A Szilikátipari Tudományos Egyesület lapja

építőanyag

Journal of Silicate Based and Composite Materials

A TARTALOMBÓL:

2022/3

ICCM 2022

XVI. International Conference on Composite Materials

August 08-09, 2022 in Amsterdam, Netherlands

XVI. International Composite Materials is the premier interdisciplinary forum for the presentation of new advances and research results in the fields of Materials and Metallurgical Engineering.

Today more than ever before it is extremely important to stay abreast of the changing landscapes of the Materials and Metallurgical Engineering world. The multidisciplinary focus of this event aims to bring together presenters and attendees from different fields with expertise in various areas of Materials and Metallurgical Engineering, providing an excellent opportunity to participate in the international exchange of ideas, current strategies, concepts and best practices, collaborations, and cooperation, offering a broader perspective and more enriching experience.
The program includes time allocated for networking, peer-to-peer discussions, and exploring the host city.

We invite the participation of leading academic scientists, researchers and scholars in the domain of interest from around the world to submit original research contributions relating to all aspects of:

- Additive manufacturing
- Applications
- Bio-based composites
- Biomimetic composites
- Ceramic matrix composites
- Concrete and cementitious composites
- Damage and fracture
- Durability and ageing
- Experimental techniques
- Fibers and matrices
- FRP reinforced concrete
- Health monitoring
- Hybrid composites
- Infrastructure
- Interfaces and interphases
- Interlaminar reinforcements
- Joint and bearing behaviour
- Life cycle analysis and sustainability
- Low cost technologies
- Mechanical and physical properties
- Metal matrix composites
- Multifunctional composites
- Multiscale modelling
- Nanocomposites
- Nanotechnologies
- NDE technologies
- Polymer matrix composites
- Probabilistic approaches and design
- Processing and manufacturing technologies
- Recycling
- Repair technologies
- Sandwich technologies
- Standardisation
- Structural design
- Testing and characterization
- Textile composites

waset.org/composite-materials-conference-in-august-2022-in-amsterdam

építőanyag

Journal of Silicate Based and Composite Materials

2022/3

TARTALOM

CONTENT

A finomkerámia-, üveg-, cement-, mész-, beton-, tégla- és cserép-, kő- és kavics-, tűzállóanyag-, szigetelőanyag-iparágak szakmai lapja
Scientific journal of ceramics, glass, cement, concrete, clay products, stone and gravel, insulating and fireproof materials and composites

A folyóiratot referálja · The journal is referred by:
ProQuest · Google Scholar · INDEX COPERNICUS INTERNATIONAL · THOMSON REUTERS

A folyóiratban lektorált cikkek jelennek meg.
All published papers are peer-reviewed.
Kiadó · Publisher: Szilikátipari Tudományos Egyesület (SZTE)
Elnök · President: ASZTALOS István
1034 Budapest, Bécsi út 120.
Tel.: +36-1/201-9360 ▪ E-mail: epitoanyag@szte.org.hu
Tördelő szerkesztő · Layout editor: NÉMETH Hajnalka
Címlapfotó · Cover photo: GYURKÓ Zoltán

WWW.EPITOANYAG.ORG.HU
EN.EPITOANYAG.ORG.HU

Online ISSN: 2064-4477
Print ISSN: 0013-970x
INDEX: 2 52 50 ▪ 74 (2022) 79–118

Preparation of meta phase of kaolinite as a precursor for geopolymer adsorbent fabrication

Hoda S. ELDIN ▪ El Nasr Pharmaceutical Chemicals Co. (ADWIC)
Nabil A. ABDULLAH ▪ Aluminum Sulphate Co. of Egypt
Mahmoud F. ISMAIL ▪ Department of Chemistry, Faculty of Science, Ain Shams University, Egypt ▪ fawzy2010@sci.asu.edu.eg
Ahmed I. HASHEMC ▪ Department of Chemistry, Faculty of Science, Ain Shams University, Egypt

Érkezett: 2021. 03. 26. ▪ Received: 26. 03. 2021. ▪ https://doi.org/10.14382/epitoanyag-jsbcm.2022.13

Abstract
Calcined kaolinite was produced by thermal treatment of raw kaolinite obtained from high quality kaolin deposits intercalated sedimentary rocks in south Sinai (Egypt). The optimal parameters for complete de-hydroxylation of kaolinite were achieved. It was found that heating at 700 °C for 90 minutes was suitable for activation of kaolinite. The formation of meta-kaolinite was investigated by XRD, IR analyses of raw kaolinite and meta-kaolinite. The pozzolanic activity was determined by Chappell test, the obtained average value of 0.70 g $Ca(OH)_2$/g meta-kaolinite indicated that the produced meta-kaolinite can be used as an active source for fabrication of geopolymer adsorbent material.
Keywords: kaolinite, meta-kaolin, pozzolanic activity
Kulcsszavak: kaolinit, meta-kaolin, puccolán aktivitás

Hoda S. ELDIN
Researcher at El Nasr Pharmaceutical Chemicals Co. (ADWIC)

Nabil A. ABDULLAH
Researcher at Aluminum Sulphate Co. of Egypt

Mahmoud F. ISMAIL
Researcher at Department of Chemistry, Faculty of Science, Ain Shams University, Egypt

Ahmed I. HASHEMC
Researcher at Department of Chemistry, Faculty of Science, Ain Shams University, Egypt

1. Introduction

Egypt has several varieties of kaolin deposits at South Sinai and Aswan (Upper Egypt), these locations are good sources for production of meta-kaolinite. The main process for the production of meta-kaolinite as high reactive pozzolan from clay minerals is calcination. The heating process removes water from kaolin, resulting in an amorphous aluminum silicate. This process is known as de-hydroxylation [1] as exemplified in (*Eq. 1*).

$$Al_2O_3{\times}2SiO_2{\times}2H_2O \rightarrow Al_2O_3{\times}2SiO_2 + 2H_2O \quad (1)$$

Thermal treatment of kaolin has been subject of some investigations [2-5]. Heating parameters such as temperature, heating rate and time significantly affect meta-kaolinite formation. For evaluation of the performance of meta-kaolinization by thermal treatment the degree of de-hydroxylation (D_{tg}) [5] is estimated according to equation (*Eq. 2)*.

$$D = 1 - (M/M_{max}) \quad (2)$$

Where, M is the difference between the loss of ignition at 950 ±50 °C (M_{max}) and the loss at certain temperature. The de-hydroxylation of pure kaolin ($Al_2O_3{\times}2SiO_2{\times}2H_2O$) at ambient atmosphere results in mass loss of about 14% and D = 1, which corresponds to the mass of bound hydroxyl groups in kaolin.

The heating temperature for production of the reactive meta-kaolinite phase is usually in the range of 600-800 °C and this temperature plays important role in the reactivity of meta-kaolinite produced. Meanwhile, more heating, causes re-crystallization resulting in mullite mineral formation ($3Al_2O_3{\times}2SiO_2$) causing loss of reactivity [6-8].

The reactivity of meta-kaolinite is measured by its reactivity to react with $Ca(OH)_2$ in the presence of water to form compounds that have cementitious properties. This reactivity can be determined chemically by measuring of the amount of lime consumed, which is determined by various techniques such as thermographic analysis (TGA), differential thermal analysis (DTA), X-ray diffraction (XRD) and calorimetric analysis [9-11]. Also, it can be determined indirectly by measuring the compressive strength developed by the reaction of MK with alkaline silicate reactive solution.

Geo-polymer is a type of amorphous alumino-silicate cementitious material which can be produced by polymerization reaction of aluminum silicate materials with alkaline solutions. Geo-polymeric concrete can be produced by using of pozzolans, which are materials obtained from various activities as byproducts, such as type-F fly ash, low calcium fly ash and calcined Sidorajo volcanic mud [12].

Several varieties of geopolymer have been exploited from modern inorganic chemistry, physical chemistry, mineralogy, geology, analytical chemistry and engineering process technologies. The potential applications of geopolymer include refractory, low energy ceramic tiles, plates for aircraft interior and automobile decoration artifacts, thermal insulation, thermal shock refractory, cements and concretes, composites for infrastructures repair and strengthening, high-tech. resin systems, radioactive and toxic waste containments, cultural heritage and archaeology [13].

The present study aims to determine the optimum conditions for thermal activation of kaolinite for the production of meta-kaolinite using local kaolin deposits in south Sinai, Abu Zenima area for using it for the preparation of geopolymer adsorbent.

2. Experimental methods and materials

2.1 Materials

Representative samples of kaolin were collected from Abu Zenima, South Sinai. Samples were dried to remove humidity, crushed to a particle size of 3 mm. The chemical and physical characteristics were determined in the Institute of Raw Materials and Building Technology that follows the National Center for Building and Housing, using X-ray Fluorescence (XRF) apparatus (XRF Bruker S4 Pioneer) it was operated at 60 kv, and the X-Ray Diffraction (XRD) analysis using an X-Ray Diffractometer (Model Bruker D8 Advance) to determine the mineralogical structure. The metakaolin was grinded to powder of mean particle size of 4.5 μm (*Fig. 2*), to be more active in polymerization reactions. Particle size distribution was performed using particle size distribution analyzer. Differential thermal analysis (DTA) and thermal gravimetric analysis (TGA) were performed using Lenseis Thermobalance instrument.

2.2 De-hydroxylation procedure

Samples of 50 g were heated in a laboratory furnace to different temperatures (100, 200, 300, 350, 400, 450, 500, 550, 600, 650, 700, 750, 800 °C) at different heating durations. The samples were cooled to room temperature to avoid recrystallization. The difference in weights before and after heating was determined in order to calculate the weight loss after thermal treatment.

The activity of meta phase of thermally treated samples was evaluated according to Chappell test [14]. 1 g of meta-kaoliniteite was mixed with 1 g of lime ($Ca(OH)_2$ in 200 ml boiling water. The suspension was subsequently boiled for 16 h and free $Ca(OH)_2$ was determined using sucrose extraction and titration with HCl.

3. Results and discussion

In the present work, it was found that the high quality raw kaolin containing about 80% kaolinite and loss of ignition (L.O.I) at temperature of 950 ± 50 °C is about 12.5% leaving 32.2% Al_2O_3 and 51.2% SiO_2. The chemical compositions of K and MK were detected by using XRF analysis and they are listed in *Table 1*. The mineralogical characteristics of the prepared MK are shown in *Fig. 1a*. XRD analysis showed that there is no mineral in the prepared MK samples, just only quartz impurities in the raw kaolin.

XRD pattern showed the disappearance of kaolin peaks as compared to the raw kaolin (*Fig. 1b*). The major minerals of kaolin deposit are kaolinite and quartz. XRD of heated kaolin at different temperatures are given in *Fig. 1a*, after thermal treatment of kaolin at 550, 600, 650, 700 and 750 °C and heating period. The characteristic peaks of kaolinite (2θ 12.41, 20.21 and 25.49°) disappeared, while the peaks assigned for Qz (2θ 21.22 and 27.45°) remained unchanged.

Particle size-distribution of the grinded MK is plotted in *Fig. 2*, which showed that the diameter of MK in cumulative % is 90% of ~8.560 μm and 10% of ~1.262 μm with an average diameter of ~4.507 μm.

Component	Content, mass (%)	
	K	MK
SiO_2	52.0	55.3
Al_2O_3	32.3	36.0
Fe_2O_3	1.12	1.41
K_2O	0.03	0.07
Na_2O	0.12	0.16
CaO	0.29	0.51
MgO	0.16	0.19
TiO_2	2.13	3.24
P_2O_5	0.16	0.12
Cl	0.08	0.11
SO_3	0.33	0.24
L.O.I.	11.5	0.2
Total	99.70	99.53
Density (g/cm³)	2.60	2.65

Table 1 Chemical and physical characteristics of K and prepared MK
1. táblázat K és MK kémiai és fizikai tulajdonságai

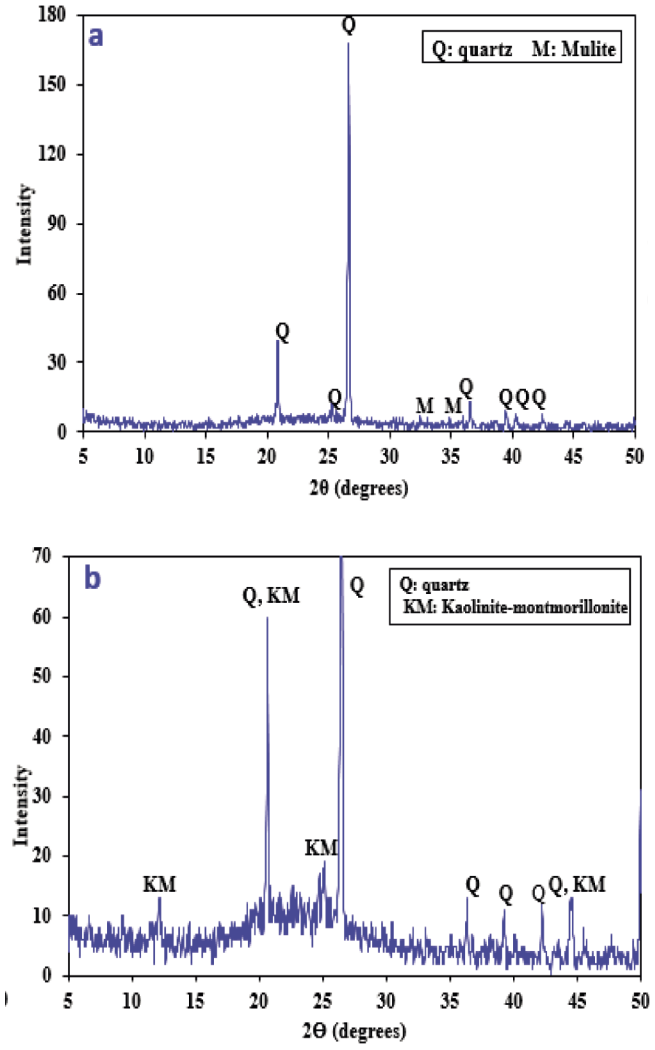

Fig. 1 XRD of (a) metakaolin treated at 700 °C and (b) kaolinite
1. ábra 700 °C-ra hevített (a) metakaolin és (b) kaolinit XRD vizsgálatának eredményei

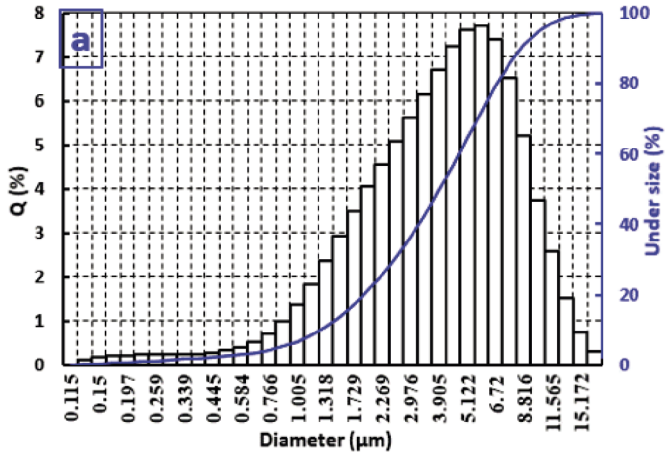

Fig. 2 Particle size-distribution of the grinded MK
2. ábra Az őrölt metakaolin szemcseméret eloszlása

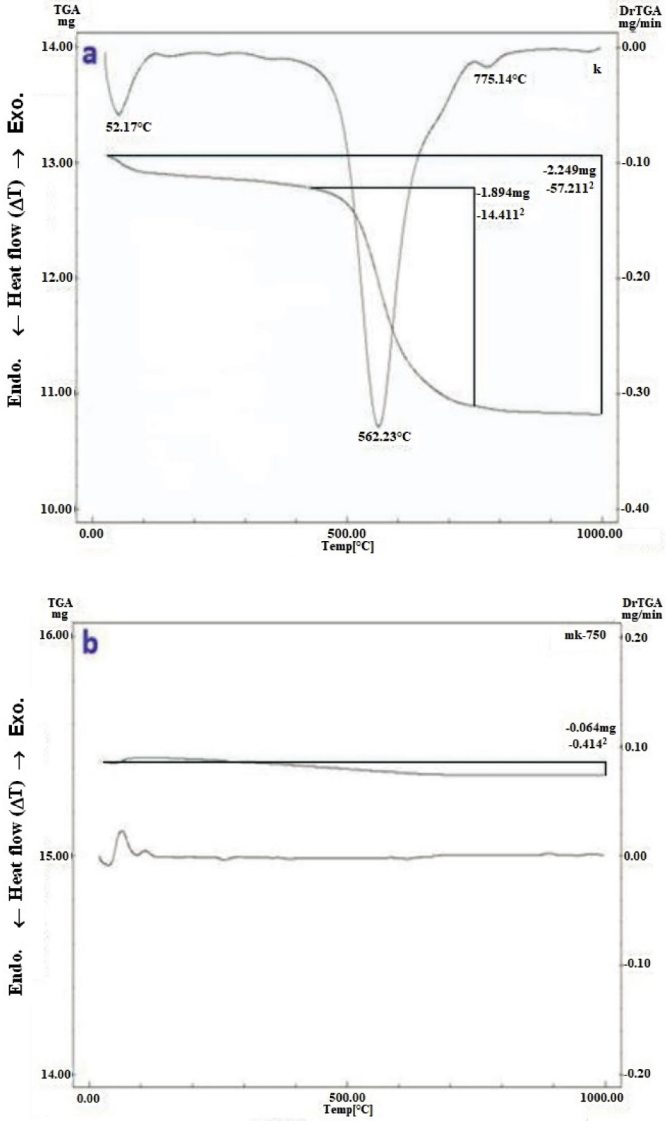

Fig. 3 Thermal gravimetric analysis (TGA/ DTGA) of (a) raw kaolinite and (b) metakaolinite after heat treatment at 750 °C for two hrs
3. ábra (a) nyers kaolinit és (b) metakaolinit termogravimetriás analízisének eredményei (TGA/DTGA) 750 °C-on történő két órás hőkezelés után

Metakaolinite was used as starting material for laboratory synthesis of geopolymer and was generated by thermal activation of kaolinite clay. *Fig. 3a* shows that the thermal activation of clay minerals is in the temperature range between 100 and 800 °C results generally in the de-hydroxylation of the clay mineral. At temperature below 200 °C, the absorbed water in the pores and on the surface was released. Between 200-450 °C, the mass loss is attributed to the pre-hydroxylation process, as a result of re-organization of the octahedral layer. In the temperature range 450-650 °C, de-hydroxylation of kaolinite and formation of meta-kaolinite occurs, while at about 1000 °C, mullite was formed, as indicated by exothermic peak. The observed endothermic peak with a maximum at 550 °C is attributed to the de-hydroxylation process [15].

The octahedral sheet loses water and decomposes into a disordered meta-state in case of collapsing clay minerals [15].

The meta-stable state of the collapsing clay is generally known to be reactive called pozzolana [16, 17]. *Fig. 3b* shows firing the clay to higher temperatures resulting in the formation of new phases such as spinel and mullite [18, 19]. Most studies have proven the utilization of secondary (waste) resources in the synthesis of geopolymer cements or concretes, such as fly ash or lava from coal and slag [20, 21].

Noteworthy, the fundamental unit of the kaolinite structure is composed of an aluminum octahedral sheet and a silicon tetrahedral sheet. Interlayer hydroxyl groups extend from the octahedral sheet into the interlayer region where they form hydrogen bonds to basal oxygens of the opposing tetrahedral silicate sheet [22, 23] (*Fig. 4*).

The first attempt to collect a crystallographic model of metakaolinite was performed by Brindley and Nakahira [24, 25] (*Fig. 5*). It was reported that, during the de-hydroxylation process the octahedral layer is likely to be changed more than the tetrahedral silica layer. Proposed structure of the metakaolinite displays no OH groups.

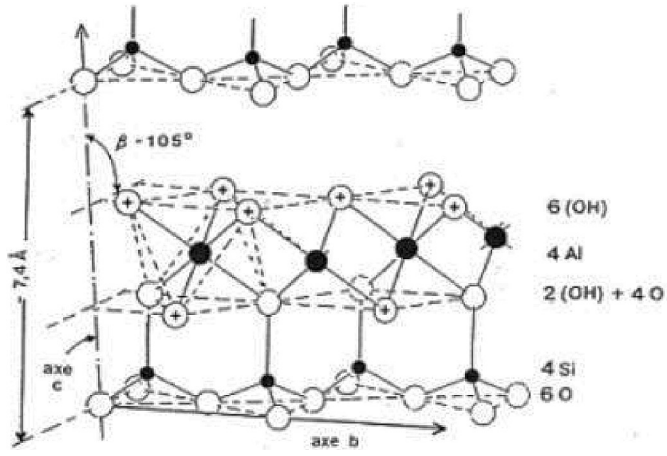

Fig. 4 Chrystalochemical structure of kaolinite [22]
4. ábra A kaolinit krisztokémiai szerkezete [22]

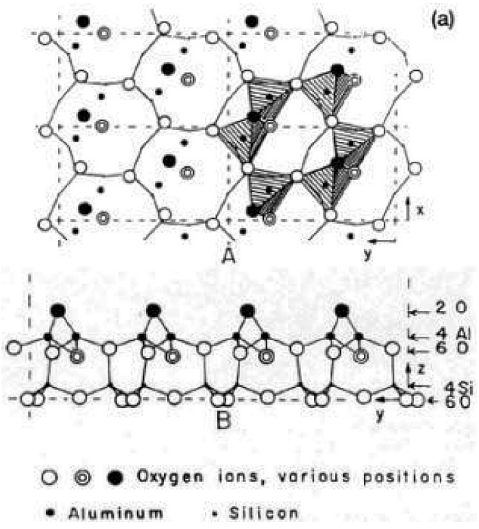

Fig. 5 Lattice of metakaolinite supposed by Brindley and Nakahira [24, 25]
5. ábra Brindley és Nakahira által javasolt metakaolinit rács [24, 25]

The aforementioned knowledge encourages us to believe that the formation of metakaolinite was produced through a stepwise mechanism as depicted in *Fig. 6*.

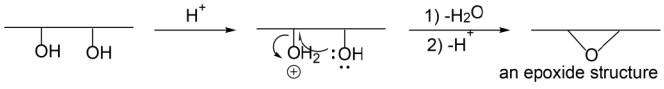

Fig. 6 A plausible mechanistic for the formation of metakaolinite
6. ábra A metakaolinit képződésének feltételezhető mechanizmusa

IR spectroscopy was performed to confirm kaolinite transformation during thermal treatment. IR spectra of raw and thermally treated kaolinite are shown in *Fig. 7a-7d*. The characteristic bands of kaolinite were presented and interpreted as reported in references [26, 27] as follows: OH^- at 3700, 3620 cm^{-1}, Al-OH at 913 cm^{-1}, Si-O at 1032, 1008, 470 cm^{-1} and Si-O-Al at 538 cm^{-1}. Al-OH band at 913 cm^{-1}, and doublet at 3700 cm^{-1} and 3620 cm^{-1}, were disappeared, in *Fig. 7b-7d*, the bands at 539 and 913 cm^{-1} and appearance of new band at 800 cm^{-1} refers to the conversion from octahedral coordination of Al(III) in kaolinite to tetrahedral coordination in meta-kaolin. The bands at 1100 and 1200 cm^{-1} are assigned to amorphous silicate.

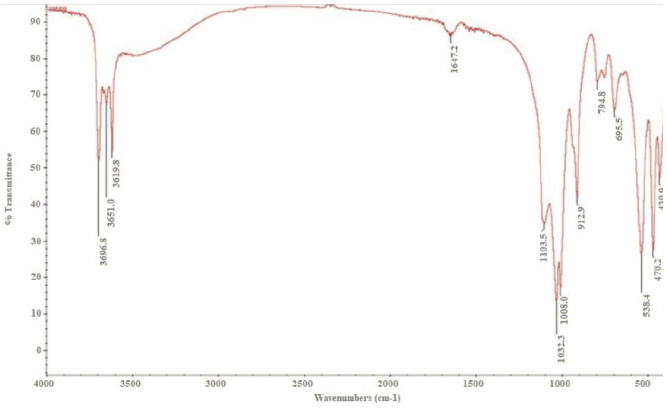

Fig. 7a IR spectrum of kaolinite
7a. ábra A kaolinit IR-spektruma

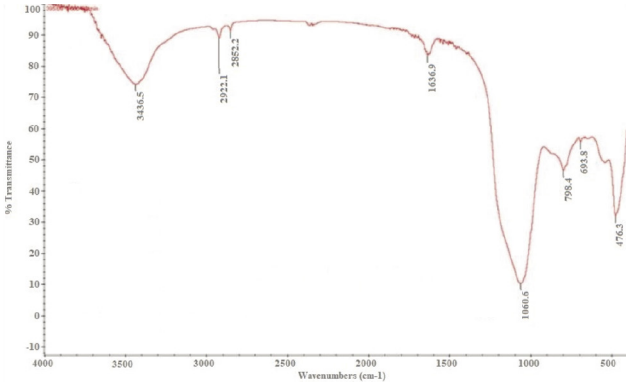

Fig. 7b IR spectrum of thermally treated kaolinite at 550 °C for 90 min
7b. ábra Az 550 °C-on 90 percig hőkezelt kaolinit IR spektruma

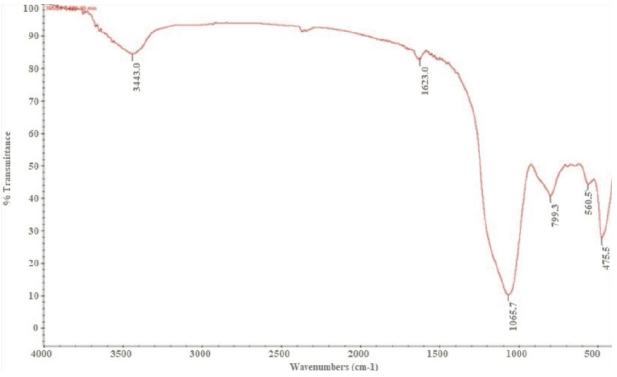

Fig. 7c IR spectrum of thermally treated kaolinite at 600 °C for 90 min
7c. ábra A 600 °C-on 90 percig hőkezelt kaolinit IR spektruma

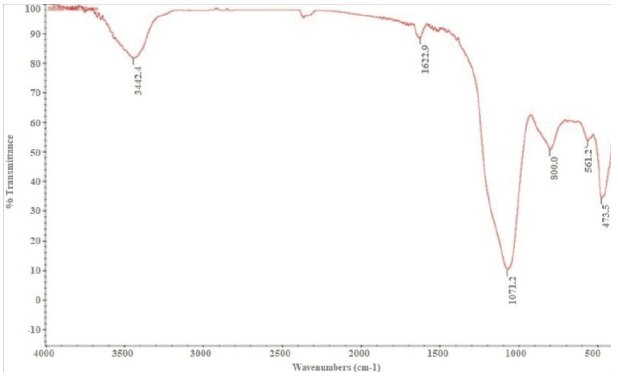

Fig. 7d IR spectrum of thermally treated kaolinite at 800 °C for 90 min
7d. ábra A 800 °C-on 90 percig hőkezelt kaolinit IR spektruma

Gravimetrically, kaolinite samples were heated at different temperatures and times, in order to determine the optimal heating parameters. The mass losses of the pre-and post-heated samples are listed in *Table 2*.

Table 2 shows that the mass loss increases up to 180 min, for heating temperatures from 100 up to 750 °C, while extending heating has no significant change of mass loss. It was found that at temperature 700 and 750 °C and heating period = 90 min., the obtained values for mass loss are the same (11%). From economic point of view and according to international trend to conserve energy, the optimal heating temperature is 700 °C and heating period is 90 min.

The mass losses during heating at different temperatures and the L.O.I obtained by chemical analysis (M_{max}), the degree of

de-hydroxylation calculated via equation (2) are summarized in *Table 3*. It was found that the de-hydroxylation has been achieved to near completion after 90 min. at temperature 700 °C, where the degree of de-hydroxylation (D_{tg}) = 0.99.

Heating period, min.	Temperature, °C										
	100 humidity	200	300	400	500	550	600	650	700	750	800
15	0.47	0.04	0.12	0.17	0.90	2.10	3.65	7.25	9.45	10.50	10.67
30	0.65	0.07	0.15	0.21	1.60	4.65	7.00	9.85	10.60	10.65	10.82
60	1.09	0.11	0.17	0.35	3.15	6.85	9.65	10.50	10.90	11.00	11.15
90	1.11	0.12	0.22	0.51	3.80	8.35	10.05	10.75	11.00	11.24	12.36
120	1.12	0.15	0.29	0.64	3.44	8.75	10.08	11.18	11.58	12.00	12.39
150	1.23	0.21	0.62	0.83	5.32	9.10	10.25	11.00	11.85	11.91	12.41
180	1.35	0.32	0.78	0.95	5.85	9.55	10.34	11.09	11.95	11.97	12.50

Table 2 *The mass losses up to 180 min, for heating temperatures from 100 up to 800 °C*
2. táblázat *180 percig, 100 és 800 °C közötti hőmérsékleten történt hőkezelés során kialakuló tömegveszteség*

Heating period, min.	Temperature, °C										
	100	200	300	400	500	550	600	650	700	750	800
15	-	0.003	0.01	0.014	0.072	0.168	0.292	0.580	0.70	0.84	0.85
30	-	0.006	0.012	0.017	0.128	0.372	0.560	0.788	0.86	0.85	0.87
60	-	0.01	0.014	0.028	0.252	0.548	0.772	0.840	0.98	0.88	0.92
90	-	0.01	0.018	0.041	0.304	0.668	0.804	0.860	0.99	1.00	1.00
120	-	0.012	0.023	0.05	0.392	0.700	0.808	0.877	1.00	1.00	1.00
150	-	0.017	0.05	0.07	0.426	0.728	0.820	0.880	1.00	1.00	1.00
180	-	0.026	0.062	0.076	0.468	0.764	0.827	0.887	1.00	1.00	1.00

Table 3 *The degree of de-hydroxylation*
3. táblázat *A dehidroxiláció mértéke*

According to the peak of kaolinite de-hydroxylation (*Fig. 8*), the transformation of kaolinite to meta kaolinite for the tested samples started at 500 °C and finished around 700 °C, the temperature which was then found to be sufficient for transformation. This temperature is in agreement with the results of previous studies. It was reported that the calcinations temperature must be higher than 700 °C to have a best reactivity of kaolinite [28] and must not exceed 800 °C.

With high temperature, alumina and silica can be re-organized again into new thermodynamically stable compounds (mullite, tridimite, etc) with no reaction with lime hydrate.

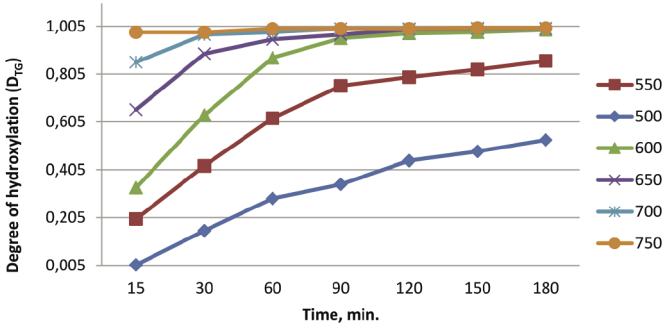

Fig. 8 *The degree of de-hydroxylation at different temperatures*
8. ábra *A dehidroxiláció mértéke különböző hőmérsékleteken*

Optimized heating process can be achieved at 700 °C for 90 min, the activity for pozzolanic meta-kaolinite ranged between 0.65 and 0.74 g $Ca(OH)_2$/g of meta-kaolin, which is in agreement with the previous studies that reported a range of (0.55 - 0.82 g $Ca(OH)_2$ for each gram of meta-kaolinite [11].

4. Conclusions

The produced meta-kaolinite as a source of active silica and alumina was prepared by thermal treatment of local kaolin deposits found in South Sinai, Egypt. The formation of meta-kaolinite was investigated by XRD, IR analyses. The optimum conditions for heating process are temperature 700 °C for 90 minutes to have a best reactivity of kaolinite. The process revealed that the de-hydroxylation degree equal 0.99. The pozzolanic activity was determined by Chappell test, the obtained average value of 0.70 g $Ca(OH)_2$/g meta-kaolinite indicated that the produced meta-kaolinite can be used as an active source for fabrication of geopolymer adsorbent material.

References

[1] Murat, M., Driouche, M. Chemical reactivity of thermally activated clay mineral estimation by dissolution in hydrofluoric acid. Cem. Concr. Res., 18(2), 1988, 221-228. https://doi.org/10.1016/0008-8846(88)90006-3.

[2] Shvarzman, A., Kovler, K., Grader, G. S., Shter, G.E. The effect of de-hydroxylation/amorphization degree on pozzolanic activity of kaolinite. Cem. Concr. Res., 33(3), 2003, 405-416. https://doi.org/10.1016/S0008-8846(02)00975-4.

[3] Kostuch, J. A., Walters, G. V., Jones, T. R. High performance concrete incorporating meta-kaolin- a review. in: R. K. Dhir, M. R. Jones (Eds.), Concrete 2000: Economic and Durable Construction Through Excellence, E&FN SPON, London, 2, 1993, 1799-1811.

[4] Arikan, M., Sobolev, K., Ertun, T., Yeginobali, A., Turker, P. Properties of blended cements with thermally activated kaolin. Constr. Build. Mater., 23(1), 2009, 62-70. https://doi.org/10.1016/j.conbuildmat.2008.02.008.

[5] Rahier, H., Wullaert, B., Van Mele, B. Influence of the degree of de-hydroxylation of kaolinite on the properties of aluminum silicate glasses. J. Therm. Anal. Calorim., 62(2), 2000, 417-427. https://doi.org/10.1023/A:1010138130395.

[6] Mackenzie, K. J. D., Meinhold, R. H., Brown, I. W. M., white, G. V. The formation of mullite from kaolinite under various reaction atmospheres. J. Eur. Ceram. Soc., 16(2), 1996, 115-119. https://doi.org/10.1016/0955-2219(95)00143-3.

[7] Wild, S., Khatib, J. M., Jones, A. Relative strength pozzolanic activity and cement hydration in super-plasticized concrete. Cem. Concr. Res., 26(10), 1996, 1537-1544. https://doi.org/10.1016/0008-8846(96)00148-2.

[8] Stroeven, P., Dau, V. D. Effect of blending with kaolin or diatomite on characteristics of Portland cement paste and morter. In: K. Dhir, T. D. Dyer, (Eds.), Modern Concrete Materials: Binders, Additions and Admixtures. Thomas Telford, London, 1999, 139-149.

[9] Cabrera, J. Rojas, M. F. Mechanism of hydration of metakaolin-lime-water system. Cem. Concr. Res., 31(2), 2001, 177-182. https://doi.org/10.1016/S0008-8846(00)00456-7.

[10] Badogiannis, E., Kakali, G., Tsivilis, S. metakaolin as supplementary cementitious material- Optimization of kaolin to metakaolin conversion. J. Therm. Anal. Calorim., 81(2), 2005, 457-462. https://doi.org/10.1007/s10973-005-0806-3.

[11] Frias, M., Cabrera, J. Pore size distribution and degree of hydration of metakaolin cement pastes. Cem. Concr. Res., 30(4), 2000, 561-569. https://doi.org/10.1016/S0008-8846(00)00203-9.

[12] Wiyono, D., Antoni, Hardjito, D. Improving the durability of pozzolan concrete using alkaline solution and geopolymer coating. Procedia Eng., 125, 2015, 747-753. https://doi.org/10.1016/j.proeng.2015.11.121.

[13] Davidovits, J. Solid phase synthesis of a mineral block polymer by low temperature polycondensation of aluminosilicate polymers. IUPAC

International Symposium on Macromolecules Stockholm; Sept. Topic III, New Polymers of high stability, 1976.
[14] Largent, R. Estimation de l'activite pouzzolanique. Bull. Liaison Lab. Ponts chaussées, 93, 1978, 61-65. http://worldcat.org/issn/04585860.
[15] Davidovits, US Patent no. 4,399,386, 1882.
[16] Dieter, G. E. Mechanical metallurgy. Mc-Graw Hill, 1987, 326-327.
[17] Astutiningsih, S. Alkali activation and curing of aluminosilicate based-geopolymers. PhD Theses, The University of Western Australia, 98, 2005.
[18] Mendelovici, E., Comparative study of the effects of thermal and mechanical treatments on the structures of clay minerals. J. Therm. Anal. Calorim., 49(3), 1997, 1385-1397. https://doi.org/10.1007/BF01983697.
[19] McManus, J., Ashbrook, S. E., MacKenzie, K. J. D., Wimperis S. ^{27}Al multiple- Quantum MAS and ^{27}Al (^{1}H) CPMAS NMR study of amorphous alumino-silicates. J. Non-Cryst. Solids, 282(2-3), 2001, 278-290. https://doi.org/10.1016/S0022-3093(01)00313-1.
[20] Buchwald, A. What are geopolymers? Current state of research and technology, the opportunities they offer, and their significance for the precast industry. Concrete Precast. Plant Tech., 72(7), 2006, 42-49.
[21] Duxson, P., Fernandez-Jimenez, A., Provis, J. L., Lukey, G. C., Palomo, A., van Deventer, J. S. J. Geopolymer technology: the current state of the art. J. Mater. Sci., 2(9), 2007, 2917-2933. http://dx.doi.org/10.1007/s10853-006-0637-z
[22] Varga, G. The structure of kaolinite and metakaolinite. Epitoanyag-j. silicate based compos. Mater., 59(1), 2007, 6-9. https://doi.org/10.14382/epitoanyag-jsbcm.2007.2.
[23] Jemai, S., Amara, A. B. H., Brahim, J. B., Plançon, A. Structural Study of a 10 Å Unstable Hydrate of Kaolinite. J. Appl. Crystallogr., 33(4), 2000, 1075-1081. https://doi.org/10.1107/S0021889800004878.
[24] Brindley, G. W., Nakahira, M. The kaolinite-mullite reaction series: I, A survay of outstanding problems. J. Amer. Ceram. Soc., 42(7), 1959, 311-314. https://doi.org/10.1111/j.1151-2916.1959.tb14314.x.
[25] Brindley, G. W., Nakahira, M. The kaolinite-mullite reaction series: II, Metakaolin. J. Amer. Ceram. Soc., 42(7), 1959, 314-318. https://doi.org/10.1111/j.1151-2916.1959.tb14315.x.
[26] Beutelspacher, H., Van der Marel, H., Van der Marel, H. W., Van der Marel, R. Atlas of Infrared Spectroscopy of clay Minerals and their Admixtures. Elsevier, Amsterdam, 1976.
[27] Russell, J. D. Infrared Spectroscopy of Inorganic Compounds Laboratory Methods in Infrared Spectroscopy. Wiley, New York, 1987.
[28] Ambroise, J., Martin-Calle, S., Pera, J. Pozzolanic Behavior of Thermally Activated Kaolin. In: Malhotra, V.M., Ed., Proceedings of the Fourth International Conference on Fly Ash, SF, Slag and natural Pozzolans in Concrete, 1, Turkey, 1992, 731-741.

Ref.:
Eldin, Hoda S. – **Abdullah**, Nabil A. – **Ismail**, Mahmoud F.– **Hashem**, Ahmed I.: *Preparation of meta phase of kaolinite as a precursor for geopolymer adsorbent fabrication*
Építőanyag – Journal of Silicate Based and Composite Materials, Vol. 74, No. 3 (2022), 82–87. p.
https://doi.org/10.14382/epitoanyag-jsbcm.2022.13

Estimation of the drying behaviour for different clay raw materials – drying sensitivity techniques review

Miloš R VASIĆ

Author is a research associate in the department Laboratory for ceramic materials of the Institute IMS Begrade from 2015. He has finished PhD in 2014 at the Faculty of technology and metallurgy, University of Belgrade. From 2006 author has praticipitated at several national research projects (ОИ 142059, ТП 19020, ТП 19017 и ИИИ 45008) as well as on the international COST „Action ELENA" project. He is author or coauthor of 98 scientific papers and 4 technicla improvemets. Research area: The processing engineering (modeling and optimization of drying and firing process, recommendations for process parameters in industrial conditions), design of new products, recycling (especially waste materials), mechanical activation of various inorganic raw materials (coal dust, clay raw materials, inorganic wastes etc), optimization of raw material mixtures.

Miloš R. VASIĆ ▪ Institute IMS ▪ milos.vasic@institutims.rs

Érkezett: 2021. 08. 29. ▪ Received: 29. 08. 2021. ▪ https://doi.org/10.14382/epitoanyag-jsbcm.2022.14

Abstract

In order to rate the drying behavior of different clay raw materials it is necessary to establish the criteria for comparison. Mineralogical composition, clay minerals content, particle size distribution, packing, porosity, forming procedure, and raw material aging are known as intrinsic parameters. Due to the fact that these parameters are cross linked and are usually inter-dependently related to each other, the attempts to set up a criteria for correlation between intrinsic parameters and drying sensitivity has been limited. That was the reason why the estimation of the cracking tendency was linked with the easiness of the drying process in each reported method. The most applied methods for estimation of the drying sensitivity of clays in the ceramic industry were proposed by Bigot, Ratzenberger, Piltz, Hermansson and Varlamov. The fact that previously mentioned methods were not compared up till know has defined the main objective of this study. The only reported comparison was between Bigot and Ratzenberg drying sensitivity index. The second objective of this review was to present these methods and to estimate the drying behavior of tree different clay raw material. It was confirmed that Varlamov method is very simple, accurate and fast. It is correlated with the mineralogical composition of clay and cannot be used for description of the drying kinetic. The other two models can provide info about the drying kinetic. Piltz model is the most relevant for describing the drying behavior at the beginning of the drying. The results have confirmed that the most suitable conclusion about the drying behavior of the tested clays is obtained when results from Bigot, Piltz and Varlamov methods are available.

Keywords: drying sensitivity, heat transfer, masonry clay units, roofing tiles
Kulcsszavak: száradási érzékenység, hőátadás, falazóelemek, tetőcserepek

1. Introduction

An experimental growth in drying requests and demands on a global scale has been registered during the last fifty years. Even though new drying technologies as well as updated operation strategies and scale up methods has a positive effect on the reduction of the production costs and better quality of the dried products, the need to qualitatively estimate the drying sensitivity of clays and consequently predict the drying behavior is still actual and present. It is expected that the closer interaction between the scientific community and industry will very soon lead to the progress in much precise determination of the drying sensitivity of clays, which is nowadays stressed as the key factor for successful drying and satisfaction of the new drying requests and demands in the near future.

It is important to state that comparison of different raw materials and its suitability regarding to crack formation during drying is possible if qualitative values of drying sensitivity are available. It is well known that mineralogical composition, clay minerals content, grain distribution, packing, porosity, forming method and raw material aging are affecting on the easiness of the drying process [1]. Previously mentioned parameters are usually inter-dependently related to each other. That is the reason why the drying sensitivity has not been related with the mentioned intrinsic parameters in most recognized and validated models. For example in Piltz, Hermansson, West, and Ford models [2, 4], the evaluation of the cracking tendency is linked with the easiness of the drying process. Previously mentioned models along with, Bigot and Ratzenberger models [5, 6], which are commonly used for qualitatively estimation of the drying sensitivity of clays and consequently the prediction of the drying behavior, are disregarding intrinsic link with the mineralogical composition of clay minerals and their physicochemical properties. More objective and rapid method was proposed by Varlamov. According to this model, based on the Thermogravimetric curve (TG), the drying behavior of clays is closely related with the intrinsic parameter which corresponds with the clay mineral content [7]. One of the objectives of this review was to present, discuss and compare the most commonly used techniques for assessing the drying sensitivity. The second objective was to actually characterize, compare and predict the drying behavior of three raw materials by applying the previously mentioned routines.

2. Material and methods

There are several methods for measuring and characterization of the drying sensitivity of clays. Bigot, Ratzenberger, Piltz, Hermansson and Varlamov are the most used techniques. Bigot method is widely used due to the fact that necessary equipment is not expensive. Piltz, Ratzenberg and Hermansson methods require a laboratory recirculation dryer in which drying air parameters can be regulated and optionally the linear shrinkage and weight changes can be recorded during drying. Drying air parameters were regulated inside the dryer with accuracies of ±0.2 °C, ±0.2 % and ±0.1 % for temperature,

humidity and velocity, respectively. The sample mass and linear shrinkage were continually registered during drying with the accuracy of 0.01 g and 0.01 mm, respectively.

Varlamov method requires the DTA/TG device which is relatively expensive, or in other words it is necessary to have the TG curve of the corresponding raw material. Nevertheless this method can precisely provide us with important parameters such as mineralogical composition of clay which can tell us in advance if montmorillonite, montmorillonized hydrous micas or hydrochlorite, which are very sensitive to drying are present in the raw material.

Samples for Bigoth and Ratzenberg methods are prepared in a similar way. The raw material was dried at 60 °C and then the pan mill was feed with it until the whole content has passed through the sieve of 5 mm. After that the crashed material was simultaneously moisturized and further milled, using the rotor crusher which gap was set to 3 and afterwards to 1 mm. Rectangular and cylindrical bars were formed from the previously homogenized clay in the extruder "Hendle" type 4, under a vacuum of 0.8 bar. From the rectangular bar two samples of 120 × 20 × 14 mm were formed. From each formed tile a rectangular sample 30 × 15 × 15 mm was cut. These samples were dried and Bigots curve was registered.

From cylindrical bar with the diameter of 33 mm four samples with 150 mm length were created. The side surface of two samples was coated with polyurethane resign in order to prevent the moisture evaporation. Only two uncoated circular ends were served as evaporation surfaces. Previously prepared cylindrical samples were dried and the corresponding Ratsenzberg drying curves were recorded.

2.1 Bigoth method

The graph which represents the relationship between shrinkage and water content, registered during natural drying of the formed clay sample is usually called the Bigot curve. A special device which was capable for registration of such drying curves was firstly reported in 1921 under the name "barrellograph" [6]. It is important to note that the Bigot's curve has a characteristic shape, which is directly correlated with the simultaneous activation of internal transport mechanisms which are dictating the moisture flow up to the surface of the clay product. In other words, as the moisture is transported out of the product, the clay particles in the body are getting closer together. For more detail information see the paper [8].

The shrinkage rate is liner until the critical moisture content (M_c) is reached. Around the critical point (CP) some clay particles are already in contact and the rate of shrinkage is decreased. Consequently, the slope on the Bigot's curve will gradually decrease. In this stage, the sample volume variation is no more proportional to the evaporated water volume. After the CP the shrinkage is nearly realized and almost all of the material particles are in contacts [9].

Bigot has firstly taken the value of moisture loss in critical point as a tool for comparing different clay drying sensitivity. Based on this value clays were classified as: insensitive ($M_c \leq 5\%$; $0 < K_c < 1$), poorly sensitive ($5 < M_c < 7\%$), sensitive ($7 < M_c < 10\%$; $1 < K_c < 2$) and highly sensitive ($M_c > 10\%$; $K_c > 2$). The same author has also proposed the *Eqs. (1)* and *(2)* for calculation of the drying sensitivity index (DSI-B and K_c), where M_i, M_c and DS represents respectively initial moisture content of the green heavy clay product, critical moisture at which the drying shrinkage finishes (%) and drying shrinkage of specimens dried at 110 °C for 24 h (%). DSI-B index is used if it is necessary to compare clays which M_c values are similar

$$DSI - B = (Mi - Mc)/100 \cdot DS\ (\%). \quad (1)$$

$$Kc = (Mi - Mc)/Mc. \quad (2)$$

2.2 Ratzenberg method

This method is based on the determination of the moisture difference between the external water and internal water content registered after previously prepared coated cylindrical samples were dried at 65 °C for 7.5 h. After drying, the two cylinder ends of each specimen were cut so that the thickness of the cut disks was 20 mm. The remained cylinder was divided into three pieces. The cut disk with the thickness of 20 mm which represent the middle part of the previous cylinder was kept. These end disks, middle disk and the uncoated cylindrical sample were dried at 110 °C for 24 h in order to find out the moisture content and linear drying shrinkage. Determined moisture content in the end disks was averaged and marked as external water content, while the determined moisture content in the middle disk was marked as internal moisture content. The uncoated cylindrical sample was used for measuring the linear drying shrinkage.

Ratzenberg has suggested the *Eq. (3)* for calculation of the drying sensitivity index, where MD and LDS represents respectively the moisture difference (between internal and external moisture content in %) and linear drying shrinkage of the uncoated samples in %. Based on this value clays were classified as: insensitive (DSI-R ≤ 30), sensitive (30 < DSI-R < 70) and highly sensitive (DSI-R > 70).

$$DSI - R = MD \cdot LDS \quad (3)$$

Aungaticard and Wada have updated this method by drying more coated samples at the same temperature but at different times of 2.5, 5, 7.5, 10, 15 and 20 h. The maximal MD for each sample was detected from the graph between moisture difference and drying time. This value was used for calculation of DIS-R index. If the updated method is used it is important to mention that MD_{max} value can be different from the $MD_{7.5}$ value. It is suggested to always calculate the DIS-R using both MD_{max} and $MD_{7.5}$ values [10].

2.3 Pilltz method

This method assumes that the hand-shaped specimen is exposed to the forced drying in a laboratory recirculation dryer in which values of drying air velocity, temperature and humidity are respectively set at 0.5 m/s, 80 °C and 10 %. During drying the appearance of the first crack is registered. This vale was used as a tool for comparing different clay drying sensitivity. Piltz classification is reported in *Table 1*. Piltz has also suggested the *Eq. (4)* for calculation of the drying sensitivity index which is labeled as T_b. Low drying sensitivity will have clays for which $T_b > 0.9$.

$$Tb = \text{Linear drying shrinkage (\%)} / \text{time to form the first crack (min)} \quad (4)$$

Time to form the first crack (min)	Drying sensitivity	Industrial sensitivity degree
0 - 2	Absolutely sensitive	(1 - 2)
2 - 4	Extraordinary sensitive	(2 - 3)
4 - 6	Highly sensitive	(3 - 4)
6 - 8	Sensitive	(4 - 5)
8 - 10	Moderately sensitive	(5 - 6)
10 - 12	Lowly sensitive	(6 - 7)
12 - 20	Slightly sensitive	(7 - 8)
> 20	Insensitive	(8 -10)

Table 1 Drying sensitivity according to Piltz
1. táblázat Szárítási érzékenység Piltz szerint

2.4 Hermansson method

The drying sensitivity of ceramic bodies with large dimensions (industrial green products) is calculated according to Hermansson as the time related difference between volume shrinkage and surface shrinkage during the drying stage. The total linear shrinkage was determined using the linear variable differential transformer placed above the sample. The surface shrinkage was detected from the pictures by measuring the shrinkage between two lines which were marked prior to the drying experiment.

This method requires in general drying and shrinkage-curves to be determined for both mild and hard drying conditions. In other words it is recommended to dry four samples. Drying air velocity and humidity was set respectively as 1.5 m/s, and 20% in each experiment. The drying air temperature was set at 50 °C and was raised for 10 °C in each following experiment.

For this method *Eq. (5)* was proposed for calculation of the drying sensitivity index labeled as S. Based on this value clays were classified as: insensitive (S < 1.1), sensitive (1.1 < S < 1.3) and highly sensitive (S > 1.3). It is important to state that S values are dependent of drying conditions, initial moisture content etc. and that the single S value for a body is not sufficient to evaluate the drying sensitivity.

The most important finding was the fact that the tendency for crack formation is related to the time relation between surface and total linear shrinkage. Crack formation was found to occur not or from the exposed surface but within the body and parallel to the faces exposed to drying. After a certain time the outer parts of the body have been dried out and consequently have become rigid with increased strength. The preceding drying of inner parts will probably create share stresses parallel to the exposed surfaces which will eventually led the crack formation [2].

$$S = \text{time to reach half of the final mid (plane shrink)} / \text{time to reach half the final surface shrink.} \quad (5)$$

2.5 Varlamov method

It was proposed to determine only the portion of the losses that is released in the temperature range above the drying temperature, at 100-200 °C in order to compare different clays as regards the interlayer moisture lost during drying. A relationship was found between the amount of moisture liberated at temperature up to 200 °C, mineralogical composition and drying behavior of clays. Varlamov has arranged 14 clay materials with different drying sensitivity. These clays were arranged in such way that the first clay was kaolin and the last one was montmorillonite. The remaining 12 clays were arranged between previously mentioned one according to complex technological test results in a series according to decreasing drying sensitivity.

The first and last clay were not used as a common raw material and were taken as a standard material. The raw materials listed in *Table 2* were further divided with regards to technological parameters in three subgroups: well drying, medium drying and poorly drying clays. According to Varlamov [6] well drying clays by their chemical composition belong to semi-acid clay minerals and by their plasticity to moderately plastic one. Medium drying clays are placed into a group from semi acid to acid clay and from moderately to medium plastic clay raw materials. Poorly drying clays are commonly classified as acid clay materials, and their plasticity vary in a range from moderately plastic to medium plastic ones.

It is important to say that in literature plasticity classification based on the value of Pfefferkorn plasticity index PI is in most cases recognized as low (PI<20), moderate (20<PI<25), good (25<PI<30), high (30<PI<35) and highest (PI>40) [7]. Nevertheless in older literature such as for example reference [6] classification limits are stated as low (PI<25), moderate (25<PI<30), medium (30<PI<35) and high (PI >35).

Clays	SiO_2 %	Al_2O_3 %	Fe_2O_3 %	CaO %	Mineralogical composition	Interlayer loss of moisture at 200 °C	Drying Sensitivity
1.	45.74	40.57	0.38	traces	K with traces of HM	0.25	well drying
2.	68.88	14.28	7.27	0.60	K, HM,H	1.20	
3.	64.04	18.69	3.41	1.83	HM, K	1.55	
4.	55.62	15.17	5.23	7.83	HM,K	1.96	
5.	60.46	16.18	3.72	6.10	HM, K, HC	2.09	
6.	63.12	16.25	6.75	1.10	HM, with ferrous hydroxide,H	2.17	medium drying
7.	59.64	18.21	6.78	1.80	K, HM, H	2.46	
8.	67.32	12.18	4.02	4.55	K-HC, M and Carbonate	2.53	
9.	75.56	10.51	5.61	0.50	MHM,K-HC	2.73	
10.	69.74	10.80	4.30	5.05	MHM,K-HC	3.17	poor drying
11.	62.38	15.00	5.50	4.40	MHM,M,HC	3.82	
12.	68.52	11.72	6.53	1.60	MHM, K-HC	4.05	
13.	61.56	12.90	6.05	5.75	MHM with carbonate	4.50	
14.	53.50	18.08	6.51	1.50	M	9.93	

K – kaolinite, HM – hydrous mica, H – hematite, HC – hydrochlorite, K-HC – kaolinite-hydrohlorite composition, M – montmorillonite, MHM – montmorillonitized hydrous micas

Table 2 Estimation of Varlamov clay sensitivity index based on interlayer loss of moisture
2. táblázat A Varlamov-agyag érzékenységi indexének becslése a rétegközi nedvességveszteség alapján

3. Results and discussion

Three clay raw materials were characterized. XRD and TG results were reported at *Figs. 1* and *2*. Drying plasticity, sensitivity and chemical composition of the investigated clays were reported in *Table 3* and *4*.

All three clays have different mineralogical composition. Kaolin is mostly present in clay B, along with small amounts of illite (hydrous micas). Kaolinite-hydrochlorite composition along with some montmorillonite is present in clay A. Montmorillonitized hydrous micas with some montmorillonit, hydro-chlorite and small amounts of illite and kaolin are detected in clay C.

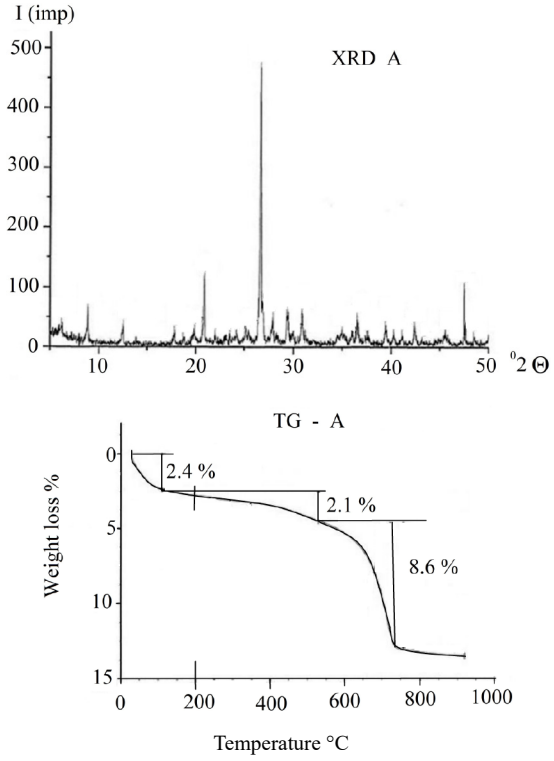

Fig. 1 XRD and TG diagrams of investigated raw materials A
1. ábra A vizsgált A jelű nyersanyagok XRD és TG diagramja

If detected mineralogical composition, as well as interlayer loss of moisture at 200 °C are compared with the Varlamov clays classification (see *Table 2*) it can be seen that clays A, B and C are similar as clays 8, 4 and 11. In other words clays A and C are consisted of swelling minerals which are problematic for drying and consequently the deterioration of drying sensibility is expected. Linear drying shrinkage, plasticity as well the shape of DTA/TG curves are in accordance with the previously reported mineralogical composition.Results have shown that all commonly used method for determination of drying sensitivity can classify different clay raw materials in the same designating order.

It is interesting to note that drying sensitivity determined using Bigoth, Ratzenberg, and Varlamov method is similar, while the one determined using Piltz and Hermanson method can be slightly different. These two methods can provide much precise information about the drying behavior at the beginning of drying. For example clay C is classified as highly sensitive to drying in accordance to Bigot and Ratzenberg routine while in accordance with the Piltz and Hermanson routine it is classified as extraordinary sensitive with a possibility of deep crack formation especially at the beginning of drying.

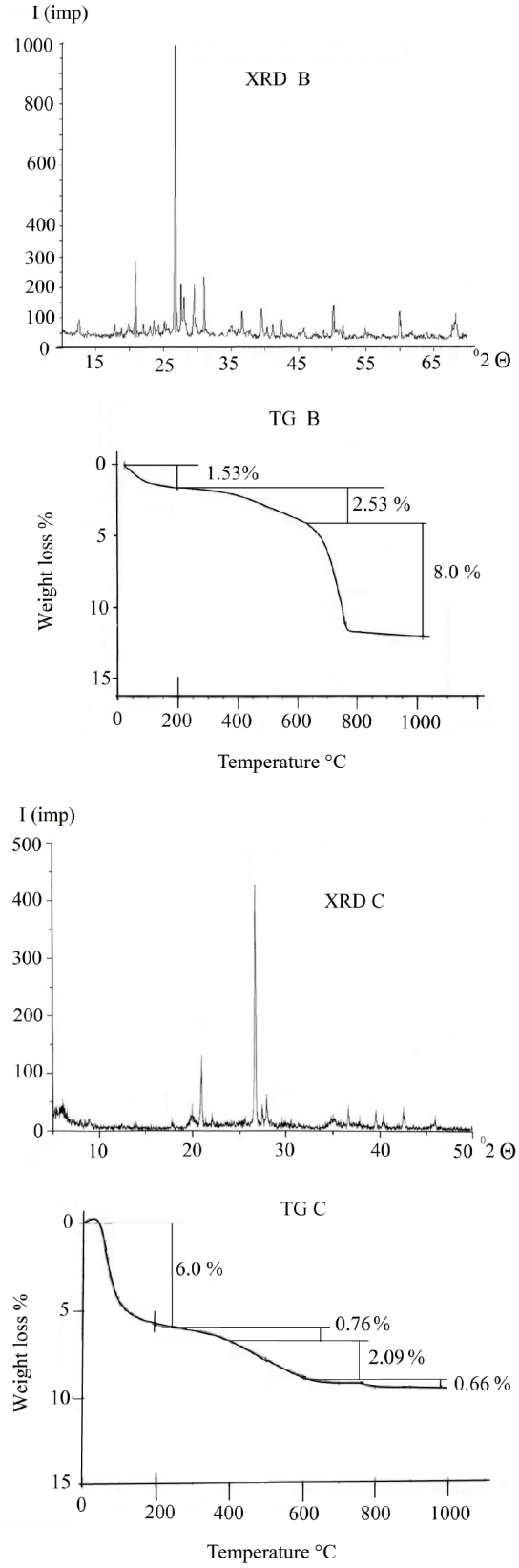

Fig. 2 XRD and TG diagrams of investigated raw materials B and C
2. ábra A vizsgált B és C jelű nyersanyagok XRD és TG diagramjai

It is also interesting to note that even though calculated DSI-B values are in accordance with the Bigot classification Kc values are not. As it was earlier stated if $1 < K_c < 2$ the clay is classified as sensitive. Calculated Kc value for clays A and C are equal to 1.01 and 1.46. So if this parameter is used alone for classification of the drying sensitivity the corresponding drying behavior of those clays could be estimated as safe and a little bit problematic respectively. That assessment does not correspond with the actually determined drying behavior in which clay A is characterized as a little bit problematic, while clay C is characterized as problematic for drying.

Clay		A	B	C
Moisture cont. after forming (wt. %)		24.22	23.08	25.26
Plasticity according to Pfefferkorn	PI	29.8	27.30	35.1
	Plasticity	Good	Good	highest
	h_0/h	1.53	1.60	1.29
	ctg α	0.59	0.31	0.50
Bigoth		**A**	**B**	**C**
Linear shrinkage at 105°C (wt. %)		6.27	3.97	9.40
Shrinkage at critical point (wt. %)		5.69	3.51	6.78
Moisture loss at critical point (wt.%)		9.81	6.41	12.00
Moisture content in critical point %		12.03	15.19	10.23
DSI - B		0.90	0.66	1.24
Kc		1.01	0.51	1.46
Drying sensitivity at critical point		sensitive	poorly	highly
Ratzenberg		**A**	**B**	**C**
Linear shrinkage at 105°C (wt. %)		6.38	4.05	9.50
$MD_{7.5}$		7.36	4.40	8.42
DSI – R		47	18	80
Drying sensitivity		sensitive	poorly	highly

Table 3 Drying plasticity and Bigoth drying sensitivity
3. táblázat Szárítási képlékenység és Bigoth szárítási érzékenység

Piltz	A	B	C
Time to form the first crack (min)	7	14	3.5
Industrial sensitivity degree	4	7	3
Drying sensitivity	Highly	Slightly	Extraordinary
Hermanson	**A**	**B**	**C**
Mid plane shrinkage %	6.45 / 6.38 / 6.25 / 6.23	3.65 / 3.58 / 3.55 / 3.52	8.82 / 8.78 / 8.67 / 8.55
S index	1.14 / 1.20 / 1.34 / 1.36	1.01 / 1.05 / 1.1 / 1.1	1.31 / 1.91 / 2.52 / 3.68
Drying sensitivity	Exp.1 - crack tendency Exp.2 - crack formation Exp. 3&4 - deep cracks	No crack formation	Cracks and deep cracks in all 4 experiments

Varlamov Clay	SiO_2 %	Al_2O_3 %	Fe_2O_3 %	CaO %	MgO %	TG loss at 200°C	Drying Sensitivity
A (8)	63.25	13.19	4.88	5.59	2.37	2.65	Medium
B (4)	55.37	13.65	6.94	7.66	1.53	1.53	Well
C (11)	58.57	19.08	5.59	2.43	0.68	5.82	Poor

Table 4 Pilthz, Hermanson and Varlanov drying sensitivity
4. táblázat Pilthz, Hermanson és Varlanov-féle szárítási érzékenység

4. Conclusions

The drying sensitivity of three clays was investigated using five commonly used drying sensitivity models. Results have confirmed that all commonly used method for determination of drying sensitivity can classify different clay raw materials in the same designating order. The most objective characteristic of clay drying sensitivity can be determined if TG curve of the raw material is available. This method is usually known as Varlamov. It is a rapid method based on the mineralogical composition and physico-mechanical nature of clays. Bigot method is very important due to the fact that the shape of this curve is directly correlated with the simultaneous activation of internal transport mechanisms which are dictating the moisture flow up to the surface of the clay product. In other words, this curve can be correlated with the kinetic of drying. DSI – B is widely used for quantification of the drying sensitivity of different clays which M_c values are similar. Piltz methods can provide much precise information about the drying behavior at the beginning of drying, then other models. For complete view of the drying behavior it is recommended to combine at least Bigoth, Piltz and Varlamov method.

Acknowledgements

This paper was financed by ministry of education science and technological development of Serbia, contract number 451-03-9/2021-14/200012. Author M. Vasic is fully employed in the Institute IMS.

References

[1] Chairi B.von., Drying sensitivity studies. An overview, Ceramic Forum International, DKG Vol.63, No. 9/10, pp. 482-486, (1986).
[2] Piltz G., Technical Paramters of Drying Heavy clay Raw Materials, Ziegel Industrie Interantional, Vol.7, pp. 294 – 300, (1971).
[3] Hermansson L., Carlsson R., An Empirical Method of Measuring the Drying Sensitivity of Ceramic, Transcript of the British Ceramic Society Vol. 78, No. 5, pp. 98-102, (1979).
[4] West H.W.H., Ford R.W., Evaluation of drying sensitivity of clays, Transcript of the British Ceramic Society Vol. 66, pp. 511-517, (1967).
[5] Bigot A., Retrait au séchage des kaolins et argiles. In Report of Academy of Sciences, Paris, (1921).
[6] Ratzenberg H., An accelerated method for the determination of drying sensitivity, Ziegel Industrie Interantional, Vol.6, pp. 348-354, (1990). https://www.zi-online.info/download/20194/1990.pdf
[7] Varlamov P.V., Kroichuk A.L., Toporkova A.A, A new method for estimating the drying sensitivity of clays, Ceramugia International, Vol. 2 No.2, 98-101, (1978). https://doi.org/10.1016/0390-5519(76)90054-5
[8] Vasić M., Grbavčić Ž., Radojević Z., "Analysis of Moisture Transfer During the Drying of Clay Tiles with Particular Reference to an Estimation of the Time-Dependent Effective Diffusivity", Drying Technology, Vol. 32 No.7, pp.829-840, (2014). https://www.tandfonline.com/doi/abs/10.1080/07373937.2013.870194
[9] Mancuhan E., Ozen S., Sayan S., Sargut T.S., Experimental investigation of green brick shrinkage behavior with Bigot's curves, Drying Technology, Vol. 34 No.13,pp.1535-1545, (2016). https://www.tandfonline.com/doi/full/10.1080/07373937.2015.1135340
[10] Aungatichart P., Wadam S., Correlation between Bigoth and Ratzenberg drying sensitivity indices of red clay from Ratchaburi province (Thailand), Applied Clay Science, Vol.43 No.2, pp.182-185, (2009). https://doi.org/10.1016/j.clay.2008.08.001

Ref.:
Vasić, Miloš R.: *Estimation of the drying behaviour for different clay raw materials – drying sensitivity techniques review*
Építőanyag – Journal of Silicate Based and Composite Materials, Vol. 74, No. 3 (2022), 88–92. p.
https://doi.org/10.14382/epitoanyag-jsbcm.2022.14

A study on thermophysical properties of clay from Agbani: its assessment as potential walling material for naturally-cooled building design

Sunday Edet ETUK ▪ Department of Physics, University of Uyo, Uyo, Nigeria
Ubong Williams ROBERT ▪ Department of Physics, Akwa Ibom State University, Ikot Akpaden, Mkpat Enin, Nigeria
Okechukwu Ebuka AGBASI ▪ Department of Physics, Michael Okpara University of Agriculture, Umudike, Nigeria ▪ agbasi.okechukwu@gmail.com
Sunday Samuel EKPO ▪ Department of Physics, University of Uyo, Uyo, Nigeria

Érkezett: 2021. 10. 12. ▪ Received: 12. 10. 2021. ▪ https://doi.org/10.14382/epitoanyag-jsbcm.2022.15

Abstract

Thermophysical properties of clay sample obtained from Agbani in Enugu State, Nigeria, were investigated, analyzed and compared with similar properties reported for some walling and roofing materials, including clay samples from other locations for the purpose of establishing its suitability as walling material for the design of naturally-cooled building. Agbani clay sample exhibits bulk density value of (2111.4 ± 13.1) kgm^{-3}, specific heat capacity value of (1253.99 ± 2.03) J/kgK, thermal conductivity value of (0.1105 ± 0.0014) W/mK, thermal resistivity value of (9.05 ± 0.11) $W^{-1}mK$, thermal diffusivity value of (4.17 ± 0.06) x 10^{-8} m^2s^{-1}, and thermal absorptivity value of (29.52 ± 0.42) m^{-1}. The outcome of the comparison of the values obtained with values of similar properties reported for other walling materials evidences that Agbani clay is a better choice material for the design of naturally-cooled building.

Keywords: Agbani, bulk density, thermal conductivity, thermal diffusivity, specific heat capacity
Kulcsszavak: Agbani, térfogatsűrűség, hővezetőképesség, hődiffúzivitás, fajlagos hőkapacitás

Sunday E. ETUK
Principal Chief Technologist in the Department of Physics at University of Uyo, Uyo, Nigeria. Fellow of the Nigerian Institute of Science Laboratory Technology and Member of Governing Council, Nigeria Institute of Science Laboratory Technology. Author of more than 81 scientific Research Publications. His research interest, includes Instrumentation, Thermal physics, Material Science, Environmental Studies and Geophysics.

Ubong W. ROBERT
Academic Technologist at the Department of Physics, Akwa Ibom State University, Mkpat Enin, Nigeria. A specialist in instrumentation. His research interest includes measurement techniques, Electrical / Electronic materials, Environmental studies and Sustainable building / composite materials technology.

Okechukwu E. AGBASI
Researcher at the Department of Physics, Michael Okpara University of Agriculture, Umudike, Nigeria. His research interests include Groundwater Geophysics, Petrophysics, Environmental Physics and Material Science.

Sunday S. EKPO
Lecturer II in Department of Physics, University of Uyo, Uyo, Nigeria. A specialist in Biophysics and Medical Physics. Member of Nigerian Institute of Physics, member Nigerian Nuclear Society. Research interest in environmental /health, radiation protection and safety.

1. Introduction

Clay soil obtained from Agbani in Enugu State, Nigeria, is the material of interest in this regard. Clay is natural, soft earth plastic soil with high percentage of micro pores and highly known for water logging. It is easily molded when mixed with water, forming a sticky coherent mass. Clay is hard and brittle when dried, capable of becoming soft with addition of water, but remains harder when baked to a red heat without being no longer affected by action of water. Clay minerals are hydrous, comprising majorly of alumina, silica and water. Hence, complex alumino-silicates and sheet silicates are clay minerals. Clays form major components of soil. Lithified clay minerals form shale [1]. It is formed as a result of weathering and breaking down of rocks and minerals [2]. Clays are described in two different words, that is, a clay-sized particle and a clay mineral. While clay-sized particle composes of any mineral with diameter not greater than 1/256 mm, clay mineral is a small silicate minerals group having a sheet-silicate structure. Most often, sediments in the clay-sized range composition develops into clay minerals. However, this is not always the case [2].

Some known properties of clay minerals include microscopic diameter smaller than 0.002 mm, capacity to absorb water, ionic double layer, cation exchange capacity, increased number of charges owing to isomorphous replacement. It is flocculating and dispersing when in solution [1, 3, 4]. Uses of clay include but not limited to, ceramics, filler and surface coating for paper, bricks making, sewer pipes and drain tiles, cement making, production of refractories, paint making, insulation materials, removal of surface contamination, natural medicine and pelotherapy, export, face powder, polishing powders, lead pencils, glazes, porcelain, water treatment systems, shower trays, decorative concrete. Studies on clay samples got from some locations have been reported.

Recently, Robert et al [3] have reported on comparison of clay soils of different colors existing under the same conditions in a location. Ihaddadene et al [5] have reported on clay-based building material. Armijo et al [6] studied on thermal properties of mixture of clays with water for applications in pelotherapy. Babatunde and Adeyemo [7] studied influence of heavy metals on thermal conductivity of clay as building material. Etuk et al [8] reported on comparison of the thermal properties of clay samples as potential walling material for naturally-cooled building design. Fgaier [9] reported on thermal performance of unfired clay bricks used in construction in the North of France, whereas Ekpe and Akpabio [10] reported on comparison of the thermal properties of soil samples for a passively-cooled building design, among other reports. Yet, thermal properties of clay sample found in Agbani in Enugu State, Nigeria, has not been reported on. The aim of this study is to investigate some thermophysical properties of clay sample found at the Nigerian Law School premises located at Agbani, Enugu State, Nigeria, for the purpose of using it as a walling material for passively-cooled building design. Agbani is in Enugu State located between Latitudes 6.4497°N and Longitudes 3.4032°E. A model for forecasting variation of temperature with thickness of the clay soil sample will be proffered, employing the result of the investigation. The outcome of the investigation will likely reveal

the potentials and possible applications of the sample especially in solving some of the problems caused by the global warming.

2. Theory

Bulk density is a physical parameter of choice to be investigated. Bulk density, ρ, a very important physical parameter is mathematically defined as

$$\rho = \frac{M}{V} \quad (1)$$

where M = mass and V = bulk volume

In materials that are homogeneous as well as isotropic,

$$\frac{\partial^2 T}{\partial x^2} = \left(\frac{\rho c}{k}\right)\frac{\partial T}{\partial t} \quad (2)$$

is an expression for one-dimensional unsteady state heat conduction mathematical model.

The above equation can also be expressed as

$$\frac{\partial^2 T}{\partial x^2} = \left(\frac{1}{\lambda}\right)\frac{\partial T}{\partial t} \quad (3)$$

where λ signifies thermal diffusivity, mathematically defined as [11, 12]

$$\lambda = \frac{k}{\rho c} \quad (4)$$

where k denotes thermal conductivity and c is specific heat capacity.

Several elements decide soil temperature and solar radiation is the dominant determinant of it. It causes change in soil temperature when it is partly absorbed by soil. Robert et al [3], among other authors, express heat budget equation thus

Heat flow through the soil
= Heat absorbed from the atmosphere
+ Part of solar radiation absorbed – Re-emitted radiant energy

The heat balanced equation in one dimension gives

$$-k\left(\frac{\partial T}{\partial t}\right)_{x=0} = h\left(T_{atm} - T_{(x=0)}\right) + \alpha I - \epsilon \Delta R \quad (5)$$

where T represents soil temperature, h is heat transfer coefficient of the soil surface, T_{atm} is atmospheric air temperature, α is solar radiation absorptivity at the soil surface ($\alpha = \left(\frac{\omega}{2\lambda}\right)^{\frac{1}{2}}$), I being intensity of solar radiation, ε is long-wave emissivity of the soil surface, ΔR is the difference between the incident long wave radiation and the radiation emitted from the surface of the soil.

The solar temperature, T_s is given as

$$T_s = T_{atm} + \left(\alpha\, {}^{I}/_{h}\right) - \left(\epsilon \Delta R/_{h}\right) \quad (6)$$

The assumed form of general solution to one-dimensional heat conduction equation as given by several authors including [3, 10] is expressed as

$$T(x,t) = a_0 + \sum_{m=1}^{\infty}\{a_m exp[i(m\omega t + \alpha_m x]\} \quad (7)$$

resulting in

$$T(x,t) = a_0 + \sum_{m=1}^{\infty}\{a_m \exp(-\alpha_m x)\, Cos(m\omega t - \alpha_m x\} \quad (8)$$

as the real part of *Eq. 7*

where $\alpha_m = \left(\frac{m\omega\rho c}{2k}\right)^{\frac{1}{2}}(1-i)$ and $\omega = 2\pi/period$

The variation of soil temperature with depth with respect to periodic change of soil surface temperature can be predicted using the modified form of *Eq. (8)* given as

$$T(x,t) = T_m - A_s \exp(\alpha x)\, Cos\,\{\omega[(t-t_0) - (\alpha x)/\omega]\} \quad (9)$$

where x = depth or thickness of the soil, t = time of the day (in hours), t_0 = time of minimum temperature at the soil surface (in hours), A_s = daily temperature amplitude (in °C) at x=0. T_m is calculated from the hourly temperature average at the soil surface, T_{hss} (in °C) on 24-hour period thus

$$T_m = \sum_{m=1}^{24}\left(\frac{T_{ss}}{24}\right) \quad (10)$$

causing *Eq. 9* to be

$$T(x,t) = T_m - A_s \exp(-\alpha x)\, Cos\left\{\left(\frac{\pi}{12}\right)[(t-t_0) - (12\alpha x)/\pi]\right\} \quad (11)$$

3. Material and method

The main material used in this study was clay soil sample obtained from Agbani in Nkanu West Local Government Area of Enugu State, Nigeria, located between Latitudes 6.4495° N and Longitudes 3.4032° E.

3.1 Preparation of test sample

The clay sample was first subjected to sun-drying, as picked from the source (*Fig. 1*). The dry clay was pulverized and the existing stones removed, leaving behind a starch-like material free from large particle sizes. The sieved starch-like clay sample was divided into four parts by mass. Each portion of the sieved sample was wetted with clean water. The wetted sample proportions were molded differently using identical sized mold measuring 20.0 cm × 20.0 cm × 2.0 cm each. Each developed test sample was compacted to uniform thickness for 48 hours at room temperature using a laboratory-made compaction machine at 20 kN for simultaneous compression of the prepared samples in their respective mold.

3.2 Properties determination

Thermal conductivity, k was determined in triplicates, using three of the molded sun-dried, non-plastic and hard prepared samples. The standard procedure for measurement of thermal conductivity employing Heat Flow Meter (HFM 100 series) described elsewhere ASTM C518 [13], was adopted and followed for the determination of the thermal conductivity of the samples. Dry samples were used for the determination to eliminate the effect of redistribution of water that could emanate due to the influence of temperature gradient. The samples were then after cut into small bits. The mass of bits of each sample was weighed in triplicates with the aid of an electronic weighing balance, while Modified Water Displacement method was used to determine bulk density of each bit as described elsewhere [14]. Bulk density, ρ in each case was computed employing *Eq. (1)*. The specific heat capacity, c was also determined in each case by calorimetry method of mixture using temperature-cooling correction as described elsewhere [15, 16, 17, 18].

Thermal diffusivity, λ values of the respective sample as treated in triplicates were computed using their corresponding thermal conductivity value, bulk density value, and specific heat capacity value, with the aid *Eq. (4)*. Thermal absorptivity value, α for each sample treated also in triplicates was equally computed. It is expedient to mention here again for the purpose of clarity that each test in this study was carried out in triplicates, their mean values were calculated with associated standard error as seen tabulated in the table of results.

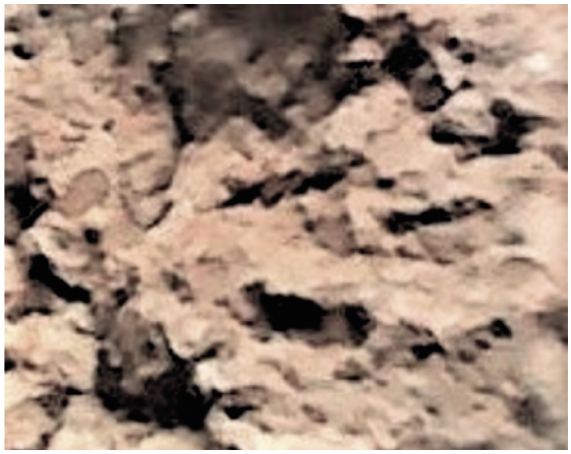

Fig. 1 Agbani clay soil used in the study
1. ábra A vizsgálatok során használt Agbani agyagos talaj

4. Results and discussion

Table 1 exhibits the measured values obtained for the bulk density, thermal conductivity, and specific heat capacity for the clay sample investigated taken in triplicates. *Table 2* shows the summary of the test results as well as summary of mean measured values and computed test results inclusive.

Trials	Bulk density, ρ (kg/m³)	Thermal conductivity, k (W/mK)	Specific heat capacity, c (J/kg/K)
1	2094.5	0.1089	1251.29
2	2133.7	0.1132	1257.39
3	2105.9	0.1093	1253.28
Mean ± std. error	2111.4 ± 13.1	0.1105 ± 0.0014	1253.99 ± 2.03

Table 1 Measured values obtained
1. táblázat A vizsgálati eredmények

Properties investigated	Values obtained
Bulk density, $\rho\ (kg/m^3)$	2111.4 ± 13.1
Specific heat capacity, $c\ (J/kg/K)$	1253.99 ± 2.03
Thermal conductivity, $k\ (W/mK)$	0.1105 ± 0.0014
Thermal resistivity, $r\ (W^{-1}mK)$	9.05 ± 0.11
Thermal diffusivity, $\lambda\ (10^{-8}m^2/s)$	4.17 ± 0.06
Thermal absorptivity, $\alpha\ (m^{-1})$	29.52 ± 0.42

Table 2 Summary of the test results
2. táblázat A vizsgálati eredmények összefoglalása

The mean bulk density value for our sample recorded in *Table 2* is compared with the bulk density values reported by Robert et al [3] for clay soils with pink and yellow colors as 2127.372 ± 1.465 kg/m³ and 2023.737 ± 1.435 kg/m³ respectively. Our sample's bulk density value is greater than the values reported for Terra-cotta, kaolinatic, stoneware, ball, kaolin, and earth-ware clays [8]. This suggests that our sample has pore size similar to the pink and yellow colored clay, but percentage pore size higher than the clay samples reported by Etuk et al [8]. That may plausibly be due to differences in particle sizes of the samples.

The mean specific heat capacity value obtained for our sample is far less than the values reported by Robert et al [3] for pink clay (2007.795 ± 1.796 J/kg/K) and yellow clay (1800.248 ± 1.981 J/kg/K) samples obtained from same topographic relief in Uyo, Akwa Ibom State, Nigeria. Ours is equally less than the values reported by Etuk et al [8] for Terra-cotta, kaolinatic, stoneware, ball, and earth-ware clays as 2.19 × 10³ J/kg/K, 1.70 × 10³ J/kg/K, 2.94 × 10³ J/kg/K, 1.68 × 10³ J/kg/K, and 1.64 × 10³ J/kg/K respectively. However, it is slightly higher than the value reported by Etuk et al [8] for kaolin as 1.19 × 10³ J/kg/K. The differences may be due to the variations in the alumina as well as oxidized ferric iron oxide contents of the samples. This assumption follows the fact that constituents of soil determine the specific heat capacity of the soil. Considering the volumetric heat capacity value (product of the value of bulk density value and specific heat capacity value) recorded for our sample, it can be inferred that the mean value is about 2.648 MJ/m³/K. This signifies that 2.648 MJ of heat would be required to change the temperature of a unit volume of clay sample obtained from Agbani by one Kelvin whereas the specific heat capacity value recorded for the sample is the amount of heat required to change the temperature of its unit mass by one Kelvin.

Considering the mean thermal conductivity value recorded for the test clay sample being lower than the values reported by Robert et al [3] and Etuk et al [8] ranging between 0.2237 and 0.463 W/mK for pink, yellow, Terra-cotta, Kaolinatic, stoneware, ball, kaolin, and earth-ware clays obtained from Uyo, Idim Afia in Eket, Mkpat Enin, Oruk Anam, Ukpom Edem Inyang in Oruk Anam, Itam in Itu and Ikot Akpan Udo in Ikot Abasi respectively, it means that more dead air spaces exist in the test sample obtained from Agbani than others. This gives rise to a high value of thermal resistivity (inverse of thermal conductivity). Hence, thermal energy exchange by process of conduction between the adjacent particles would be greatly retarded in the case of clay sample from Agbani, which is the test sample in this work. This is supported by the fact that still air is a poor heat conductor; hence, the more dead air space a soil has, the more it can retard heat flow through its thickness as well as its cross-section. 0.1105 ± 0.0014 W/mK is the recorded thermal conductivity value for the test clay sample. This value is within the recommended range for good construction material [19].

The thermal diffusivity value shown by the result in *Table 2* is (4.17 ± 0.06) × 10⁻⁸ m²/s. This value, when compared with the values of (6.139 ± 0.006) × 10⁻⁸ m²/s to (6.413 ± 0.014) × 10⁻⁸ m²/s and 0.73 × 10⁻⁷ m²/s to 1.74 × 10⁻⁷ m²/s as reported by Robert et al [3] and Etuk et al [8] respectively for clay samples from other locations, shows that clay sample obtained from Agbani has a lower value of thermal diffusivity. Hence, clay sample from Agbani would respond more sluggishly to a change in temperature than the ones reported by Robert et al [3] and Etuk et al [8]. With this, it is obvious that it would take a longer time for heat to be spread within the test sample obtained from Agbani than other clay samples reported on as stated above. The fact is that the test sample is characterized by a lower thermal conductivity value than those clay samples earlier reported by those other researchers above. This can equally be explained in terms of the linear relationship that exists between thermal conductivity and thermal diffusivity as evident in the mathematical model expressed here in *Eq. (4)*.

Considering thermal absorptivity, the test sample exhibits a mean value of 29.52 ± 0.42 m^{-1}. This indicates its ability to absorb thermal radiation which equals its homogeneous layer internal absorptance. Solar radiation that gets to soil and is absorbed by the soil determines the soil temperature variation. A model for predicting soil temperature variation with thickness, x at any given time for the test clay sample is derived by substituting the mean value of thermal absorptivity into *Eq. (11)*, thus yielding

$$T(x,t) = T_m - A_s \exp(-29.52x)\, Cos\{(0.262)[(t - t_0) - (112.74x)]\} \quad (12)$$

More so, comparing the results of thermal properties recorded for the clay sample tested with the range of values reported by Oktay et al [20], Ajibola and Onabanjo [21] for some established walling and roofing materials shows thermal conductivity values for briquette, brick, blockbims, concrete, plaster, hardwood, plywood, woodchip board, glass to be within the range 0.124 W/mK to 1.370 W/mK with specific heat capacity values ranging from 840 J/kgK to 1047 J/kgK and thermal diffusivity values ranging from 2.99×10^{-7} m^2/s to 7.50×10^{-7} m^2/s for briquette, brick, blockbims, concrete, and plaster [20]. The thermal conductivity values of brick, Portland cement, asbestos mill board, asbestos (loosely packed) are reported to be 0.69 W/mK, 0.29 W/mK, 0.14 W/mK, 0.15 W/mK respectively [22]. It shows that the values recorded for Agbani clay sample would make for a more preferred walling material for a naturally-cooled building design over some already known and commonly used walling materials.

5. Conclusions

A very close observation has shown that clay sample obtained from Agbani in Enugu State, Nigeria exhibits a low thermal conductivity value, hence a higher thermal resistivity than most of the reported clay samples and other materials commonly employed as walling materials for building design. Not only that, its mean specific heat capacity value (approximately 1254 J/kgK) is greater than 840 J/kgK to 1047 J/kgK possessed by some walling materials used for building purposes. The studied clay exhibited high mean thermal resistivity value (9.05 ± 0.11) W^{-1}mK and value (4.17 x 10^{-8} m^2s^{-1}). These are good evidences to conclude that Agbani clay would make a better walling material over some established walling materials for naturally-cooled building design.

References

[1] Carlson, D. H., Plummer, C. C., McGeary, D. (2006) Physical Geology: Earth Revealed. McGraw Hill, Boston, pp. 231, 343

[2] Hillier, S. (1995) Erosion, sedimentation and sedimentary origin of clays, in: Velde B (ed) Origin and Mineralogy of clays. New York, Springer-Verlag, p. 162 – 219

[3] Robert, U. W., Etuk, S. E., Agbasi, O. E., Umoren, G. P. (2020) Comparison of clay soils of different colors existing under the same conditions in a location. Imam Journal of Applied Sciences, vol. 5, no. 2, pp. 68 – 73, https://doi.org/10.4103/ijas.ijas_35_19

[4] Velde, B. (1995) Composition and Mineralogy of clay minerals, in: Velde B (ed) Origin and Mineralogy of clays. New York, Springer-Verlag, pp. 8 – 41

[5] Ihaddadene, N., Ihaddadene, R., Betka, A., Logerais, P., Delaleux, F., Riou, O. (2019) Study of the thermal conductivity of a clay-based building material. IAPE 19 Conference Paper. At: Oxford UK

[6] Armijo, F., Maraver, F., Pozo, M., Carrelero, M. I., Armijo, R. (2016) Thermal behavior of clays and clay-water mixtures for pelotherapy. Applied Clay Science, vol. 126, pp. 50 – 56

[7] Babatunde, G. E., Adeyemo, A. J. (2019) Influence of heavy metals on thermal conductivity of clay as a building material. Egyptian Journal of Basic and Applied Sciences, vol. 6, no. 1, pp. 1 – 5

[8] Etuk, S. E., Akpabio, I. O., Udoh, E. M. (2003) Comparison of the thermal properties of clay soil samples as potential walling material for naturally cooled building design. Journal of Environmental Science, vol. 15, pp. 65 – 68

[9] Fgaier, F. E., Lafhaj, Z., Brachelet, F., Antczak, E., Chapiseau, C. (2015) Thermal performance of unfired clay bricks used in construction in the North of France: Case study, ScienceDirect. www.elsevier.com/locate/cscm

[10] Ekpe, S. D., Akpabio, G. T. (1994) Comparison of the thermal properties of soil samples for passively cooled building design. Turkish Journal of Physics, vol. 18, pp. 117 – 122

[11] Incropeda, F. P., Witt, D. (1990) Fundamentals of Heat and Mass Transfer, 3rd edn., John Wiley and Sons, New York, pp. 4, 45 – 51, A7, A9, A10, A11, A13

[12] Etuk, S. E., Akpabio, L. E., Akpabio, K. E. (2005) Determination of thermal properties of Cocos nucifera trunk for predicting temperature variation with its thickness. Arabian Journal for Science and Engineering, vol. 30, no. 1, pp. 121- 126

[13] ASTM C518. (2017) Standard Test Method for steady state thermal transmission properties by means of the Heat Flow Meter Apparatus, West Conshohocken, PA. ASTM International.

[14] Robert, U. W., Etuk, S. E., Agbasi, O. E. (2019a) Modified Water Displacement Method and its use for determination of bulk density of porous materials. Journal of Renewable Energy and Mechanics, vol. 1, no. 1, pp. 1 – 16

[15] Okeke, P. N., Osuwa, J. C., Menkiti, A. I., Ofoegbu, C. O., Okeke, C. E., Emereoke, H. U. (1991) /Nigerian University Physics Series 2, 2nd edn., Ibadan, Nigeria. Physics Writers Series Creation, pp. 222 – 232

[16] Tyler, F. A. (1971) Laboratory manual of Physics, 4th edn., London. Edward Rnold, pp. 118 – 119

[17] Robert, U. W., Etuk, S. E., Umoren, G. P., Agbasi, O. E. (2019b) Assessment of Thermal and Mechanical Properties of composite board produced from coconut (Cocos nucifera) husks, waste newspapers, and cassava starch. International Journal of Thermophysics, vol. 40, no. 9, p. 83

[18] Robert, U. W., Etuk, S. E., Agbasi, O. E., Umoren, G. P., Inyang, N. J. (2021) Investigation of thermophysical and mechanical properties of board produced from coconut (Cocos nucifera) leaflet. Environmental Technology and Innovation, vol. 24, pp. 1 – 9

[19] Twidell, J., Weir, T. (1990) Renewable Energy Resources, London. E and FN Spon, p. 416 – 418

[20] Oktay, H., Argunhan, Z., Yumrutas, R., Isik, M. Z., Budak, N. (2016) An Investigation of the influence of Thermophysical Properties of Multilayer Walls and Roofs on the Dynamic Thermal Characteristics. Mugla Journal of Science and Technology, vol. 2, no. 1, pp. 48 – 54

[21] Ajibola, K., Onabanjo, B.O. (1995) Investigation of Cocos nucifera as a potential insulator for buildings. Renewable Energy, vol. 6, no. 1, pp. 81 – 84.

[22] Engineering Toolbox (2001). http://www.engineeringtoolbox.com/thermal-conductivity-d_429.html

Ref.:
Etuk, Sunday Edet– **Robert**, Ubong Williams– **Agbasi**, Okechukwu Ebuka– **Ekpo**, Sunday Samuel: *A study on thermophysical properties of clay from Agbani: its assessment as potential walling material for naturally-cooled building design*
Építőanyag – Journal of Silicate Based and Composite Materials, Vol. 74, No. 3 (2022), 93–96. p.
https://doi.org/10.14382/epitoanyag-jsbcm.2022.15

Performance of self-compacting concrete in hot arid climate

Hachemi BENADDI ▪ Civil Engineering and Hydraulic Department, University Mohamed Khider of Biskra, Algeria ▪ hachembenmoh@gmail.com
Bouzidi MEZGHICHE ▪ Civil Engineering and Hydraulic Department, University Mohamed Khider of Biskra, Algeria ▪ mezghichebm@yahoo.fr
Mohamed SALHI ▪ Civil Engineering Department, University of Relizane, Bourmadia, Algeria ▪ salhi8@yahoo.fr
Abdecharif BOUMAZA ▪ Chemistry Department, University Abbes Laghrour of Khenchela, Algeria ▪ boumaza.abdecharif@gmail.com

Érkezett: 2021. 10. 12. ▪ Received: 12. 10. 2021. ▪ https://doi.org/10.14382/epitoanyag-jsbcm.2022.16

Abstract

This article analyzes the effects of the hot climate on the fresh and hardened properties and the durability of self-compacting concrete (SCC) and ordinary concrete (OC). The experimental program makes it possible to produce in the laboratory three concretes (SCC1), (SCC2) and an ordinary concrete (OC). In order to evaluate rheological tests such as: spreading, L-box and sieve stability immediately after the end of mixing and to measure the maintenance of self-placing, compressive strength. The samples of concrete were stored in water for an initial curing period of 7 days, before being exposed to the hot and dry natural climate in a desert region of Biskra for up to 120 days. Durability against sulphate and acid attack was assessed by curing concrete samples in air for 28 days, followed by full immersion in H_2SO_4 and Na_2SO_4 solutions for 180 days. The results showed the positive effect of limestone filler on the fluidity of SCC in a hot climate just after mixing, on the other hand, the compressive strength is improved at young age and poor in the long term. Concrete SCC2 containing limestone seems to be the least attacking by sulfuric acid compared to SCC1 without substitution and ordinary concrete.

Keywords: rheology, compressive strength, durability, sulphate attack, X-ray
Kulcsszavak: reológia, nyomószilárdság, tartósság, szulfáttámadás, röntgen

Hachemi BENADDI
Assistant Professor, LRGC Institute of Civil and Hydraulic Engineering, University of Biskra, Algeria. Research interests: Self-compacting concrete technology, Building Materials.

Bouzidi MEZGHICHE
Doctor at the Institute of civil and hydraulic engineering, University of Biskra, Algeria. Research interests: Building materials.

Mohamed SALHI
Doctor at the Faculty of Science and Technology, Civil Engineering and Public works Department, University of Relizane, Algeria. Research interests: Building Materials, Rheology, Mechanical and Durability properties of Self-compacting concrete, Waste valorization.

Abdecharif BOUMAZA
Professor at the Faculty of Science and Technologies, Department of Material Sciences, Abbes Laghrour, University Khenchela, Algeria. Research interests: Solid State Physics Materials and Metallurgy.

1. Introduction

Algeria is a country in the subtropical zone of North Africa, apart from the northern fringe with a Mediterranean climate; more than 85% of its area is characterized by a semi-arid climate on the highlands and the centre of the country, and an arid climate as soon as one crosses the chain of the Saharan Atlas. That is to say, a hot and a dry climate which is defined any combination of high air temperature, low relative humidity, wind speed and solar radiation, which tend to affect the quality of fresh or hardened concrete [1].

The analysis of climatic data from the Biskra region as an example of an arid zone with a hot and a dry climate shows that the summer period is the hottest with a temperature exceeding 47 °C at 11:00 am in the month of July 2019 (*Fig. 1*) [2].

The average daily incident shortwave solar radiation experiences considerable seasonal variation throughout the year. The daily-obtained energy on a horizontal surface of 1 m² is about 2263kWh/m²/year in the south of Algeria country [3]. For the period 2000-2014, these data undoubtedly explain the severe climatic conditions which exceed the tolerances that can alter the quality and the rheological behavior of the concrete in the fresh state such as the rapid loss of fluidity over time, the increase in compressive strength to young ages, and the adverse consequences on the mechanical properties and durability of concrete structures in the long term.

Several studies have been carried out on vibrated or self-compacting concrete fresh. Ana et al. [4] used two SCCs containing a binder (OPC + lime plaster) and a PCP superplasticizer in simulated hot weather conditions, and found that when the temperature increased from 20 to 50 °C, the additions of additional water or superplasticizer was needed to maintain constant self-compacting until the end of mixing. Ghafoori et al. [5] reported that the deterioration in spreading immediately after mixing appears above the temperature of 28 °C for three compositions only vary by the dosages of superplasticizer and viscosity agent. [6] found that raising the ambient temperature from 22 to 32 °C contributes to raising that of vibrated concrete and causes a loss of slump regardless of the consistency range studied.

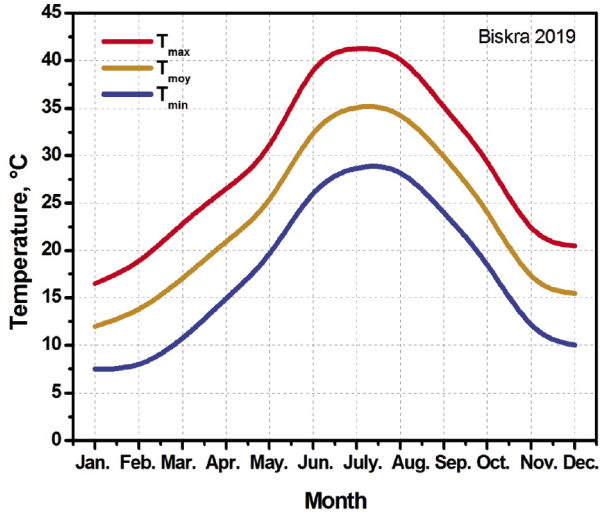

Fig. 1 Temperature in 2019 at Biskra (Infoclimat2019)
1. ábra Hőmérséklet 2019-ben Biskrán (Infoclimat2019)

As for a SCC, according to previous study [7], when the G/S ratio close to 1, the flow properties are not strongly altered by raising the initial temperature up to 30 minutes after mixing. Cygan et al. [8] have reported that the increased rate of hydration caused by the rise in temperature leads to deterioration of the workability of concrete. However, in the hardened state, Abd-ElAziz et al. [9] found that the compressive strength at the age of 90 days drops considerably for concretes stored in hot air. The study conducted by Salhi et al. [10] revealed that the compressive strength is strongly influenced by the curing method, seven days of initial curing in water followed by a ripening in a hot climate was the optimal duration for a better development of compressive strength.

Tao et al. [11] observed that the hot compressive strength of SCC decreases with increasing temperature. Kodur et al. [12] found that the increase in the temperature of the SCC in the period 7-90 days favored the compressive strength from 46-72 MPa. Pichler et al. [13] studied the Influence of curing temperature dependent microstructure on early-age concrete strength development and found that the higher the temperature, the lower the resistance which is due to the increase of a wider porous network, as a result of a coarser microstructural development, the hydrates being denser at high temperature and more heterogeneously distributed.

Nehdi et al. [14] have disclosed that the hot climate leads to premature desiccation which delays or completely stops the hydration reaction of the cement, thus influencing the compressive strength. Concerning the durability of concretes against sulphate attack, which is an issue for many studies, as sulphate attack can significantly deteriorate concrete in a relatively short period of time 10 to 15 years (GCI, 714).

In 1989, a survey by the Organization for Economic Cooperation and Development (OECD) indicates that sulphate attacks is the second most common cause of degradation after steel corrosion with the risk of an internal sulphate reactions due to an increase in temperature from 60 °C to 70 °C [15]. However, [16] described the coupling between temperature and external sulphate attack on cementitious materials and observed that no damage occurred in samples exposed to the sulphate solution at 50 °C. Denecker et al. [17] reported that sodium sulphates (Na_2SO_4) are accepted as the most destructive salts for porous materials. Mohsen et al. [18] found that under severe Na_2SO_4 solution conditions, the SCC made from marble and tile waste has a lower mass gain than vibrated concretes. Salhi et al. [7] found that with W/B=0.38 and 0.44 of different SCC formulations of crystallization-induced expansions by increasing the compactness of the concrete which leads to an increase in compressive strength at the micropore level in the first stage; however in the second stage new cracks begin to appear which cause a decrease in this strength. Khalifa et al. [19] reported that the lowest sulphate resistance in the same SCC cement is that of the concrete with a ratio of W/C=0.59, which degrades faster and more significantly than that of concrete with a ratio of W/C=0.49. Chiraz et al. [20] found that the loss of compressive strength of specimens immersed in H_2SO_4 is greater than that of specimens immersed in Na_2SO_4. Senhadji et al. [21] found that the substitution of cement with limestone fillers for mortars increases chemical resistance against attack by 5% H_2SO_4, and the loss of mass is lower than mortars without additions.

This work involves studying the concrete behavior under real conditions of hot and dry climate (Biskra area). It studied the effect of high ambient temperature over 35 °C on the fresh state characteristics of self-compacting concrete (spreading-deformability-stability) and slump for vibrated concrete. Furthermore, the compressive strength in different ages of these concretes subjected to solar radiation and without any curing applied has also investigated. This is the case of our worksites in the south of Algeria (Biskra), which raises many questions, especially about concreting during the summer period, as well as durability in aggressive environments of sulphate attacks, by applying accelerated aggression by immersing the samples in solutions of sulphuric acid H_2SO_4 and sodium sulphate Na_2SO_4 with concentrations of 5%, i.e. 50 ml/l and 50 g/l, respectively, at an ambient temperature above 35 °C.

2. Experimental

2.1 Materials used

For all the experiments, only one type of cement (CPJ-CEM II / 42.5A) from the GIGA group of Ain-Touta cement plant was used. Its physical, chemical and mineralogical properties communicated by the producer have shown in the *Table 1* and *2*. The crushed limestone is available in the quarries of Ain-Touta. According to our laboratory analysis, the crushed limestone of the following properties: Absolute density = 2.76, bulk density = 1.09 and specific surface = 3070 cm^2/g. The sand used in this investigation is a local siliceous sand of granular class 0/5 mm taken from Oued Ittel 85 km south of Biskra. *Table 3* presents the physical properties of this sand. There is only one type of gravel (7/15) was used to fabricate self-consolidating concrete. Whereas, the types of (7/15) and (15/25) (*Fig. 2*) were used for the preparation of vibrated concrete. Crushed gravel and limestone in nature were brought from AinTuta sediments in Batna city (*Table 4*). The superplasticizer "MEDAFLOW30" is an adjuvant produced by the company "GRANITEX", in light brown liquid form which is based on Pol carboxylates. According to the manufacturer, the physical properties of the superplasticizer are shown in *Table 5*. It has used drinking water from the tap of the public network of Biskra city with a quality conforming to the standard P18-303.

Chemical compositions (%)									
CaO	SiO_2	Al_2O_3	Fe_2O_3	MgO	SO_3	Na_2O	K_2O	Loss on fire	Insoluble Residue
61.37	22.28	4.56	3.88	1.40	1.72	0.06	0.33	3.71	3.29
Mineralogical compositions (%)									
C_3S		C_2S			C_3A			C_4AF	
59.2		14.1			6.1			11.4	

Table 1 Chemical and mineralogical properties of the cement used
1. táblázat A felhasznált cement kémiai és ásványtani tulajdonságai

Physical properties	Values
Absolute density	3.1
Apparent density	1.09
Blaine specific surface area (cm^2/g)	3775
Normal consistency (%H_2O)	25.6
Start of setting	171
End of setting	232
Hot expansion (mm)	1.80

Table 2 Physical properties of the cement used
2. táblázat A felhasznált cement fizikai tulajdonságai

Physical properties	Values
Absolute density	2.56
Apparent density	1.54
Fineness modulus	2.54
Visual sand equivalent	78.32
Sand equivalent per piston	73

Table 3 Physical properties of the sand used
3. táblázat A felhasznált homok fizikai tulajdonságai

Physical properties	Gravel 15/25	Gravel 7/15
Absolute density	2.62	2.61
Apparent density	1.255	1.283
Coefficient of absorption (%)	0.64	0.60
Porosity (%)	0.96	0.56
Los Angeles coefficient (%)	26	26

Table 4 Physical characteristics of the gravel used
4. táblázat A felhasznált durva adalékanyag fizikai jellemzői

Physical properties	Values
Aspect	Liquid
Color	Light brown
PH	6-6.5
Density	1.07
Chlorine content	Less than 0.1g/l
Dry extract	30%

Table 5 Physical properties of the superplasticizer used
5. táblázat Az alkalmazott folyósítószer fizikai tulajdonságai

2.2 Mixtures and formulations

The formulation used in this study is conformed to the guide [22], which provided guidelines and proposed a typical range of quantities of the main constituents in SCC. These guidelines are summarized in the mass ratio G/S close to 1 unity, to the volume of the paste which must be from 330-400 l/m^3. In addition, the total quantity of binder (cement + addition) varies from 400 to 600 kg/m^3. Furthermore, the dosage of the superplasticizer must not exceed the dosage of saturation. On the basis of these directives, it proceeded to several preliminary formulations in order to optimize and characterize the SCC which meets the criteria and recommendations in the fresh state of the [23]. 100% of cement concrete was synthesized, and then limestone fillers (24.73%) was replaced part of the cement.

Dreux-Gorisse method [24] was used to synthesis an ordinary concrete. The compositions of the three concretes are given in *Table 6*.

After the tests in the fresh state, cubic pieces of dimensions 10×10×10 cm^3, were made in molds previously oiled covered with a plastic film in order to avoid any type of evaporation. These samples were kept under shelter at an ambient temperature over 35 °C and relative humidity between 11 and 28% until demoulding after 24 hours. The cubic pieces are affected directly in the middle of the open air of the hot and dry climate under the sun's rays, up to the crushing age of 7, 14, 28 and 120 days to study the compressive strength. To study the durability against sulphate attacks, a series of specimens (after 28 days) were immersed in three different accelerated ageing environments in order to follow the effect of sulphate attacks: solution containing 5% sodium sulphate Na_2SO_4, solution containing 5% of sulphuric acid H_2SO_4, fresh water as a witness.

To keep the pH of the sulphate solution between 6 and 8, the method of Mehta [25] was adopted which recommended the correction of the solution already used by daily adding a quantity (0.1% H_2SO_4) of acid sulfuric during the first weeks of the test, then it becomes weekly. The solutions will be renewed every month.

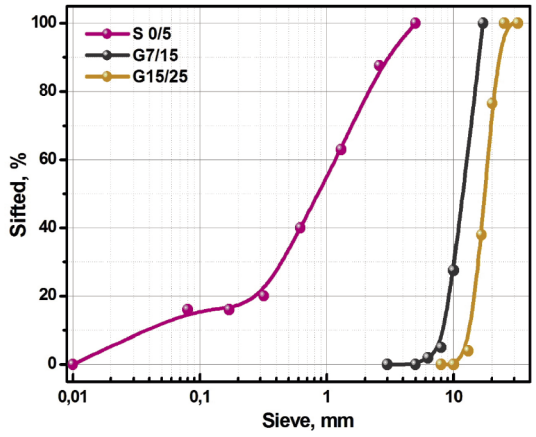

Fig. 2 Particle size curve of the gravel used
2. ábra A felhasznált durva adalékanyag szemeloszlás görbéje

3. Results and discussions

3.1 Effect of climate temperature on the fresh state of SCC

The behavior of concrete in an arid climate (hot and dry) is very complex and depends on several factors. Various studies simulated in the laboratories were carried out but far from the real conditions of the sites. The characterization tests in the fresh state to test the workability according to [23] are: Slump flow test, L-box test and Sieve stability.

For vibrated concrete, subsidence is measured at the Abrams cone (according to the specifications of EN 206-1) [26].

Maintaining workability which is important factor for all concretes, it is essentially altered by the increase of ambient temperature, which leads to the increase in temperature of the fresh concrete. *Fig. 3* shows that up to 25 minutes, the SCC

Type of concrete	W/B	Cement kg/m^3	L.fillers kg/m^3	Sand 0/5 kg/m^3	Gravel 7/15 kg/m^3	Gravel 15/25 kg/m^3	Water l	Sp% kg/m^3	G/S
SCC1	0.48	465	00	741.46	804	00	220.16	4.65	1.08
SCC2	0.48	350	115	741.46	804	00	220.16	4.65	1.08
OC	0.55	350	00	697	395	757	192.5	00	1.65

Table 6 Composition of the synthesized concretes
6. táblázat A betonkeverékek összetétele

at an ambient temperature above 35 °C and relative humidity between 11 and 28% retains its self-compaction. It can be seen that the spread decreases from 76 cm after 5 minutes to 65 cm after 25 minutes of mixing, and a reduced filling rate from 0.88 after 5 minutes to 0.81 after 25 minutes of mixing. At the same time, the stability rate becomes 7.5% at 25 minutes after mixing. These results are very consistent with the literature [27, 28]. These studies reported that up to 30 minutes after mixing, the flow properties are not strongly altered with the increase of the initial temperature, especially for the mixture with a G/S ratio close to 1.

Fig. 3 shows the effect of temperature on the workability of self-compacting concrete. It is clear to observe that the high ambient temperature causes an excessive loss of sag, which is canceled out at 65 minutes after mixing. This loss is due to a rapid acceleration of hydration and evaporation of water which consistent previous studies [6]. In these investigations it was found that the rise in the ambient temperature of 22 to 32 °C contributes to raising that of the concrete and causes a loss of slump regardless of the range of the consistency studied.

The effect of calcareous fillers on the rheology of SCC is very significant. Numerous researches have proven that fine limestone increases the stability and workability of fresh SCC [16], due to the incorporation participates in its behavior to obtain self-compacting more easily.

Immediately after mixing, workability tests showed the positive and beneficial effect of lime fillers on the fluidity and rheology of SCC. The spreading test records a slight increase for SCC2 containing limestone fillers comparable to SCC1 100% Cement (78 cm for SCC2 against 76cm for SCC1); the same for the tests of deformability and sieve stability, the results are consistent with several studies [16, 29, 30]. However, at 25 minutes after mixing, the loss of fluidity of SCC2 containing limestone fillers becomes more noticeable and very rapid as shown in *Fig. 3*. This loss of fluidity may be due to the calcareous nature of the fillers, which requires a request for water or super plasticizer to maintain its fluidity. Moreover, the effect of limestone fillers which improves the rheological properties of SCC and increases their stability depends on several factors such as fineness which strongly influences the flow [31] as well as the nature and quantity [32].

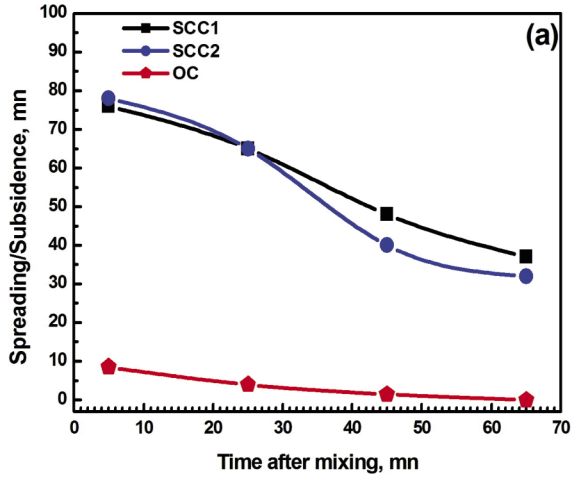

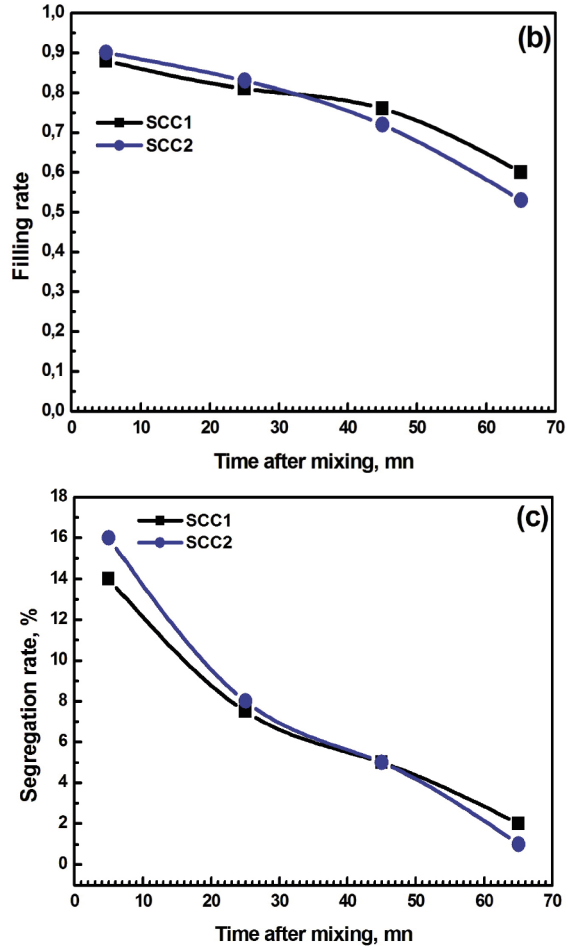

Fig. 3 Effect of the temperature on the workability of self-compacting concrete: (a) spread/sag, (b) deformability, and (c) stability
3. ábra A hőmérséklet hatása az öntömörödő beton megmunkálhatóságára: (a) terjedés/süllyedés, (b) deformálhatóság és (c) stabilitás

3.2 Effect of climate temperature on compressive strength of SCC

In the early days, as shown in *Fig. 4*, all the concretes developed very high compressive strengths such as SCC1 at seven days its strength reached 86.79% of the strength at 28 days. SCC2 contain limestone fillers reach 81.08% in resistance while the OC registered 82.5% in 28-day compressive strength. These results explain the effect of high temperature in the early days on the hydration reaction which leads to a rapid change in compressive strength. At young age, the higher the temperature the faster the development of compressive strength.

In the long term, the temperature plays a detrimental role on the mechanical behavior of the concrete, at 120 days we recorded a drop of 9.43% in the 28-day strength of SCC1 containing 100% cement, 5.40% for SCC2 containing 24.73% of limestone fillers and 7.5% for vibrated concrete. This is due to a coarser microstructural development, the hydrates (in particular the C-S-H) being dense at high temperature and distributed in a more heterogeneous manner; thus allowing the development of a larger porous network at the origin of the loss of resistance. At the same age, in all the concretes, one notices the favoring of SCC1 containing 100% cement, which has shown good resistant values comparable to SCC2 containing

24.73% of fillers and vibrated concrete due to the effect of the composition, which plays a primary role in the development of compressive strength. The SCC2 recorded poor strengths and lower than those of SCC1 100% cement, and closer to that of vibrated concrete in all ages, perhaps it is the fineness (less than that of cement) and the quantity substituted (24.73%) of the fillers used which are the reason of these resistant results.

Soufiane et al. [33] reported that the substitution of part of the Portland cement by limestone fillers is the origin of a decreasing of compressive strengths. Whereas, [34] found that the tests of the compressive strength on cubic specimens show an increase until a replacement of 20% after which the resistance begins to decrease. [35] Found that the compressive strength of high performance SCC decreases by 20% of cement substitution. Taoufik et al. [36] (disclosed that for superplasticized concrete (SCC), a quantity of 60 to 80 kg/m^3 makes it possible to increase the compactness and significantly improve the mechanical performance of the concrete. Shamir et al. [37] disclosed the amount of 30% substitution of mineral additions in mortars is optimal, beyond which the compressive strength begins to drop.

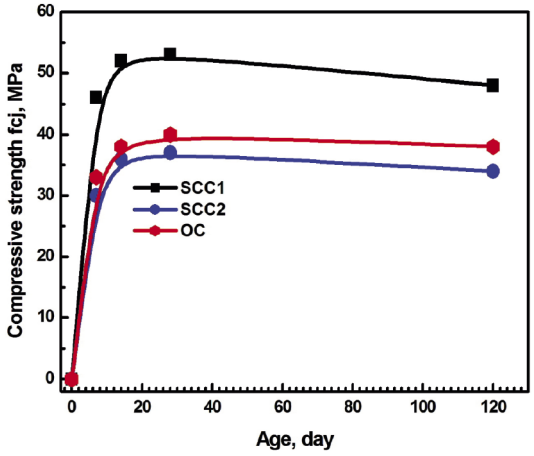

Fig. 4 Effect of the temperature on compressive strength of SCC
4. ábra A hőmérséklet hatása az öntömörödő beton nyomószilárdságára

3.3 Study of durability in the face of sulphate attacks

After 24 weeks of immersing of the samples in the various environments, visual inspection reveals the following (*Fig. 5*): in fresh water no changes or degradation on the samples; in the Na_2SO_4 solution, a slight yellowish layer is formed on the surface of the specimens; in the H_2SO_4 solution formation of a white layer on the surface and deterioration of the corners and edges of the specimens.

The variation in the mass of each specimen is calculated from the following equation:

$$VM=\left[\frac{M_0-M_i}{M_0}\right]\times 100\% \quad (1)$$

With VM: variation of the mass in (%);

M0: the mass of the specimen before exposure to media attack in (grams);

M_i (i = 1, 2, 3, ..., 24): the mass after 1, 2, ..., 24 weeks of attack in (grams).

After immersion in a solution of 5%Na_2SO_4 | *After immersion in a solution of 5%H_2SO_4* | *After immersion in fresh water*

Fig. 5 State of the samples after 24 weeks of immersion in the different environments
5. ábra A minták állapota 24 hetes tárolás után a különböző közegekben

The kinetic of mass gain of different concretes submerged in fresh (sweet) water according to *Fig. 6a* is the same. The reference is the last measurement before immersion. After the first week of immersion, the variation becomes stationary for the three concretes with a slight superiority of SCC1 and SCC2, this superiority is perhaps due to the porous structure of self-compacting concretes in a hot climate comparable to ordinary concrete.

The variation in the mass of different concretes immersed in the sodium sulphate solution at a concentration of 5% is shown in *Fig. 6b*. A gain in mass was observed for all concretes as a function of immersion time. Firstly, it observed a rapid increase in mass gain during the first six weeks for all concretes up to 4.7% for SCC1 cement compared to the last measurement before immersion, 5.2% for SCC2 containing limestone fillers and 5.1% for ordinary vibrated concrete. Later, the growth becomes slow where we recorded after 24 weeks of immersion, a mass setting of 5.5% for SCC1, 7.6% for SCC2 and 6.4% for ordinary vibrated concrete; these results coincide with the results found by [18, 38]. This increase in mass is explained by the absorption of water and the penetration of SO_4^{2-} ions into the capillary pores of the samples. A slight increase in mass gain has been observed for SCC2 is due to the presence of the calcareous fillers which increase the porosity and consequently the penetration of sulphates [32, 39]. Sulphate ions react in an aqueous medium with Portlandite $Ca(OH)_2$ to form gypsum (calcium sulphate) according to the following reaction :

$$Ca(OH)_2+Na_2SO_4+2H_2O \longrightarrow Ca(SO_4).2H_2O+2NaOH \quad (2)$$

This gypsum produced by the decalcification of Portlandite participates in the formation of secondary ettringite, either from tricalcium aluminate C_3A, present in the composition of the clinker by the following reaction:

$$C_3A+3Ca(SO_4)2H_2O+26H_2O \longrightarrow C_3A.3Ca(SO_4).32H_2O \quad (3)$$

Or from hydrated calcium mono-sulfano-aluminate according to the following reaction:

$$CaSO_4.12H_2O+2Ca(OH)_2+2SO_4+12H_2O \longrightarrow C_3A.3Ca(SO_4).32H_2O \quad (4)$$

The monitoring of accelerated aging is expressed by the loss in mass as a function of time in *Fig. 6a*. The samples immersed in the solution of sulfuric acid H_2SO_4 at a concentration of 5%

and at a temperature exceeding 35 °C, show that all concretes have a significant weight. It was noticed that the SCC1 lost 30.9% of its weight after twenty-four weeks of immersion. Ordinary vibrated concrete has undergone almost the same loss of mass of 27%, while SCC2 containing limestone fillers appears to be the least attacking by sulfuric acid with a loss of only 20% of its weight, this result explains the beneficial effect substitution of limestone fillers by considerably reducing the loss of mass vis-à-vis attack by sulfuric acid, which is in agreement with other researchers [18, 21, 30].

The mechanism of the loss weight is justified by the attack of sulphuric acid which reacts with calcium hydroxide $Ca(OH)_2$, giving rise to calcium sulphate $CaSO_4$ salt which causes a very increased degradation for the concrete by reacting with tricalcium aluminates C_3A to form secondary ettringite.

$$Ca(OH)_2 + H_2SO_4 \longrightarrow CaSO_4 + 2H_2O \quad (5)$$

$$3CaSO_2.2H_2O + 3CaOAl_2O_3 + 26H_2O \longrightarrow (CaO)_3.Al_2O_3.CaSO_4.32H_2O \quad (6)$$

The monitoring of the compressive strength of the samples made and cured in a hot and dry climate with an ambient temperature exceeding 35 °C, showed that, on the contrary to the mixtures (SCC1, SCC2 and OC) immersed for six months in the fresh water (*Fig. 7*) where we have recorded changes in compressive strength. All concrete samples immersed in 5% Na_2SO_4 and 5% H_2SO_4 aggressive media have undergone external sulphate attack. For the 5% of N_2SO_4 solution, a drop in compressive strength (45.0%) for SCC1 was recorded after six-month immersion, comparable to the compressive strength at 28 days before immersion, and of 52.35% for OC, against 34.29% for the SCC2. For the 5% of H_2SO_4 solution, the drop in compressive strength is very dramatic, around 90.56% for SCC1 and 88.75% for OC against 80.54% for SCC2. These results show that concretes subjected to sulfuric acid degrade dramatically because during their immersion, the samples develop phases, which predispose materials capable of embrittlement, particularly gypsum, which turns into ettringite. These results show that the aging of concretes by the sulfuric acid solution is more intense compared to the sodium sulfate solution [38]. As well as the substitution of limestone fillers is beneficial to maintain the best resistance in a sulphate environment [30, 38] and even to its increase vis-à-vis the attack of 5% H_2SO_4 [21].

The microscopic study by XRD diffraction and Fourier transform infrared spectroscopy (FTIR) techniques of concrete samples is more than necessary to give more precise information on the behavior of concrete in the face of external sulphate attack. X-ray diffraction patterns of the mixtures materials proved to be efficient as it revealed the essential constituents of each mixture fabricated. *Fig. 8* reveals the essential products that make up the starting cement, sand and LF. Recall that for the JCPDS references, we have adopted uniform colors in all XRD (*Table 7*). The ettringite phase is given by the following JCPDS–ICDD reference: 41-1451.

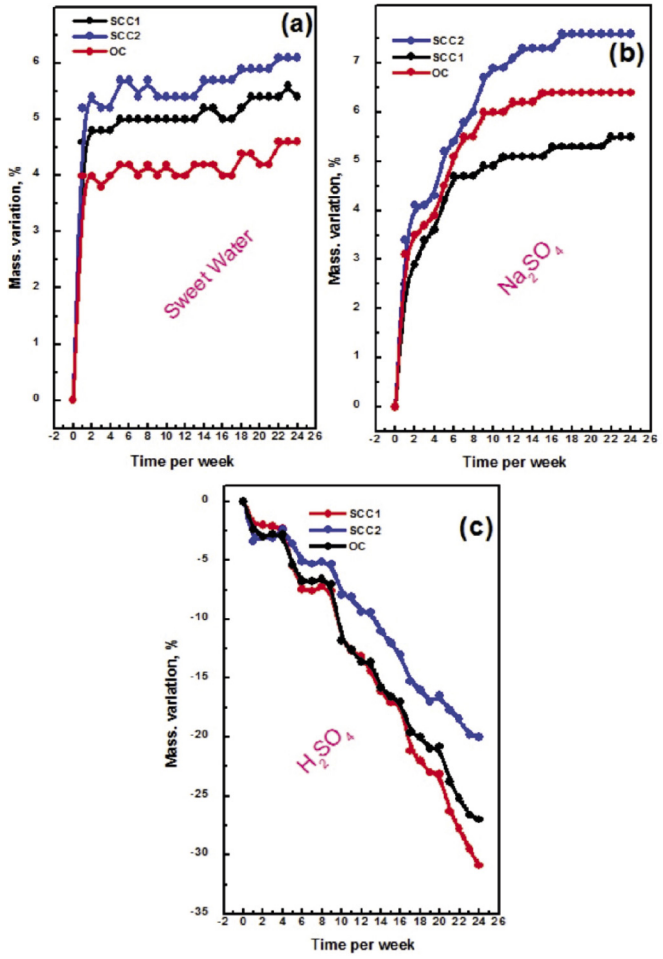

Fig. 6 Variation of the mass as a function of time of the immersed samples in different hot climates
6. ábra A minták tömegének változása az idő függvényében különböző meleg éghajlatokon

The XRD patterns reveal the presence of the compounds such as C_3S (Alite), C_2S (Belite), C_3A (Tricalcium aluminate), C_4AF (Calcium aluminoferrite), and a little quantity of SiO_2. The compounds, have been identified in accordance with the corresponding JCPDS references and the XRD spectra in *Fig. 8a*, are very similar to those given in the literature for cements. The used sand consists of a large amount of quartz (SiO_2), gypsum ($CaSO_4.2H_2O$), and a small amount of calcite ($CaCO_3$). The Limestone filler (LF) compound is mainly composed of calcite ($CaCO_3$), with a smaller amount of dolomite ($CaMg(CO_3)_2$), and also a small amount of Quartz (SiO_2). *Table 8* presents the most common peaks of these compounds and its 2θ values.

The XRD patterns of concretes powder (SCC1, SCC2, and OC) were analyzed in depth according to the effect of the aggressive environments such as sulfuric acid (H_2SO_4), sulphates of sodium (Na_2SO_4), and fresh water. The results confirm the macroscopic approach studied in the previous test. After six months of immersions in H_2SO_4 and Na_2SO_4 media, we found the following products in large quantities: Gypsum, Calcite, Quartz, and portlandite ($Ca(OH)_2$). Portlandite shows a peak around 18.13°. Note that the amount of this mineral change depending on the medium used, and that in the case of H_2SO_4, this compound seems to be reduced in favor of the formation of other more complex compounds.

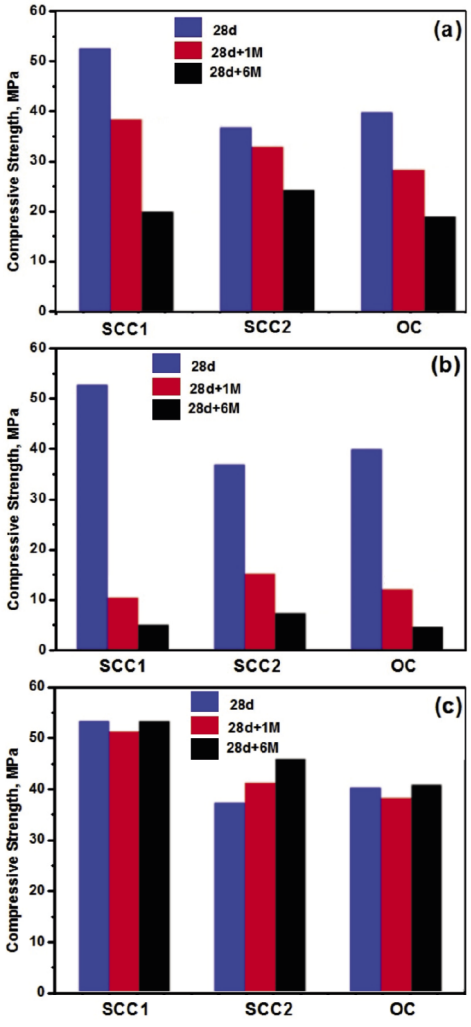

Fig. 7 Variation of the compressive strength: (a) 5%Na_2SO_4, (b) 5% H_2SO_4, (c) Sweet water
7. ábra A nyomószilárdság változása: (a) 5% Na_2SO_4, (b) 5% H_2SO_4, (c) Édes víz

From *Fig. 9*, it can be clearly seen that the concretes immersed in fresh water are those which do not present any gypsum formation, whereas, the concretes immersed in H_2SO_4 media contain sulphated quantities. At very high values, particularly in the case of ordinary concrete, for which the peak has a higher intensity even compared to that of calcite. It can see that for 2Theta, 9.08°, 15.85°, 18.91°, 22.94°, and 25.65°, very weak peaks are detected. The XRD patterns show the presence of few quantities of ettringite with the following chemical formula: $Ca_6Al_2(SO_4)_3(OH)_{12}.26H_2O$. This compound results from the reaction between gypsum and calcium oxides. The relative amount estimated by X-rays is ~ 05.70% in the case of SCC1 immersed in fresh water [40].

$$\underset{\text{Gypsum}}{CSH_2} + \underset{}{C_3A} + 10H \longrightarrow \underset{\text{Monosulfate}}{\overset{2CSH_2+16H}{C_4ASH_{12}}} \longrightarrow \underset{\text{Ettringite}}{C_6AS_3H_{32}} \quad (7)$$

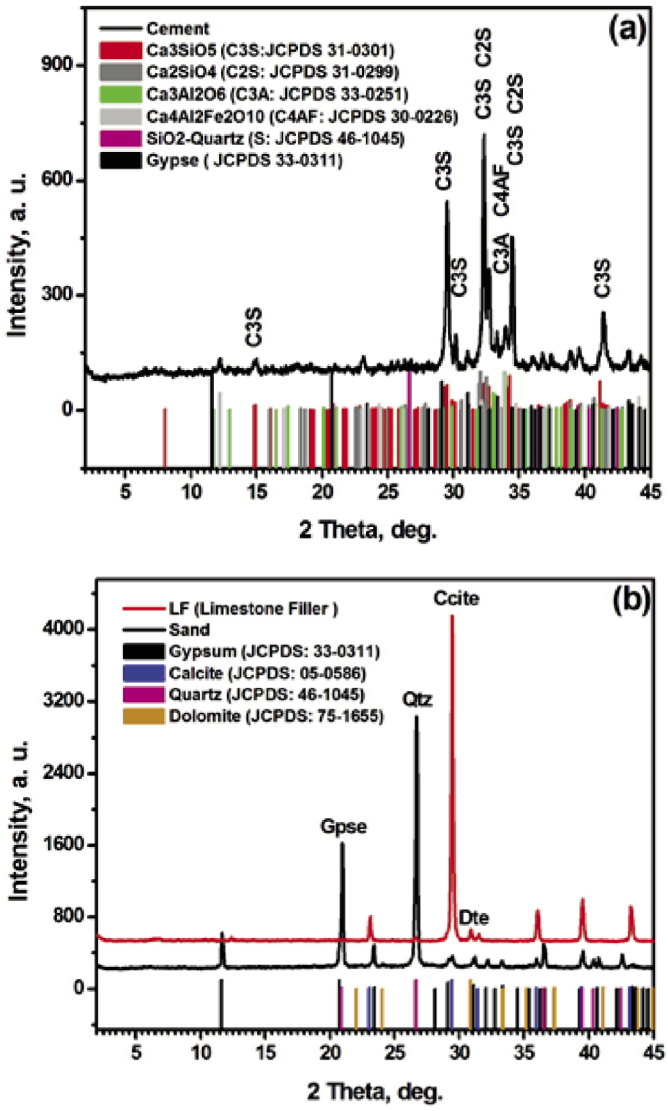

Fig. 8 X-ray patterns of materials used: (a) Cement and (b) LF
8. ábra A felhasznált anyagok röntgenképei: (a) Cement és (b) LF

Phase	C_3S	C_2S	C_3A	C4AF	Gypsum	Calcite	Quartz	Dolomite	Portlandite
Formula	Ca_3SiO_5	Ca_2SiO_4	Ca_3Al_2O	$CaAl_2Fe_2O_{10}$	$CaSO_4,2H_2O$	$CaCO_3$	SiO_2	$CaMg(CO_3)_2$	$Ca(OH)_2$
JCPDS ICDD file n°	31-0301	31-0299	33-0251	30-0226	46-1045	33-0311	46-1045	75-1655	44-1481
Color	Red	Gray	Green	Light gray	Black	Blue	Pink	Orange	Magenta

Table 7 Mineralogical formulas, JCPDS references, phases detected and colors adopted
7. táblázat Ásványi formulák, JCPDS hivatkozások, észlelt fázisok és felvett színek

Peak	C_3S	C_2S	C_3A	C_4AF	Quartz	Gypsum	Calcite	Dolomite
2θ	32.34	32.34	33.32	33.65	26.70	26.55	29.49	30.90

Table 8 2θ of the most common detected peaks
8. táblázat 2θ a leggyakrabban észlelt csúcsokon

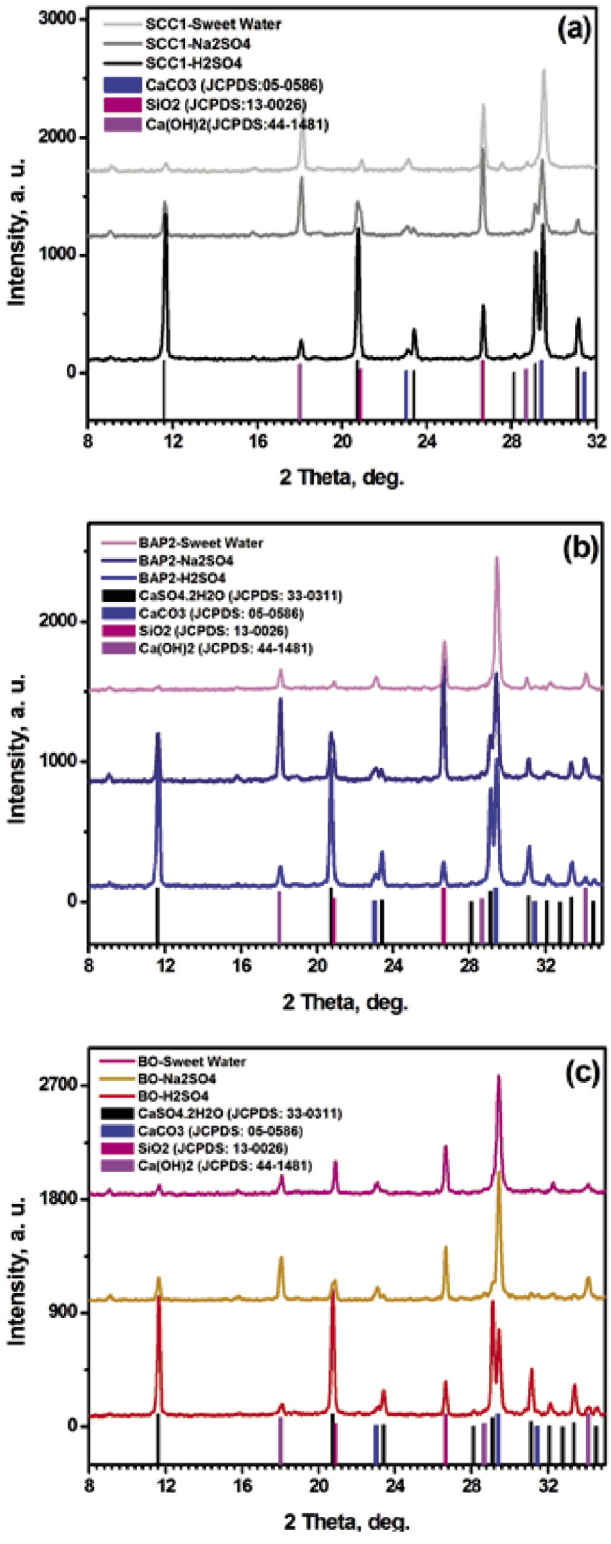

Fig. 9 X-ray patterns of different concretes after immersion in different media for six months

9. ábra Különböző betonok röntgenképei hat hónapig tartó különböző közegbe való merítés után

The analysis by FTIR spectroscopy, allows to a better understanding of the different concretes compositions in various aggressive environments. Furthermore, the spectroscopy also makes it possible to characterize even the amorphous products added to those crystallized found by X-ray diffraction technique. The FTIR spectra of the materials used are shown in *Fig. 10*. The analysis and assignments of the peaks obtained by allow characterizing the constituent products of sands, cement, and limestone fillers. In all cases, these analyses corroborate and supplement the results already found by XRD.

This part based on FTIR spectroscopy characterization to identify the various compounds formed after immersion for six months in the different media. Once having carried out this identification, we evaluated the relative quantities of each compounds found in this amalgam by exploiting the region of the FTIR spectrum between 900 and 1600 cm^{-1}. The relative and qualitative values of CSH-SiO_2, $CaSO_4 2H_2O$ and $CaCO_3$ are detected in the regions of 900-1050 cm^{-1}, 1050-1250 cm^{-1} and 1300-1600 cm^{-1} (*Table 9*), respectively. However, these compounds reflect the reality of the phenomena encountered.

Fig. 11 shows FTIR spectra of different concretes prepared and matured in a dry and arid climate for six months of immersion in different environments. *Table 10* estimates the relative quantities of concretes constituent minerals. It is clear that the percentage of gypsum is the highest which is responsible for the formation of ettringite. The calculated rates show that immersion in fresh water presents the most gypsum-free concretes which explain their good compressive strengths. The best percentage is given for SCC2 concrete with only 5.39% of gypsum, which confirms the positive effect of limestone fillers on concrete behavior. The effect of H_2SO_4 is very significant and leads to the predominant formation of gypsum (63.78%) for ordinary concrete which is mixed with calcite (26.39%) and a small amount of CSH-SiO_2 (09.83%) (*Table 10*) this is the most unfavorable case for which we predict poor mechanical behavior. To a lesser degree, the effect of Na_2SO_4 on relative quantities of constituents is also negative, as it allows the formation of a large amount of gypsum and reduces significant parts of the CSH, SiO_2 and $CaCO_3$ in gypsum by only about 19.64% for ordinary concrete, 41.85% for SCC1 and 35.48% for SCC2 containing limestone fillers. These results lead us to conclude that the substitution of a portion of cement by the limestone fillers is very beneficial, such as the SCC2 subjected to an aging of H_2SO_4 for six months contains a quantity of gypsum (58.35%), a small quantity of CSH –SiO_2 (12.48) against 61.05 and 11.61% for SCC1 (100% cement), and 63.78 and 9.83% for ordinary concrete. Results were found in our macroscopic study confirming the positive effect of lime fillers to maintain better compressive strength in a sulphate environment [32] and even to increase it against attack by 5% H_2SO_4 [21].

Concrete	Relative quantities	Sweet water	Na_2SO_4	H_2SO_4
SCC1	Gypsum	7.72	41.85	61.05
	CSH-SiO_2	27.94	15.95	11.61
	$CaSO_3$	64.34	42.2	27.34
SCC2	Gypsum	5.39	35.48	58.35
	CSH-SiO_2	17.96	14.78	12.48
	$CaSO_3$	67.65	49.74	29.17
OC	Gypsum	6.31	19.64	63.78
	CSH-SiO_2	18.66	13.72	9.83
	$CaSO_3$	75.03	66.64	26.39

Table 10 Relative quantities of constituents of different concretes after immersion for six months in different media

10. táblázat Különböző betonok összetevőinek relatív mennyisége hat hónapig tartó különböző közegekbe való merítés után

Material	Mineral/other	Wavenumber, cm^{-1}	Quantity
Cement	Oxide (SiO_2, ...)	444-522-1102-1126-	Significant
	$CaSO_4$, $2H_2O$	602-658-1140-1154-	Significant
	CSH	920	Significant
	Calcite, $CaCO_3$	712-876-1428-1796-2514-	Main part
	CH_3/CH_2 (Oil residues)	2862-2924-2980-	Small amount
	Water	1622-3450-3544-3644	Significant
	Portlandite	3640	Small amount
Limestone fillers	Calcite, $CaCO_3$	712-874-1420-1798-2514-2874	Main part
	Oxide (SiO_2)	470-1007-1041	Very weak
	Water	1622-3450	Very weak
Sand	SiO_2	460-516-692-778-796-1040	Significant
	$CaSO_4$, $2H_2O$	602-670-1116-1142	Very significant
	Calcite, $CaCO_3$	712-874-1428-1798-2513-2858	Less quantity
	CH_3/CH_2 (Oil residues)	2858-2923	Small amount
	Water	1622-1686-3245-3406-3494-3546-3614-3698	Important

Table 9 Results of analyzes of the constituent products of the materials used
9. táblázat A felhasznált anyagokat alkotóelemeinek elemzésének eredményei

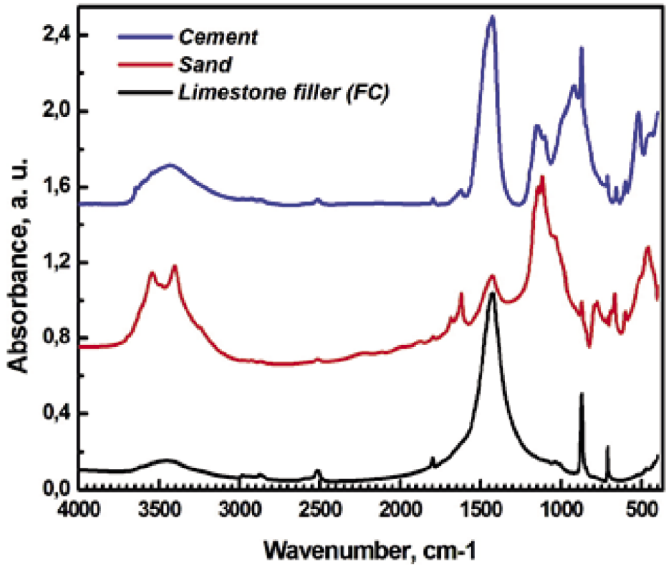

Fig. 10 FTIR Spectra of the materials used for cement synthesis
10. ábra A cementszintézishez használt anyagok FTIR spektruma

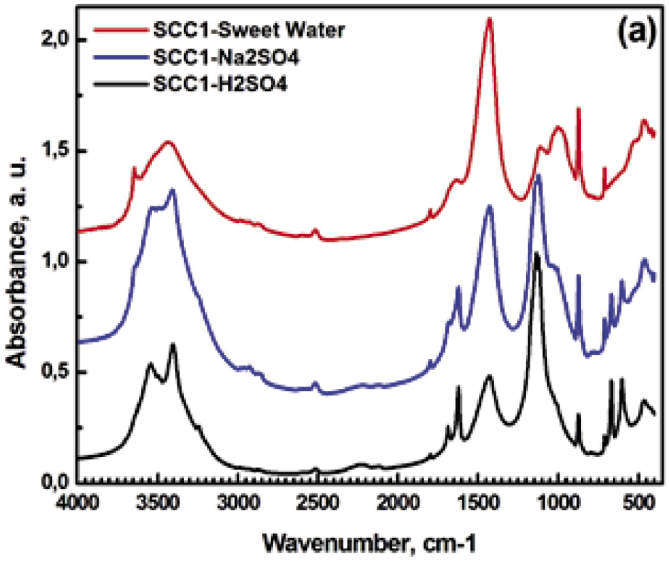

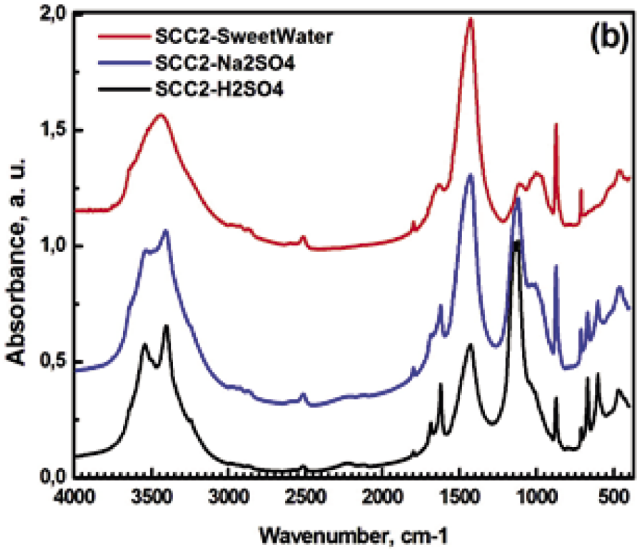

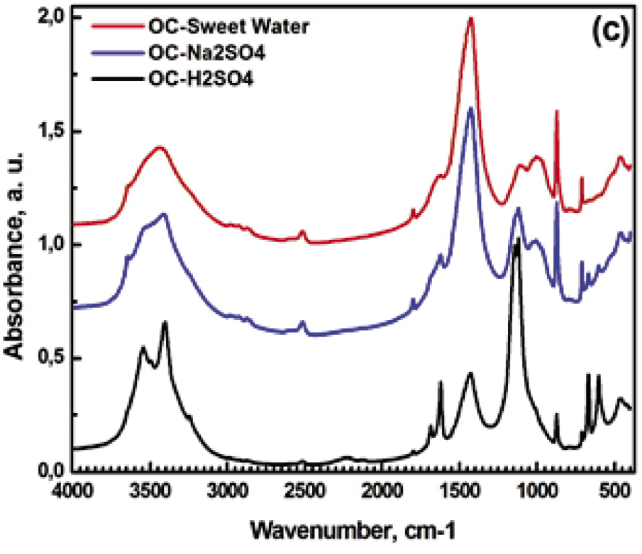

Fig. 11 FTIR spectra of: (a) SCC1, (b) SCC2 and (c) OC, after immersion for six months in different media
11. ábra (a) SCC1, (b) SCC2 és (c) OC FTIR spektruma hat hónapig tartó különböző közegekbe való merítés után

4. Conclusions

In this work, the effect of real climate (hot and dry) of area Biskara, on the concretes (SCC1,SCC2 and OC) behavior immersed in various environments such as sweet water, Na_2SO_4 and H_2SO_4. The rheological behavior of self-compacting concrete and the time required to maintain self-compacting appearance, as well as vibrated concrete were discussed. The experimental results of this study allowed us to draw the following conclusions:

- Up to 25 minutes after mixing, the SCC made with a G/S ratio close to 1, and at a temperature above 35 °C and a humidity of between 11 and 28% kept its self-placing.
- The effect of limestone fillers on the fluidity of SCC in a hot climate is positive and significant just after mixing, but over time the loss of fluidity becomes more noticeable and faster.
- An ambient temperature exceeding 35 °C leads to a rapid evolution of the compressive strength at the early ages of different concretes (SCC1, SCC2, and OC). However, in the long term (120 days) and without any cure, the compressive strength is greatly reduced.
- Monitoring of the aging of concrete prepared and matured in a hot and dry climate for six months with the solution of sulfuric acid H_2SO_4 is more intense compared to the solution of sodium sulphate Na_2SO_4.
- SCC2 containing limestone fillers seem to be the least attacking by sulfuric acid with a loss of 20% in weight while this loss is 30.9% for SCC1 without substitution and 27% for ordinary concrete, which explains why the beneficial effect of the substitution of limestone fillers by considerably reducing the loss of mass vis-à-vis attacks by sulfuric acid.
- The results of compressive strengths of concrete immersed in sulfuric acid are insufficient compared to concretes immersed in Na_2SO_4 or fresh water after six months of immersion because it promotes the formation of phases such as gypsum, ettringite, and consequently decreases the effect of other phases such as calcite, silicates, and quartz.
- The structure of the concrete degraded in acid (H_2SO_4) studied by XRD and FTIR, confirms the existence of a considerable amount of gypsum, and a few amount of Portlandite. This gypsum occupies a considerable volume which replaces calcite and silicates. The presence of a quantity of gypsum associated with the presence of ettringite, promotes the formation of harmful phases in the concrete. The effect of Na_2SO_4 is lower than of H_2SO_4, though, it converts a quantity of calcite and silicates into gypsum.

References

[1] ACI 305. (2010). Guide to Hot Weather Concreting. Reported by *ACI Committee 305 of American Concrete Institute*, 28p.

[2] Infoclimat (2019).Temps reel de Biskra. https://www.infoclimat.fr/observations-meteo/temp reel/biskra/60525.html?graphiques

[3] Yaich, M.R., Bouhanik, A., Bekkouche, S.M.A., Malek, A., & Benouaz, T. (2014). Revised solar maps of Algeria based on sunshine duration. *Energy Conversion and Management*. 82, pp. 114–123. https://doi.org/10.1016/j.enconman.2014.02.063

[4] Ana Cecilia,Vieira da Nóbregada., Mouret.,M., Cassagnabere,F.&, Vinh-An Le. (2018). Improved 28-day compressive strength of SCC mixed and cured in hot weather. Non-conventional behavior. *Construction and Building Materials*. 173, 650–661. https://doi.org/10.1016/j.conbuildmat.2018.03.279

[5] Ghafoori, N., & Diawara, H. (2010). Influence of temperature on fresh performance of self – consolidating concrete. Construction and Building Materials. 24. pp. 946-955. https://doi.org/10.1016/j.conbuildmat.2009.11.023

[6] Hampton, J. S. (1981). Extended Workability of Concrete Containing High-Range Water-Reducing Admixtures in Hot Weather. In Development in the Use of Superplasticizers. *ACI Spec. Publ*. SP 68, Detroit. pp.409-22

[7] Salhi, M., Li, A., Ghrici, M., & Bliard, C. (2019). Effect of temperature on the behavior of self-compacting concretes and their durability. *Advances in Concrete Construction*. 7, pp. 277–288. https://doi.org/http://dx.doi.org/10.12989/acc.2019.7.4.277

[8] Cygan, G., Golazewski, J.,& Drewniok, M. (2016). The effect of temperature on the properties of fresh self- compacting concrete. *Archives of Civil Engineering*. 62(3), 23–32. https://doi.org/10.1515/ace-2015-0080

[9] Abd-El.Aziz, M.A., Abd.El.Aleem, & S., Mohamed, H. (2012). Physico-chemical and mechanical characteristics of pozzolanic cement pastes and mortars hydrated at different curing temperatures. *Construction and Building Materials, 26(1)*, 310–316. https://doi.org/10.1016/j.conbuildmat.2011.06.026

[10] Salhi, M., Ghrici, M., Li, A. and Bilir, T. (2017). Effect of curing treatments on the material properties of hardened self-compacting concrete. *Advances in Concrete Construction*. 5(4), 359–375. https://doi.org/10.12989/acc.2017.5.4.359

[11] Tao, J., Yuan, Y., & Taerwe, L. (2010). Compressive Strength of Self-Compacting Concrete during High Temperature Exposure. *Journal of Materials in Civil Engineering*. 22(10), pp. 1005–1011. https://doi.org/10.1061/(ASCE)MT.1943-5533.0000102

[12] Kodur, V., ASCE, F., & Khaliq, W. (2011). Effect of Temperature on Thermal Properties of Different Types of High-Strength Concrete. *J. Mater. Civ. Eng*. 23, pp.793–801. https://doi.org/10.1061/(ASCE)MT.1943-5533.0000225

[13] Pichler, Ch., Schmid, M., Traxl, R., & Lackner, R. (2017). Influence of curing temperature dependent microstructure on early-age concrete strength development. *Cement and Concrete Research*.102, pp. 48–59. https://doi.org/10.1016/j.cemconres.2017.08.022

[14] Nehdi, M. N.,& Soliman, A. M. (2011). Early-age properties of concrete: overview of fundamental concepts and state-of-the-art research. Proceedings of the Institution of Civil Engineers -*Construction Materials*. 164 (2), 57–77. https://doi.org/10.1680/coma.900040

[15] Divet, L. (2002). Comment se prémunir des réactions sulfatiques dans les bétons ? Point sur les normes actuelles et quelques recommandations. *Bulletin des laboratoires des ponts et chaussées*. 240 – septembre- octobre réf. 4447, pp. 87-9 https://www.ifsttar.fr/collections/BLPCpdfs/blpc_240_87-94.pdf

[16] Mehdi, B., & Abdelaziz, B. (2017). Behaviour of Self Compacting Concrete mixed with different additions at high-temperature. *Journal of Materials and Environmental Sciences*. 8(9), 3081–3092. http://www.jmaterenvironsci.com/

[17] Denecker, M.F.C., Hebert, R.L., Wassermann, J., Dosseh, G., Menendez, B., & BourgÃ¨s, A. (2014). Experimental study of the crystallization of sodium sulfate hydrates through temperature monitoring. *Environmental Earth Sciences*. 72(12). pp. 5089-5099. https://doi.org/10.1007/s12665-014-3379-2

[18] Mohsen, T., Mongi, B. O., & Abderrazak, K. (2017). Behavior of self-compacting Concrete made with marble and tile wastes exposed to external sulfate attack. *Construction and Building Materials*. 135, 335–342. https://doi.org/10.1016/j.conbuildmat.2016.12.193

[19] Khelifa, R., Brunetaud, X., Chabil, H., & Al-Mukhtar, M. (2008). Consequences mecaniques de l'attaque sulfatique externe sur les betons autoplaçants. *Sci. Technol*. 28, pp. 8–23. http://revue.umc.edu.dz/index.php/b/article/view/243

[20] Chiraz, K., Mouloud, B., & Yacine, C. (2020). Contribution to the Study of the Durability of Rubberized Concrete in Aggressive Environments. *Civil and Environmental Engineering Reports*. 30(1),111- 129. https://doi.org/https://doi.org/10.2478/ceer-2020-0009

[21] Senhadji, Y., Benosman, A. S., Escadeillas, G., Mouli, M., Laoufi, L., & Khelafi, H. (2016). Mortar incorporating supplementary cementtious materials :Streng the isothermal calorimetry and acids attack, *Journal of Fundamental and Applied Sciences*. 8 (2), 232–243. https://doi.org/10.4314/jfas.v8i2.4

[22] EFNARC. (2005). Specification and Guidelines for Self-Compacting Concrete. *European Federation of Producers and Applicators of Specialist Products for Structures*. May, pp. 1– 68. https://wwwp.feb.unesp.br/pbastos/c.especiais/Efnarc.pdf

[23] AFGC. (2008). Groupe de travail. Recommandations pour l'emploi des bétons auto-plaçants, *documents scientifiques et techniques*. https://doi.org/betonlabpro.ifsttar.fr/fileadmin/contributeurs/BetonlabPro/doc/recommandations_bap_afgc.pdf

[24] Dreux, G., & Festa, J. (1998). Nouveau guide du béton et de ses constituants, 8eme édition, *Edition Eyrolles*. https://www.eyrolles.com/BTP/Livre/nouveau-guide-du-beton-et-de-ses-constituants-9782212102314/

[25] Mehta, P. K. (1975). Evaluation of sulfate resisting cements by a new test method. *Journal ACI*. 72, 573–575. http://worldcat.org/issn/0889325X

[26] EN 206-1: Béton - Partie 1(2004). Spécification, performances, production et conformité.

[27] Le, V.A. (2014). Comportement des bétons autoplaçants par temps chaud. *Ph.D. Dissertation*, Université Toulouse III-Paul Sabatier, France. http://thesesups.ups-tlse.fr/2296/1/2014TOU30041.pdf

[28] Salhi, M., Ghrici, M., Bilir, T., Mücteba, U. (2020). Combined effect of temperature and time on the flow properties of self-compacting concrete. *Construction and Building Materials*. 240, 117914. https://doi.org/10.1016/j.conbuildmat.2019.117914

[29] Courard, L., & Michel, F. (2014). Limestone fillers cement based composites. Effects of blast furnace slags on fresh and hardened propertie. *Construction and Building Materials*. 51, 439–445. https://doi.org/10.1016/j.conbuildmat.2013.10.076

[30] Rahmani, H., A.A. & Ramzanianpour. (2008). Effect of silica fume and natural pozzolanas on sulfuric acid resistance of dense concretes, *Asian Journal of Civil Engineering (building and housing)*, 9 303-319. https://www.bhrc.ac.ir/Portals/25/PropertyAgent/2905/Files/6195/303.pdf

[31] Diederich, P., Mouret, M., de Ryck, A., Ponchon, F., & Escadeillas, G. (2012). The nature of limestone filler and self-consolidating feasibility—relationships between physical, chemical and mineralogical properties of fillers and the flow at different states, from powder to cement-based suspension. *Powder technology*, 218, 90-101. https://doi.org/10.1016/j.powtec.2011.11.045

[32] Bensebti, S., Aggoune, S., & Houari, H. (2007). Essai de caractérisation expérimentale de la ségrégation verticale des bétons autoplaçants. *Sciences & Technologie*. B, Sciences de l'ingénieur, pp. 59–64. http://revue.umc.edu.dz/index.php/b/article/view/205

[33] Soufiane, B., Fouad, G., Mohammed Amine, B.H.,& Omar, T. (2015). Influence des fillers calcaires sur la porosité et la distribution porale des pâtes autoplaçantes. *Nature &Technologie*. A- Sciences fondamentales et Engineering. 12, pp. 60-66. https://www.researchgate.net/publication/338595172

[34] Beeralingegowda, B., & Gundakalle, V. D. (2013). The effect of addition of limestone powder on the propertes of self-compacting concrete. *International Journal of Innovative Research in Science Engineering and Technology. 2(9)*, pp. 4996. https://www.ijirset.com/upload/september/75_THE%20EFFECT.pdf

[35] Abidin, N. E. Z., Ibrahim, M. H. W., Jamaluddin, N., Kamaruddin, K. &, Hamzah, A. F. (2014).The Effect of Bottom Ash on Fresh Characteristic, Compressive Strength and Water Absorption of Self- Compacting Concrete. Applied Mechanics and Materials. 660, 145–151. https://doi.org/10.4028/www.scientific.net/AMM.660.145

[36] Taoufik, A., Andre, 'L., Mongi, B.O., Rachid, M., & Imène, J. (2008). Contribution of the fillers limestones to the paste-aggregate bond: Tunisian examples. *Materials and Structures*. 41. pp. 815–830. https://doi.org/10.1617/s11527-007-9287-0

[37] Shamir, S., Sudharshan, N.R., Safiuddin, Md., A. Kaish, A. B. M., A.& Mutalib, A. (2020). Utilization of By-Products and Wastes as Supplementary Cementitious Materials in Structural Mortar for Sustainable Construction. *Sustainability*. 12, pp. 3888. https://doi.org/10.3390/su12093888

[38] Mouallif, I., Lasfar, S., Latrach, A., Chergui, M., Barbe, N. (2013). Influence du vieillissement sulfatique sur la résistance mécanique et la microstructure du béton, *21ème Congrès Français de Mécanique Bordeaux*, 26 au 30 août 2013. http://hdl.handle.net/2042/52907

[39] Da Silvaa, P. R., & de Brito, J. (2015). Experimental study of the porosity and microstructure of self-compacting concrete (SCC) with binary and ternary mixes of fly ash and limestone filler. *Construction and Building Materials*. 86, 101–112. https://doi.org/10.1016/j.conbuildmat.2015.03.110

[40] Vysvaril, M., Bayer, P., & Rovnaníková, M. (2014). Microstructural changes of fine-grained concrete exposed to a sulfate attack. *Materials and technology*. 49(6), pp. 883–888. https://doi.org/10.17222/mit.2014.138

Ref.:
Benaddi, Hachemi – **Mezghiche**, Bouzidi – **Salhi**, Mohamed – **Boumaza,** Abdecharif: *Performance of self-compacting concrete in hot arid climate*
Építőanyag – Journal of Silicate Based and Composite Materials, Vol. 74, No. 3 (2022), 97–107. p.
https://doi.org/10.14382/epitoanyag-jsbcm.2022.16

The effect of one-part magnesium oxychloride cement additive on the mechanical, mineralogical, water resistant and micro structural properties of dolomite cement

M. Ezzat TAHA ▪ Housing and Building National Research Center (HBNRC), cairo, Egypt ▪ Topaz75@gmail.com
Ayman M. KANDEEL ▪ Housing and Building National Research Center (HBNRC), cairo, Egypt
M. Ezzat EL-FAKHARANY ▪ Housing and Building National Research Center (HBNRC), cairo, Egypt

Érkezett: 2021. 10. 14. ▪ Received: 14. 10. 2021. ▪ https://doi.org/10.14382/epitoanyag-jsbcm.2022.17

M. Ezzat TAHA
Associate Professor in field of geology at Raw Building Materials Technology and Processing Research Institute, Housing and Building National Research Center (HBNRC).

Ayman M. KANDEEL
Professor of cement chemistry at Raw Building Materials Technology and Processing Research Institute, Housing and Building National Research Center (HBNRC).

M. Ezzat EL-FAKHARANY
Researcher in field of geology at Raw Building Materials Technology and Processing Research Institute, Housing and Building National Research Center (HBNRC).

Abstract
In this paper magnesium oxychloride cement (MOC) is prepared from dolomite by calcinations process. The effect of different ratios of additive prepared from magnesite MOC (0.5, 1 and 1.5%) on the mechanical properties of dolomite MOC is recorded at 7, 14 and 28 days. Infrared spectroscopy (IR-spectra) is used to characterize the effect of magnesite MOC additive on the mineralogy of dolomite MOC mixes air cured at 28 days. The results indicated that one-part MOC additive posted the mechanical compressive strength of dolomite MOC mix at addition rate of 0.5 and 1% and was declined at 1.5%. The water resistance of MOC increased with increase of additive in mix. The micro structural investigation revealed that the mechanical performance of MOC was predominantly dependent on abundance and crystals size of phase 5.
Keywords: dolomite, magnesite, magnesium oxychloride cement, compressive strength, micro-structure
Kulcsszavak: dolomit, magnezit, magnézium-oxiklorid cement, nyomószilárdság, mikroszerkezet

1. Introduction

The problem of scarcity of quality raw materials to produce magnesium oxychloride cement (MOC) in Egyptian market can be solved by replacing the caustic magnesite by caustic dolomite [1]. The presence of vast amount of dolomite deposits in different regions in Egypt ranging in grades from low to high, which can be used to produce MOC by calcinations at lower temperature. Magnesite and dolomite MOC is considered as advantage over ordinary Portland cement binder due to their high strength, and remarkable bonding ability and their ability to be mixed with broad inorganic and organic fillers [2-5].

MOC is based on the reaction between MgO and $MgCl_2$ forming a variety of phases that are highly dependent on molar ratios, temperature and magnesium reactivity. MOC is formed from hardened paste is in form of hydroxide, chloride pentahydroxide (Phase 5) and chloride trihydroxide (Phase 3) of magnesium, their content in the paste influence the material properties [6-9]. Though MOC posses superior properties than ordinary Portland cement but it have poor water resistant. Different additive are added to increase its water resistant [10-12]. Several patents and research work claimed that dolomite could be used to produce MOC binders if the dolomite was carefully calcined by firing at ~750 °C to produce MgO and $CaCO_3$. The thermal decomposition of dolomite is reported to take place on two stages, yielding MgO and $CaCO_3$, followed by $CaCO_3$ decomposition at higher temperature [13]. The suitability of dolomite as a raw material for producing MOC has been evaluated thermally and petrographicaly [14]. Meanwhile, own to the small content of MgO of caustic dolomite some researcher proposed mixing with different ratios of caustic magnesite to increase the mechanical and physical properties of the resultant MOC.

The current work aims to study the effect of using one-part magnesite MOC additive added in different ratios to dolomite MOC wet mix on the mineralogy, mechanical properties water resistance, and micro structure of resultant hardened MOC.

2. Experimental procedures

2.1 Materials

In this research two main raw materials were used mainly; calcined dolomite and light-burned magnesite in order to produce magnesium oxychloride cement (MOC). The dolomite used in making calcined dolomite (Size 6 mm) is sourced from Ataqa district, Suez Egypt and was heated to 750 °C for about 2 hrs with a rate of 10 °C /min in a muffle furnace in order to obtain calcined dolomite with high percent of reactive Magnesium oxide. Afterwards, it is subjected to dry milling using laboratory ball mill (Herzog) to the consistency of Ordinary Portland cement. The light-burned magnesite used to produce the one-part MOC was produced from local magnesite sourced from upper Egypt by heating raw magnesite (Size 6 mm) to about 2 hrs with a rate of 10 °C /min. The magnesium chloride hexahydrate ($MgCl_2 \cdot 6H_2O$) used in activating the calcined dolomite and magnesite is of analytical reagent grade of purity 99.9%, and was sourced from ThermoFisher. The chemical compositions of starting raw materials analyzed by XRF are

Oxides, %	SiO_2	Al_2O_3	Fe_2O_3	CaO	MgO	Na_2O	K_2O	P_2O_5	TiO_2	SO_3	Cl-	L.O.I	TOTAL
Calcined dolomite	1.03	0.38	0.12	38.20	22.8	0.20	-	0.22	-	0.21	0.14	36.67	99.97
light-burned magnesite	1.2	0.07	1.29	2.36	79.5	0.01	0.01	0.01	0.01	0.42	-	15.01	99.80

Table 1 Chemical composition of calcined dolomite and light-burned magnesite heated to 750 °C
1. táblázat A 750 °C-ra hevített égetett dolomit és magnezit kémiai összetétele

listed in *Table 1*, where the mineralogical compositions of these materials analyzed by XRD are given in *Fig. 1*. The XRD analysis revealed that the main component of the dolomite calcined at 750 °C (*Fig.1a*) is calcite ($CaCO_3$) and periclase (MgO) with minor amount of lime (CaO). This calcinations temperature for dolomite is chosen on the basis of earlier previous research work of different authors, which recommended this temperature, as below this temperature low amount of MgO is formed and above this temperature more lime is formed, which is not recommended in MOC [15-20]. The mineralogical analysis of light-burned raw magnesite shown *Fig. 1b*, revealed that the main components are MgO with minor amount of calcite and portlandite which is attributed to hydration of lime component from air moisture. In addition, the mineralogical analysis of one-part magnesite MOC shown in *Fig. 1c* revealed that it is mainly composed of periclase, calcite, bruchite ($MgOH_2$), and phase 5.

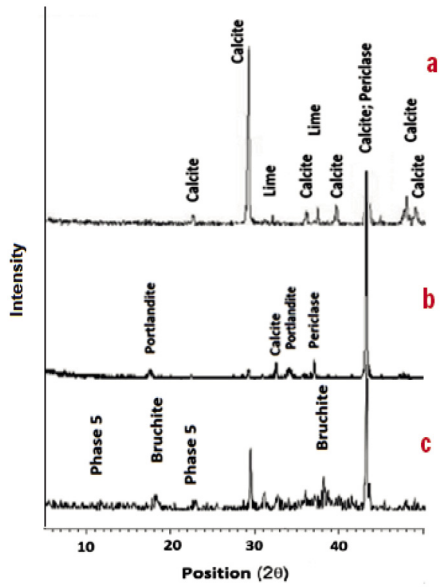

Fig. 1 XRD analysis of a) calcined dolomite b) Light-burned raw magnesite c) magnesite MOC dried at 80 °C (one-part MOC)
1. ábra a) kalcinált dolomit b) égetett nyers magnezit c) 80 °C-on szárított magnezit MOC (egyrészes MOC) XRD vizsgálatának eredménye

2.2 Processing, mixing and moulding

Saturated magnesium chloride solution was prepared by dissolving analytical reagent grade magnesium chloride hexahydrate ($MgCl_2 \cdot 6H_2O$) of purity 99.9% in tap water as mixing water before mixing with calcined dolomite and light-burned magnesite powder to make MOC paste. The mass concentration of the 1st solution was 50 gm of $MgCl_2 \cdot 6H_2O$ dissolved in 100 ml of mixing water and for 2nd solution was 133.3 gm of $MgCl_2 \cdot 6H_2O$ dissolved in 100 ml of mixing water with the addition of 1% of concentrated hydrochloric acid to each solution to ease the solubility process and turn any free CaO present into $CaCl_2$. The mix formed by mixing of 2nd solution with light burned magnesite is casted in cubic shaped silicon rubber mould and left in drier at 80 °C for 24 hrs to harden. Then the hardened product is crushed and grinded to the constancy of cement to form one-part magnesite MOC additive with mix proportion listed in *Table 2*. Four mixtures of MOC were prepared; A0, A1, A2 and A3 from calcined dolomite and the 1st solution with the mix proportions listed in *Table 2*. The water to solid ratio (w/s) in all the mixes was initially fixed at 0.32 for all mixes. The proportions of substitution of dolomite MOC with one-part MOC additive in specimens; A0, A1, A2 and A3 were 0, 0.5, 1 and 1.5% respectively. The MOC mixes were then casted in oil lubricated cubic iron mould (25 mm). The MOC specimens were left in the moulds for 24 hrs, then cured after demoulding in air and water, and examined for their mechanical properties and water resistant beside mineralogical and micro structural investigation at 7, 14 and 28 days.

MOC	$MgO/MgCl_2$	$H_2O/ MgCl_2$
Dolomite MOC	8	28
Magnesite MOC	14	14

Table 2 Mix design of dolomite MOC reference mix (A0) and one-part magnesite MOC additive
2. táblázat Dolomit MOC referenciakeverék (A0) és az egykomponensű magnezit MOC adalék keverékterve

2.3 Methods

The chemical analysis was performed on the ground pressed aggregate powder using Philips PW 1400 XRF in housing and building national research center laboratory confirming to the test methods described in the American Society for Testing and Materials (ASTM). The mechanical properties of dolomite MOC mixes were studied after 7, 14 and 28 days of air and water curing. The compressive strength was determined according to ASTM standards. Compressive strength test is performed using five tones German Brüf pressing machine with a loading rate of 100 MPa/s determined according to ASTM C109 [21]. Removing of the free water from specimens for examination was accomplished by drying of the crushed specimens for 24 hrs at 105 °C.

To evaluate the water resistance of the MOC, the specimens cured for 14 and 28 days in the air environment were dipped in water at 20 ± 3 °C, and the compressive strength of the specimens after the different immersion times was measured and used to calculate the strength retention coefficient (*Rf*) as follows [22, 23]:

$$Rf = R(W, n)/R(A, 28) \quad (1)$$

Where *R(W, n)* and *R(A, 28)* denote the compressive strength of the specimens after immersion in the water for n days and the compressive strength of the specimens cured in the air environment for 14 and 28 days.

Perkin Elmer FTIR Spectrum RX1 Spectrometer (Fourier Transformation Infrared) was used to evaluate the functional groups in the specimens. The dolomite MOC specimens cured for 28 days with different ratios of additive in air are ground into fine powder with a ceramic mortar. Then the ground specimen was mixed with KBr at a mass ratio of 1/100 and the mixture was pressed in a sample holder at about 295 MPa for 2 mins to make a specimen for FTIR examination. The wave number of Spectrometer was ranging from 400 to 4000 cm^{-1}. Scanning electron microscopy (SEM) investigation were done on dolomite MOC cured for 28 days specimens, using Inspect S (FEI Company, Holland), equipped with an energy dispersive X-ray analyzer (EDXA). Each sample was covered by gold and the accelerated voltage was set at 10 kV in order to enhance its conductivity.

3. Results and discussions

3.1 Compressive strength

Generally, it is clear that the compressive strength of air cured dolomite MOC with no MOC additive (Mix A0) increases with air curing for 7, 14 and 28 days. The compressive strength of mix A0 air cured for 7, 14 and 28 days was about 146, 238, and 309 kg/cm^2 respectively and the rate of increase in compressive strength was about 12%, 36% and 26% respectively for mix A1 with 0.5% MOC additive. However, for mixes A2 and A3 air cured for 7 days, it was obvious that there is slight decrease in compressive strength by about 9% and 23% when compared to same curing time of A0 mix. This slight decrease in compressive strength compared to the reasonable increase in compressive strength noticed in A1 mix, suggests that with increase of MOC additive above 0.5%, the amount of formed hydration product of MOC phases are affected and thus the mechanical performance is negatively affected. However, an increase in compressive strength is noticed for MOC mixes A2 and A3 air cured for 14 and 28 days. The percentage of increase in compressive strength of these mixes was about 33% and 24% for mix A2 air cured for 14 and 28 days. Moreover, the percentage of increase in compressive strength was about 22% and 12% for mix A3 air cured for 14 and 28 days respectively. This result imply that MOC mixes A1 and A2 achieved the best mechanical performance, but on increase of MOC additive above 1%, the mechanical performance of dolomite MOC cement declined noticeably. This can be explained that on increase of MOC additive in mixes as mix A3, the hydration phases that are responsible for compressive strength decrease. This finding is confirmed by FTIR spectra in *Fig. 3* in which the bending vibration O-H (hydrogen bond) formed at 1630 cm^{-1} as indicative of water of crystallization and MOC phases bands which is very clear in MOC mixes A0, A1 and A2 and not distinctive in A3 mix. Moreover, the bands in FTIR spectra band at about 1155-1160 cm^{-1} of the hydrogen bonding between H_2O and Cl^-, which is indicative of hydration phases of MOC is very distinctive and strong in mixes A0, A1 and A2 and decrease in mix A3.

Further, from *Fig. 2* it is obvious that the water curing negatively affects the dolomite MOC mechanical performance and the compressive strength of water cured mixes dropped significantly compared to the air cured counterparts. The clearest effect of water on MOC was very clear after 28 days of curing. The compressive strength water cured mixes for 28 days; A0, A1, A2 and A3 were about 199, 195, 320 and 280 kg/cm^2 respectively. The decline in compressive strength of water cured mixes compared to the air cured counterpart were about 36%, 29%, 22% and 21%. This noticeable decline in strength could be explained than when MOC specimens was immersed in water for a certain period, needle-like phase five decomposed to $Mg(OH)_2$, which led to a noticeable decrease in the compressive strength of the MOC [24] due to formation of a highly porous structure [25].

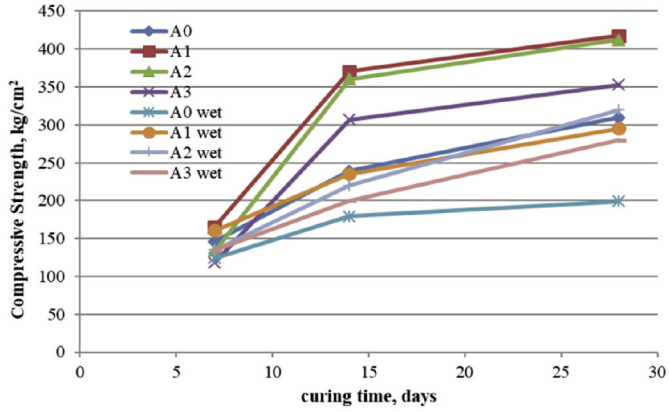

Fig. 2 Compressive strength of air and water cured dolomite MOC mixes cured at 7, 14 and 28 days
2. ábra 7, 14 és 28 napot levegőn valamint víz alatt tárolt dolomit MOC keverékek nyomószilárdsága

3.2 Strength retention coefficient

Unfortunately, the use of MOC in engineering applications is restricted because of its poor performance in water. The compressive strength retention coefficients of the MOC mixes after complete immersion in the water for 14 and 28 days are shown in *Table 3*. It is clear from the strength retention coefficient values of MOC specimens after 14 and 28 days of water curing, that there is a noticeable increase with increasing of magnesite MOC additive in MOC mixes with curing time and that the best water performance value was mix A3. The increase of water resistance of MOC mixes with MOC additive may be attributed to the water environment that provides sufficient free water that facilitates the secondary hydration of the MOC, which form more main crystal phases after the water immersion [26, 27]. The higher strength retention coefficient (*Rf*) value of MOC mix, the better water resistance it has. Which imply that the strength of MOC still develops in immersion condition.

Mix	14 days	28 days
A0	0.48	0.64
A1	0.65	0.70
A2	0.61	0.77
A3	0.65	0.79

Table 3 The strength retention coefficients (Rf) of the MOC mixes cured for 14 and 28 days
3. táblázat A 14 és 28 napig kezelt MOC keverékek szilárdsági megtartási együtthatói (Rf)

3.3 FTIR spectroscopy

FTIR spectra of minerals display characteristic features, usually absorption features, which can be related qualitatively to variations in the constituent minerals. The FTIR spectra of dolomite MOC cured at 28 days for mixes A0, A1, A2 and A3

with different proportions of one-part MOC additive are shown in *Fig. 3*. The characteristic bands for the MOC are represented by three small absorption peaks at 3693, 3652 and 3612 cm^{-1} [28], and they are very distinctive at MOC mixes A0, A1 and A2.

The bands at 3400 to 3600 cm^{-1} are attributed to the O-H bending vibrations of crystallization water. Moreover, the bending vibration O-H (hydrogen bond) at about 1630 cm^{-1} is indicative of water of crystallization and increase of MOC phases. These Function groups produced in MOC could enhance compressive strength of the final mix. This is confirmed by the stretching vibration OH (hydroxyl function group) appeared at 3420 cm^{-1}, which is composition of phase 5 and phase 3 thus contribute to increased strength of the products. A gradual increase of intensity of peaks is noticed with increasing of MOC additive up to mix A2, owing to increase of hydration products.

The FTIR spectrum of pure calcium carbonate formed from calcinations of dolomite at 750 °C is confirmed by the presence of a strong band centered around 1425 cm^{-1}, characteristics of the C–O stretching mode of carbonate together with a narrow band around 875 cm^{-1} of the bending mode. In addition, it is clear from the FTIR spectra that decrease of Carbonates band intensity may interfere the phase formation of the MOC, since the results shifts towards a higher mechanical strength with increasing of MOC additive up to percentage of mix A2. The bands at about 1440 and 1155-1160 cm^{-1} indicate the hydrogen bonding between H_2O and Cl^-, and vibrational signals in the range of 640-400 cm^{-1} can be attributed to the stretching and bending of the Mg-O bonds in the MgO_6 octahedral coordination [29].

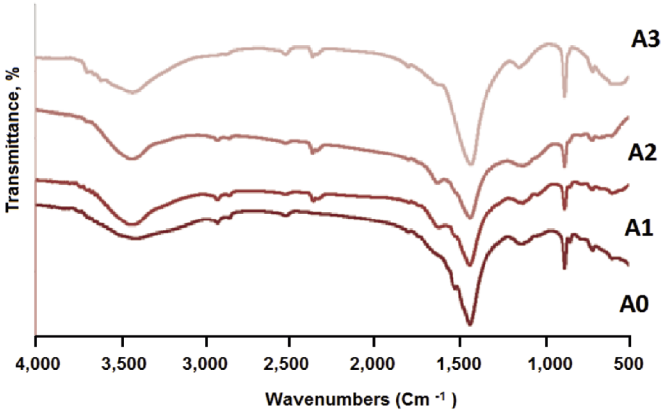

Fig. 3 *FTIR spectra of dolomite MOC mixes (A0, A1, A2 and A3) air cured for 28 days*
3. ábra *28 napig levegőn tárolt dolomit MOC keverékek (A0, A1, A2 és A3) FTIR spektruma*

3.4 Micro structural investigation

The SEM images of dolomite MOC mixes A0, A1, A2 and A3 air cured for 28 days are shown in *Fig. 4*. It is clear from the SEM that the abundance phases in all of the mixes are Phase 5 (P5), periclase (Per.) and bruchite (Br.). Generally across the MOC matrix, spherical particles of MgO were observed in form of clusters, $Mg(OH)_2$ crystals appeared in form of plate like crystals and phase 5, which is responsible for acquired mechanical strength of MOC appeared in form of needle like crystals of different sizes and orientation in matrix of MOC mixes. *Fig. 4a* of MOC mix A0 shows the formation of small interlocked needle like and plate like crystals of phase 5 and abundance of $Mg(OH)_2$ crystals with some unconsumed clusters of MgO in matrix. On the other hand, *Fig. 4 b* and *c* showing SEM micrographs of MOC mixes A1 and A2 show the formation of interlocked distinctive needle like crystals of phase 5 of size 300-500 nanometer in width and with fewer clusters of MgO in matrix compared to MOC mix A0. This finding leaded the structure of MOC to be more compact and denser [30, 31] and thus influenced the mechanical performance of A1 and A2 MOC mixes. Further, *Fig. 4d* shows the formation of larger needle like Phase 5 of size 1000 nanometer (1 micrometer) in width and abundance of bruchite and periclase crystals in matrix of A3 MOC. It is obvious that the formation of these larger P5 crystals in MOC A3 (*Fig. 4d*) compared to the other mixes, results in increase in water resistance of A3 compared to the other mixes, but it negatively affected its mechanical performance compared to the other mixes, owing to formation of larger pore spaces in matrix of A3 MOC as shown in SEM image (*Fig. 4d*).

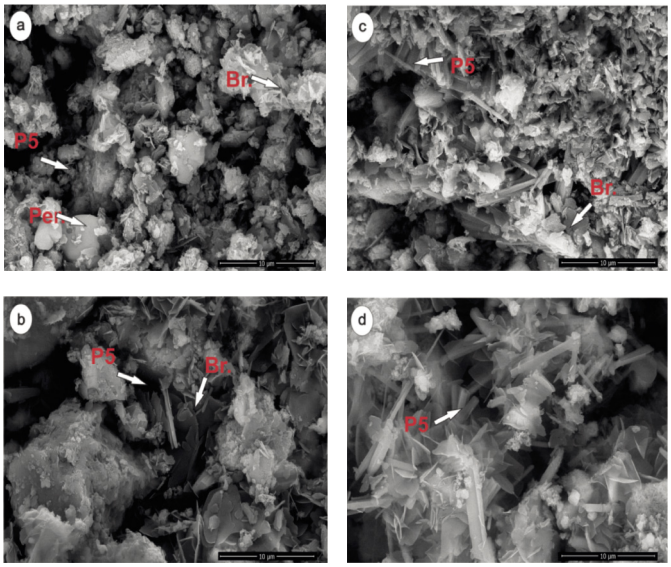

Fig. 4 *SEM images of dolomite MOC mixes with different percentage of one-part MOC additive*
4. ábra *MOC adalékot különböző százalékban tartalmazó dolomit MOC keverékekről készült SEM felvételek*

4. Conclusions

This study disclose the effect of one-part MOC additive prepared from light-burned magnesite on the mineralogy, compressive strength, water resistance and micro structure of dolomite MOC, the conclusions can be drawn as follows:

(1) The magnesite MOC additive increased the dry compressive strength of all mixes at different curing ages compared to the reference mix of MOC with no additive. However, on curing of MOC in water the strength noticeably declined due to dissolution of phases of MOC.

(2) The magnesite MOC additive increased the water resistance of all mixes compared to the reference mix A0, especially MOC mix A3 that showed the best water resistance.

(3) Micro structural investigation revealed formation of phase 5 was responsible for mechanical performance and structure compactness of dolomite MOC, and when the width the width of theses formed crystals in MOC increases, the mechanical performance of MOC is negatively affected.

References

[0] Khuziahmetov, R.K., Ibragimov, R.A., Khuziahmetova, R.N. (2020) Production process of dolomite-based facing building materials. IOP Conference Series: Materials Science and Engineering, P. 962. https://doi.org/ 10.1088/1757-899X/962/2/022019

[2] Sglavo, V.M., De Genua, F., Conci, A., Ceccato, R.; Cavallini, R. (2011) Influence of curing temperature on the evolution of magnesium oxychloride cement. Journal of Materials Science 2, Vol. 46, pp. 6726-6733. https://doi.org/ 10.1007/s10853-011-5628-z

[3] Xu, B., Ma, H., Hu, C.; Yang, S., Li, Z. (2016) Influence of curing regimes on mechanical properties of magnesium oxychloride cement-based composites. Construction and Building Material. Vol. 102, pp. 613-619. https://doi.org/ 10.1016/j.conbuildmat.2015.10.205

[4] Xu, B.; Ma, H., Hu, C., Li, Z. (2016) Influence of cenospheres on properties of magnesium oxychloride cement-based composites. Materials and Structures/Materiaux et Constructions. Vol. 49, pp. 1319-1326. https://doi.org/ 10.1617/s11527-015-0578-6

[5] Chau, C.K., Chan, J., Li, Z. (2009) Influences of fly ash on magnesium oxychloride mortar. Cement and Concrete Composites. Vol. 31, pp. 250-254. https://doi.org/ 10.1016/j.cemconcomp.2009.02.011

[6] Chumak, V. (2003) A new product that is more than 100 years old. Stroitel'nye material [Building Materials]. Vol. 9, pp. 10-11 (in Russian).

[7] Rogic, V., Matkovic, B. (1972) Phsesin magnesium oxychloride cement (in Croatia). Cement (Zagreb). Vol. 16 (2), pp. 61-69.

[8] Sims, C. Industrial minerals. Vol. 2, p. 43.

[9] Zhang, X., Ge, S.,Wang, H., R. Chen, R. (2017) Effect of 5-phase seed crystal on the mechanical properties and microstructure of magnesium oxychloride cement. Construction and Building Materials. Vol. 150, P. 409-17. https://doi.org/ 10.1016/j.conbuildmat.2017.05.211

[10] Deng, D. (2003) The mechanism for soluble phosphates to improve the water resistance of magnesium oxychloride cement. Cement and Concrete Research, Vol. 33 (9), pp. 1311-1317. https://doi.org/ 10.1016/S0008-8846(03)00043-7.

[11] Li, Y., Li, Z., Pei, H., Yu, H. (2016) The influence of FeSO4 and KH2PO4 on the performance of magnesium oxychloride cement. Construction and Building Materials. Vol.102, pp. 233-238. https://doi.org/ 10.1016/j.conbuildmat.2015.10.186

[12] Zhang, X. (2018) Study on compound modified MOC material and its application in thermal insulation board. Thesis. Henan, Xinyang Normal University. (in Chinese).

[13] Altiner, M. and Yildirim, M. (2017) Study of using dolomite as starting material resource to produce magnesium oxychloride cement. Journal of Advanced Concrete Technology. Vol. 15 (6), pp. 269-277. https://doi.org/10.3151/jact.15.269

[14] Kacker, K.P., Mehrotra, G.S., Rai, M. (1970): Petrographic and thermal evaluation of dolomite for the manufacture of magnesium oxychloride cement. Journal of Applied Chemistry, Vol. 20, pp. 189-193. https://doi.org/10.1002/jctb.5010200607

[15] Mitina, A., Lotov, A., Sukhushina, V. (2015) Influence of heat treatment mode of various magnesia rocks on their properties. Procedia Chemistry. Vol. 15, pp. 213–218. http://doi.org/10.1016/j.proche.2015.10.034

[16] Erdman, S., Gapparova, K., Khudyakova, T., Tomshinaa, A. (2014) Magnesia binder preparation from local natural and technogenic raw materials. Procedia Chemistry. Vol. 10, pp. 310-313. https://doi.org/10.1016/j.proche.2014.10.052

[17] Heystek, H. Haul, R.A.W. (1952) Differential thermal analysis of the dolomite decomposition. Am. Mineralogist. Vol. 37, pp.166 -179.

[18] Wieczorek-Ciurowa, K., Paulik, J., Paulik, F. (1980) Influence of foreign materials upon the thermal decomposition of dolomite, calcite and magnesite (part II). Thermochimica Acta. Vol. 38 (2), pp. 165-172.

[19] Wieczorek-ciurowa, K., Paulik, J., Paulik, F., (1980) Influence of foreign materials upon the thermal decomposition of dolomite, calcite and magnesite (part I), Thermochimica Acta. Vol. 38 (2), pp.157-164.

[20] Shand, M., Al-Tabbaa, A, Qian J., Mo. L, Jin, F. (2020) Magnesia Cements: From Formulation to Application. Elsevier publishing. 334 p. https://doi.org/10.1016/C2010-0-68998-X

[21] ASTM C109 (2016) Standard test method for compressive strength of Hydraulic Cement Mortars.

[22] Huang, Q., Xiao, X., Li, Y. (2018) Research on the properties of magnesium oxychloride cement prepared with simulated seawater. Advances in Cement Research, Vol. 30 (7), pp. 277-284. https://doi.org/10.1680/jadcr.17.00127

[23] Huang, Q., Li, Y., Zheng, W. (2019) Investigation on the properties of magnesium oxychloride cement prepared with seawater. Advances in Cement Research. Vol. 32 (8), pp. 379-398. https://doi.org/10.1680/jadcr.18.00159

[24] Qiao, H., Cheng, Q., Wang, J., Shi, Y. (2014) The application review of magnesium oxychloride cement." Journal of Chemical and Pharmaceutical Research, Vol. 6(5), pp. 180-185.

[25] Zhang, C. and Deng, D. (1994) Research on the water-resistance of magnesium oxychloride cement I, the stability of the reaction products of magnesium oxychloride cement in water. Journal of Wuhan Univ. Technol. Material Sci. Ed., Vol. 9, pp. 51-59. https://doi.org/10.1680/jadcr.17.00127

[26] He, P., Poon, C.S., Tsang, D.C. (2017) Effect of pulverized fuel ash and CO2 curing on the water resistance of magnesium oxychloride cement (MOC). Cement and Concrete Research. Vol.97, pp. 115-122. https://doi.org/10.1016/j.cemconres. 2017.03.005

[27] Jiříčková, A., Lojka, M, Lauermannová, A. M., Antončík, F., Sedmidubský, D., Pavlíková, M., Záleská, M., Pavlík, Z., Jankovský, Ondřej. (2020) Synthesis, structure, and thermal stability of magnesium oxychloride 5Mg(OH)2·MgCl2·8H2O. Applied Science. Vol. 10 (5). https://doi.org/10.3390/app10051683. doi:10.3390/app10051683

[28] CHEN, X. G., LV, S., LI, X., ZHANG, L., ZHANG, P., YE, Y. (2011) Preparation of magnesium hydroxide chloride hydrate nanowires using calcined dolomite. Journal of Inorganic Material. Vol. 26, pp. 214-218. https://doi.org/10.3724/SP.J.1077.2011.10535

[29] He, P., Poon, C., Tsang, D. (2017) Using incinerated sewage sludge ash to improve the water resistance of magnesium oxychloride cement (MOC). Construction and Building Material. Vol. 147, pp. 519-524. https://doi.org/10.1016/j.conbuildmat. 2017.04.187. https://doi.org/10.1016/j.conbuildmat.2017.04.187

[30] Liu, Z., Wang, S., Huang. J. (2015) Experimental investigation on the properties and microstructure of magnesium oxychloride cement prepared with caustic magnesite and materials and structures. Construction and Building Materials. Vol. 85, pp. 247-255. https://doi.org/10.1016/j.conbuildmat.2015.01.056

[31] Chau, C. K., Li, Z. (2008) Microstructures of magnesium oxychloride. Material Structure. Vol. 41, pp. 853-862. https://doi.org/10.1617/s11527-007-9289-y

Ref.:
Taha, M. Ezzat – **Kandeel,** Ayman M. – **El-Fakharany,** M. Ezzat: *The effect of one-part magnesium oxychloride cement additive on the mechanical, mineralogical, water resistant and micro structural properties of dolomite cement*
Építőanyag – Journal of Silicate Based and Composite Materials, Vol. 74, No. 3 (2022), 108–112. p.
https://doi.org/10.14382/epitoanyag-jsbcm.2022.17

Investigation and characterization of eco-friendly healing efficiency for sustainable building materials

H. M. KHATER ▪ Professor of cement and geopolymer chemistry, Institute of raw materials and processing technology, housing and building national research center, Egypt ▪ Hkhater4@yahoo.com
A. M. EL NAGAR ▪ Researcher, Institute of raw materials and processing technology, housing and building national research center, Egypt

Érkezett: 2022. 01. 09. ▪ Received: 09. 01. 2022. ▪ https://doi.org/10.14382/epitoanyag-jsbcm.2022.18

H. M. KHATER
Professor of cement chemistry at Raw Building Materials Technology and Processing Research Institute, Housing and Building National Research Center (HBRC). Supervisor of XRF laboratory for the chemical analysis of all type of raw building materials.

Abdeen EL NAGAR
Researcher in the field of geology at Raw Building Materials Technology and Processing Research Institute, Housing and Building National Research Center (HBRC).

Abstract
Concrete repairs are foreseeable to enhance its service life and provide additional expenditure separate to the building cost; so it is necessary to seal cracks which occur due to drying shrinkage or exposed to external factors. Recently, the most promising healing materials that can be applied for concrete repairs are alkali activated materials which have high efficiency in dealing with crack propagation, while this efficiency can be increased by immersion in saturated lime solution or using fibers to heal the produced cracks or even suppress the crack formation. This work focuses on formation alkali activated materials that exposed to artificial cracking then immersed in water, saturated lime using steel fiber as well as basalt fiber to examine their capability in healing the produced cracks. Results demonstrates the healing of the formed cracks with most of the used techniques, while the most promising were those used steel fiber as well as basalt fiber where the crack propagation were terminated and diminished.
Keywords: slag, steel fiber, basalt fiber, damage
Kulcsszavak: salak, acélszál, bazaltszál, károsodás

1. Introduction

Concrete damage is usually the result of a series of events. Not all microcracks progress to become dangerous or unstable cracks. If micro-cracks can be mended once they've formed, concrete damage can be prevented from worsening.Structures can be made safer, and maintenance costs can be drastically lowered.Many academics have looked at this fascinating concrete phenomenon.The self-healing process of micro-cracks in concrete was explored by Hannant et al. [1].When concretes degraded due to freeze and thaw, Stefan et al. [2] discovered crystals of ettringite and $Ca(OH)_2$ traversing the fissures at various locations using a scanning electron microscope (SEM).

Later on, Li et al. stated the complete closing of the cracks without leaking [6]. Reinhardt et al. [7] examined the effect of temperature and crack width on self-healing behavior of concrete and they the fastest self-healing at the concrete surface.

Geopolymer is an inorganic polymer, synthesized by alkali activation of aluminosilicate materials and results in three-dimensional Si-O-Al-O bonds [8]. Despite its strength and versatility as a construction material, geopolymer concrete has a significant drawback resulting from its defects, which could affect its durability and service life. The major defects are either direct cracking, or other forms of defects which are linked to cracking [9]. Cracking is generally initiated by the formation of microcracks, which may later propagate into macrocracks [10-11]

Fiber addition has been proved to be an efficient method in improving the mechanical performance as well as the shrinkage control of brittle mortars and concretes matrices based on alkaline-cements by crack arresting. Also, it is well known that the fracture toughness provided by fiber bridging on the main crack plane prior to crack extension increases. Debonding, sliding and pulling-out of the fibers are the local mechanisms that control the bridging action [12-14]. At the beginning of macrocracking, the opening and growth of cracks is controlled by the bridging action of fibers, which increase energy demand of crack to be propagated. The linear elastic behaviour of the matrix could not be affected significantly for low volumetric fiber fractions. However, post-cracking behaviour can be substantially modified, with increases of strength, toughness and durability of the material [14].

The enormous existence of microcrack in alkali activated slag's framework causes a preterm failure, large interfacial zone, high permeability, and low durability. Crack healing is an interesting concept that received much attention in recent years [15], prominently using self-healing material [16-17]. Based on previous investigations, there were several self-healing agents available for microcrack refinement purpose. Several works were performed by using bacteria or polymer to fill the voids in the microstructure of concrete [18-19] either using external intervention or self-healing methods. The mechanism involves the releasing of self-healing agent into the crack path when the embedded microcapsule ruptured by crack progression.

The purpose of this research focus on the formation alkai activated slag materials that exposed to artificial cracking then immersed in water, saturated lime, and using steel fiber as well as basalt fiber to examine their capability in healing the produced cracks. The sequence of crack healing are characterized petrographic examination; also ultrasonic pulse velocity as well as compressive strength will be studied.

2. Material and methods

2.1 Materials

Blast furnace slag (BFS) was used as raw materials for alkaline activation process [Iron and Steel Factory- Helwan, Egypt]. Steel fiber and basalt fiber were used as healing agents. Sodium hydroxide was used as an alkaline activator for the reaction [99%, Sigma Aldrich], while calcium hydroxide [99%, Sigm Aldrich] was used for the preparation of saturated lime solution for immersion of geopolymer. The used steel fiber was of length 5 mm and diameter 0.2 mm with aspect ratio of 25.

The complete compositions of the used materials are given in *Fig. 1*, as well as their mineralogical properties; where its mineralogical composition reflects its high amorphous structure as a results of fast quenching process, while the chemical composition depicts that it has mainly SiO_2, CaO, and Al_2O_3 as major constituents.

2.2 Alkali mateials preparation and curing

Activation of the used binder was done using 6 wt., % NaOH from dry mixes, while their water content was 23% as indicated in the *Table 1*. The dried binder was stirred mechanically for 2 min followed by another 5 min with activator solution, then were poured in 10 cm length cylindrical shaped mold with diameter of 5 cm. The cast binders were exposed to vibration for compaction, and then sealed with plastic sheet to avoid water loss evaporation. The molded mixes were cured undisturbed at 23 °C (r.t.) for 24 hrs, then they were cured at 40 °C with 100% relative humidity (R.H.) up to 28 days. In order to stimula cracking for the samples, they were exposed to strength equal 0.2 of the 28 days compressive strength of the control paste [20] in order propagate a crack with a width between 0.1 and 0.3 mm. After that the samples were treated using different healing conditions as in *Table 1*.

Mix no.	Water cooled slag(WCS), %	Steel fiber, %	Basalt fiber, %	NaOH, %	Water immersion	Saturated lime immersion	Water/ binder, %
A0	100	–	–	6	√	×	0.23
A1	100	–	–	6	×	√	0.23
S	100	0.50	–	6	√	×	0.23
B	100	–	0.50	6	√	×	0.23

Table 1 Composition of the geoplymer mixes (Mass %)
1. táblázat A geopolimer keverékek összetétele (tömeg %)

During immersion, at specified time all samples were tested using ultrasonic puls velocity to attain the healing efficiency of the used agent. At the end of immersion time, the samples were tested using compressive strength testing, followed by stopping of the reaction using acetone solution for 24 hrs at 60 °C [21]. All samples were tested visually as well as using petrographic microscocopic imaging.

2.3 Methods of investigation

Chemical investigation for starting material performed using XRF-Axios (PW4400) WD-XRF Sequential Spectrometer, while mineralogical characterization done by XRD-Philips PW 3050/60 Diffractometer using a Cu-Kα source. Compressive strength was measured using five tones German Brüf pressing machine with a loading rate of 100 MPa/s [22].

Petrographic examination was done on fluorescent dyed alkaline hybrid samples using a stereo-microscope (Olympus Gx70) equipped with a blue filter (BG-12) and under magnification 50×. Flat polished section was and lapped by using a series of silicon carbide grit followed by polishing using diamond paste, until a smooth surface is obtained [23].

For nondestructive in-situ testing for concrete, ultrasonic pulse velocity (UPV) test is the most promising technique for checking the quality of the cement binders using Proceq's Tico instrument, by measuring the velocity of an ultrasonic pulse passing through a hardened binder structure, in addition it can be helpful in quantifying the damage of the hardened binder [24, 11] according to the following equation:

$$UPV = L/T \quad (1)$$

Where T is the elapsed time and L is the distance of the ultrasonic propagation through the concrete matrix, whereas UPV readings were taken in accordance with ASTM C597 [25].

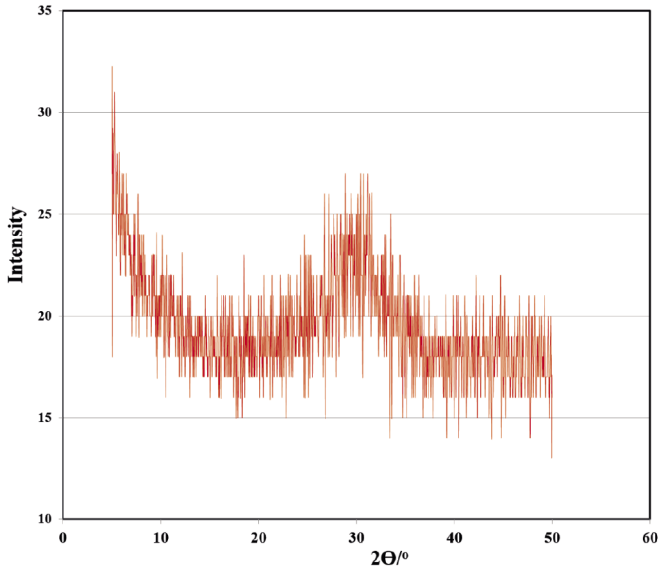

Material	Water – Cooled Slag (GGBFS)
SiO_2	36.67
Al_2O_3	10.31
Fe_2O_3	0.50
CaO	38.82
MgO	1.70
SO_3	2.17
K_2O	1.03
Na_2O	0.48
TiO_2	0.57
MnO_2	4.04
P_2O_5	0.04
Cl^-	0.05
L.O.I.	0.12
SrO	0.18
BaO	3.28
Total	99.96

Fig. 1 Chemical and mineralogical properties of blast furnace slag
1. ábra A kohósalak kémiai és ásványtani tulajdonságai

3. Results and discussion

Ultrasonic concrete tester is shown in *Fig. 2* of alkali activated slag treated using various healing parameters. As known, the main principle of this test consists of measuring the time of ultrasonic pulse travel passing through the

tested samples. Relatively, as the specimen quality is good in terms of density, uniformity, homogeneity, etc., the higher the velocity is obtained. From the figure we can deduce that tap water as well as saturated lime solution immersed samples possess high UPV values and increases with time up to more than 100% from its original value giving an indication about the continuous healing of the precracked samples with time. On the other hand, samples incorporating basalt fiber as well as steel fiber have lower UPV readings by about 50% from the previous two groups as well as from their original readings; inspite their readings increase with time reflecting also the continuous healing of the precracked hardened samples. One can classify the resulting data according to ASTM C597 [25], where UPV more than 4.5 resulting in formation of excellent binder quality, while reading below 3; results in doubtful quality of the formed binder. This means that the immersion in tap water as well as in saturated lime solution has good potential in formation of excellent quality binder (UPV more than 5) rather than fiber incorporated sample (UPV less than 3).

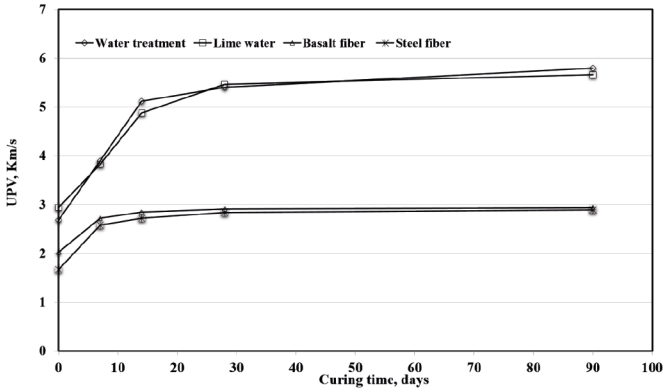

Fig. 2 UPV of alkali activated slag treated with various healing parameters
2. ábra Különböző gyógyító paraméterekkel kezelt lúgaktivált salak UPV értékei

The results from UPV tests indicate that the UPV of damaged hardened paste recover almost completely during subsequent storage in tap water as well as saturated lime solution environment, but the recovery of UPV is influenced by many factors, such as damage degree etc.

Lastly, any increase in mortar moisture content causes an increase in UPV which negatively affect compressive strength; where any discontinuity as a crack in the wave path, results in refelction of part of the energy from the flaw surface.

According to other researchers' investigations [26, 11], the UPV decreases significantly as the secant modulus decreases during uniaxial compressive loading.So, according to Wenhui Zhong and Wu Yao, a damage degree is defined as: Damage efficiency:

$$D= 1-(V/V_0) \quad (2)$$

Where D denotes the degree of concrete damage, V denotes the UPV prior to self-loading, and V_0 denotes the UPV prior to loading. As a result, the decrease in UPV by D could be used to infer microstructure changes in concrete.

From *Fig. 3* we can conclude that all damage data is in the negative zone which refelcts the increased UPV of the healed specimens as compared with the comtrol unhealed one at all studied healing parameters.

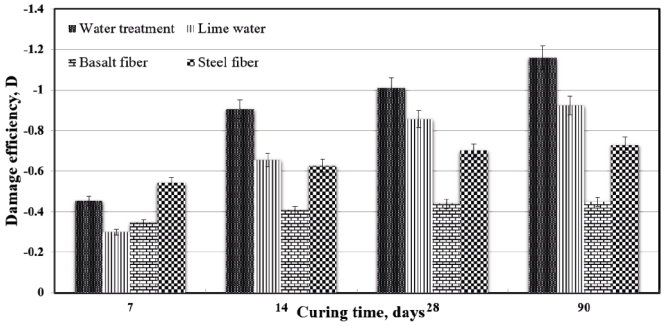

Fig. 3 Damage efficiency of 90 days alkali activated slag treated with various healing parameters
3. ábra Különböző öngyógyulás segítőket tartalmazó, 90 napos korú lúgaktivált salak károsodási hatékonysága

Fig. 3 shows also the highest negstive values for tap water, followed by saturated lime solution and then steel fiber mixes. This indicates that those mixes can retain their orginal uniformity steadily with time resulting in uniform compact structure as well be emphasized later by petrographic examination.

The result of damage degree illustrates the increased UPV after healing as compared with control reading as reflected on the negative reading of the damage degree for all samples. However, tap water as well as saturated lime solution followed by steel fiber treated samples have lowest D values which confirmed by highest healing efficiency for those treatments. Samples treated with basalt fiber has highest D values as compared with other tratments which reflected negatively on the healing efficiency of this treamtemt.

Fig. 4 shows the strength and K value of hardened geopolymer exposed to various healing parameters. It appears that the compressive strength of all specimens is from 300 to 480 kg/cm^2, whereas mixes immersed in saturated lime solution retain a high level of strength, basalt fibre and tap water mixtures do not.

It is clear that specimens reinforced with steel fibres have a weaker effect on self-healing than those reinforced with other parameters.The self-healing ratio (K) was proposed to define the self-healing capabilities. It represents the ratio of the compression strength after self-healing ($P0$) to the original compression strength (P) of UHPCC.

$$K=P/P0 \quad (3)$$

The self-healing ratio K of alkali activated slag treated with various healing parameters of both tap water and saturated lime approaches 1.2 and the self-healing ratio K of both basalt fiber and steel fiber approaches to 1. Steel fibre specimens have superior mechanical properties, but a poorer self-healing ratio than specimens treated with other factors.Wenhui Zhong and Wu Yao [11] discovered that there is a damage degree threshold on concrete, and that if the damage degree is less than this threshold, the concrete's self-healing ratio will grow as the damage degree increases.

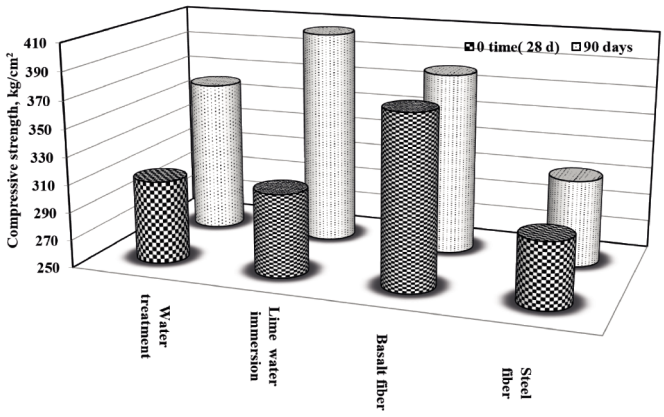

Fig. 4 Compressive strength of alkali activated slag treated with various healing parameters for zero and 90 days of treatment
4. ábra Különféle gyógyulás segítőket tartalmazó lúgaktivált salak nyomószilárdsága nulla és 90 napos korban

As we know, the degree of damage to the concrete can affect its ability to self-heal, but it is not the only issue. In tap water as well as saturated lime solution environment, the unhydrated cement particles re-hydrate, and the fine cracks are bridged and narrowed gradually. If the damage degree is too low, the exposure number of unhydrated cement particles is small and it is not helpful for re-hydration. However, if the damage degree is too high and excess a limit, the length of new hydration products cannot bridge the cracks, as a result, K decreases.

Fig. 5 illustrates the visual as well as petrographic examination of 90 days prereacked alkali activated hardened specimens**.** One can depict from the visual patterns that the microcracks almost healed under the studied healed parametes, which emphasized by their petrofgraphic images where some re-hydration products clustering along the edges of cracks could be seen in microcracks clearly through the petrographyic images, and the rehydration products filled in the center part were less dense than those along the edges, as well as the width of cracks is narrowed [3]. From the figure we can deduce also that microcrakcs in tap water is the most filled one followed by basalt fiber and saturated lime solution and finally steel fiber samples.

4. Conclusions

Self-healing of alkali activated slag is markedly affected by the treamtemt methods as well as the materials used for promoting their healing efficiency. The cuurent work has some main findings:

a. Damage degree of all treatments were vey low but mixes immersed in tap water as well as saturated lime solution has the lowest damage degree. Where the damage degree affected markedly by ultrasonic pulse velocity reading.
b. The results obtained from mechanical and ultrasonic properties showing that the self-healing ratio of alkali activated slag increases with the decreasing of damage degree depending on the ways of treatment.
c. Precracked hardened alkali activated samples in both tap water as well as saturated lime solution exhibit higher self healing performance wih high UPV that increased to about 100% of its orginal value indicating high retention of structure with time. Also, they acquire high healing efficiency more than 1.2.

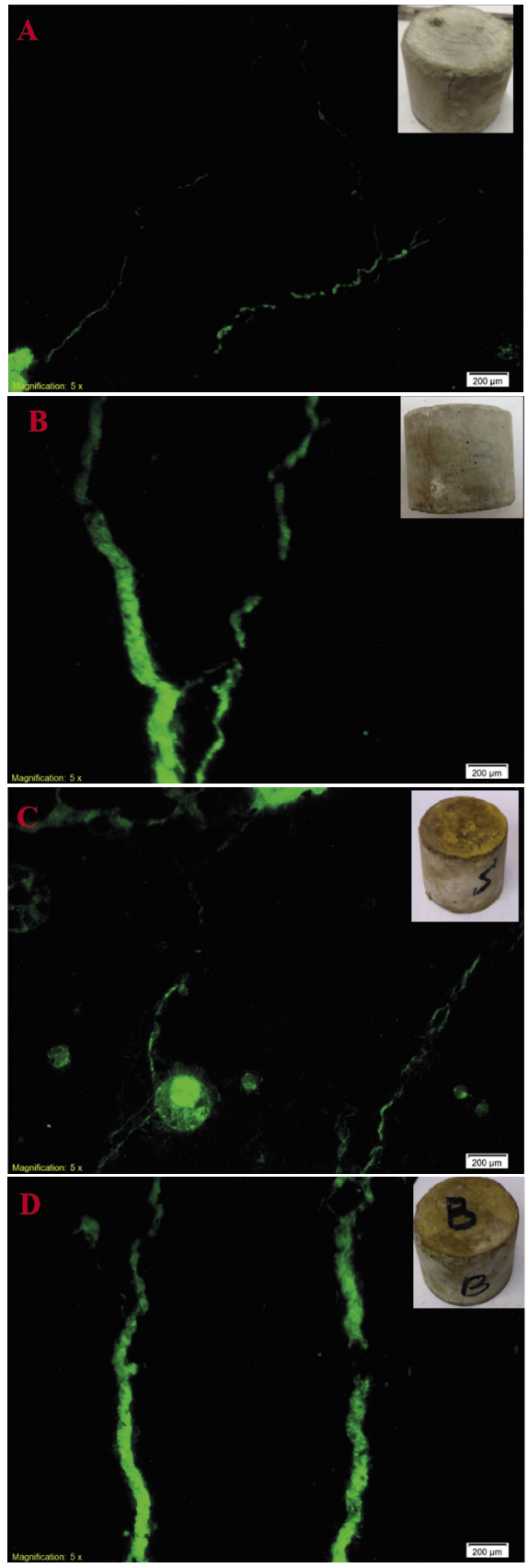

Fig. 5 Fluorescent images of 90 days alkali activated slag treated with various healing parameters; A) water immersion, B) saturated lime immersion, C) steel fiber in water, D) basalt fiber in water
5. ábra Fluoreszcens képek 90 napos, különféle gyógyulás támogatókat eljárásokkal kezelt, lúgaktivált salakról; A) vízben tárolt, B) telített mészben tárolt, C) vízben tárolt, acélszálat tartalmazó, D) vízben tárolt, bazaltszálat tartalmazó

d. Basalt fiber aas well as steel fiber has lower UPV values while improved with the increasing of curing ages, whereas their healing efficiency reached to about one. The UPV has been greatly restored after self-healing for the final time, and the damage degree can be extrapolated from the UPV growth.

References

[1] Hannant, D.J., Keer, J.G., (1983) Autogeneous healing of thin cement based sheets, Cement Concrete Research, Vol. 13, No. 3, pp.357–365, https://doi.org/10.1016/0008-8846(83)90035-2

[2] Stefan, J., Jacques, M., Hugues, H., (1995) SEM observations of the microstructure of frost deteriorated and selfhealed concretes, Cement Concrete Research, Vol. 25, No. (8), pp. 1781–1790.

[3] Stefan, J., Jacques, M., Luc, B., (1996) Effect of cracking and healing on chloride transport in OPC concrete,Cement Concrete Research, Vol. 26, No.6, pp. 869–881.

[4] Nataliya,H., 1998, Self-sealing, autogenous healing and continued hydration: what is the difference?, Materials and Structures, Vol 31, No.212, pp.563–567.

[5] Liu, X.Y., Yao, W., Zheng, X.F., Wu, J.P., (2005) Experimental study on self-healing performance of concrete, Chinese Journal of Building Materials, Vol. 8, No.2, pp.184–188, https://doi.org/10.3969/j.issn.1007-9629.2005.02.014

[6] Li, H.X., Tang, C.A., Zeng, S.H., Li, S.N., (2004), Research on self-healing of concrete cracks. Chinese Journal of Wuhan University of Technology, Vol. 26, No. 3, pp. 27–29, https://doi.org/10.3321/j.issn:1671-4431.2004.03.008

[7] Reinhardt, H.W., Jooss, M., (2003), Permeability and self-healing of cracked concrete as a function of temperature and crack width, Cement Concrete Research, Vol 33, No. 4, pp. 981–985. https://doi.org/10.1016/S0008-8846(02)01099-2

[8] Davidovits, J., (1994), High-Alkali Cements for 21st Century Concretes, Am. Concr. Inst., Vol. 144, pp. 383–398.

[9] Zhu, J., Popovics, J.S.,(2007) Imaging Concrete Structures Using Air-Coupled Impact-Echo, J. Eng. Mech. , Vol. 133, pp. 628–640. https://doi.org/10.1061/(ASCE)0733-9399(2007)133:6(628)

[10] Shah, S.P. , Choi, S., (1999) , Nondestructive Techniques for Studying Fracture Processes in Concrete", Int. J. Fract. Vol. 98 , pp. 351–359.

[11] Zhong, W., Yao, W. , (2008), Influence of damage degree on self-healing of concrete, Constr. Build. Mater., Vol. 22 , pp.1137–1142, https://doi.org/10.1016/j.conbuildmat.2007.02.006

[12] Silva, F.J., Thaumaturgo, C.,(2003), Fiber reinforcement and fracture response in geopolymeric mortars, FatigueFract Engng Mater Struct. Vol., 26, pp. 167–72.

[13] Silva, F.J., Thaumaturgo, C., (2003), The chemistry, reinforcement and fracture in geopolymeric cementcomposites", In: Proceedings of the 11th international congress on the chemistry of cement (ICCC). cement's contribution to the development in the 21st century, Durban – South Africa; pp. 1379–1387.

[14] Penteado, D. D., Thaumaturgo, C.,(2005), Fracture toughness of geopolymeric concretes reinforced with basaltfibers, Cem Concr Compos Vol. 27, pp.49–54, https://doi.org/10.1016/J.CEMCONCOMP.2004.02.044

[15] He, H. , Guo, Z. , Stroeven, P. , Stroeven, M., Sluys, L.J., (2011), Self healing capacity of concretecomputer simulation study of unhydrated cement structure, Image Anal. Stereol. Vol. 26 pp. 137, https://doi.org/10.5566/ias.v26.p137-143

[16] Li, W., Dong, B., Yang, Z., Xu, J. , Chen, Q., Li, H. , Xing, F., Jiang, Z., (2018), Recent Advances in Intrinsic Self-Healing Cementitious Materials, Adv. Mater. Vol. 30, No. 17, e1705679, https://doi.org/10.1002/adma.201705679.

[17] Yıldırım, G. ; Şahmaran, M., (2018), Ö.A.-P. of 3rd International, U. 2018, Determination of Self- Healing Performance of Cementitious Composites Under Elevated CO2 Concentration by Resonant Frequency and Crack Opening , in: Proc. 3rd Int. Sustain. Build. Symp., pp. 592, https://doi.org/10.1007/978-3-319-64349-6_47

[18] Dong, B. , Wang, Y., Fang, G. , Han, N., Xing, F., Lu, Y. , (2015), Smart releasing behavior of a chemical selfhealing microcapsule in the stimulated concrete pore solution, Cem. Concr. Compos. Vol. 56 , pp.46–50, https://doi.org/10.1016/j.cemconcomp.2014.10.006

[19] Snoeck, D., Van Tittelboom, K. , Steuperaert, S., Dubruel, P. , De Belie, N., (2014), Self-healing cementitious materials by the combination of microfibres and superabsorbent polymers, J. Intell. Mater. Syst. Struct., Vol. 25, pp. 13–24, https://doi.org/10.1177/1045389X12438623

[20] Shim, K.B., Kishi, T., Choi, C.S., Ahn, T.H., (2015), Cementitious materials for crack self-healing concrete, Journal of Ceramic Processing Research. Vol. 16, No. 1, pp. s1~s13

[21] Ke, X., Bernal, S. A., Ye, N., Provis, J. L., Yang, J.,(2014), One-Part Geopolymers Based on Thermally Treated Red Mud/NaOH Blends, J. Am. Ceram. Soc., Vol.98, No.1, pp. 1–7, http://dx.doi.org/10.1111/jace.13231

[22] ASTM C109,(2016), Standard test method for compressive strength of Hydraulic Cement Mortars .

[23] Khater, H.M.; Ezzat, M.,(2018), Preparation and characterization of engineered stones based geopolymer composites, Journal of building engineering (El Sevier), Vol. 20, pp. 493-500, https://doi.org/10.1016/j.jobe.2018.08.004

[24] Qasrawi, H., Marie, I., (2003). The use of USPV to anticipate failure in concrete under compression. Cement and Concrete Research, Vol. 33, pp. 2017-2021, https://doi.org/10.1016/S0008-8846(03)00218-7

[25] ASTM C597. (2016). Standard Test Method for Pulse velocity Through Concrete. West Conshohocken:American Society for Testing and Materials.

[26] Suaris, W., Fernado, V., (1987), Ultrasonic pulse attenuation as a measure of damage growth cyclic loading of concrete, ACI Materials Journal, Vol. 84, No. 3, pp.185-193

Ref.:
Khater, H. M. – **El Naga**, A. M.: *Investigation and characterization of eco-friendly healing efficiency for sustainable building materials* Építőanyag – Journal of Silicate Based and Composite Materials, Vol. 74, No. 3 (2022), 113–117. p. https://doi.org/10.14382/epitoanyag-jsbcm.2022.18

GUIDELINE FOR AUTHORS

The manuscript must contain the followings: title; author's name, workplace, e-mail address; abstract, keywords; main text; acknowledgement (optional)**; references; figures, photos with notes; tables with notes; short biography** (information on the scientific works of the authors).

The full manuscript should not be more than 6 pages including figures, photos and tables. Settings of the word document are: 3 cm margin up and down, 2,5 cm margin left and right. Paper size: A4. Letter size 10 pt, type: Times New Roman. Lines: simple, justified.

TITLE, AUTHOR

The title of the article should be short and objective.

Under the title the name of the author(s), workplace, e-mail address.

If the text originally was a presentation or poster at a conference, it should be marked.

ABSTRACT, KEYWORDS

The abstract is a short summary of the manuscript, about a half page size. The author should give keywords to the text, which are the most important elements of the article.

MAIN TEXT

Contains: materials and experimental procedure (or something similar), results and discussion (or something similar), conclusions.

REFERENCES

References are marked with numbers, e.g. [6], and a bibliography is made by the reference's order. References should be provided together with the DOI if available.

Examples:

Journals:

[6] Mohamed, K. R. – El-Rashidy, Z. M. – Salama, A. A.: In vitro properties of nano-hydroxyapatite/chitosan biocomposites. *Ceramics International.* 37(8), December 2011, pp. 3265–3271, http://doi.org/10.1016/j.ceramint.2011.05.121

Books:

[6] Mehta, P. K. – Monteiro, P. J. M.: Concrete. Microstructure, properties, and materials. *McGraw-Hill*, 2006, 659 p.

FIGURES, TABLES

All drawings, diagrams and photos are figures. The **text should contain references to all figures and tables**. This shows the place of the figure in the text. Please send all the figures in attached files, and not as a part of the text. **All figures and tables should have a title**.

Authors are asked to submit color figures by submission. Black and white figures are suggested to be avoided, however, acceptable.

The figures should be: tiff, jpg or eps files, 300 dpi at least, photos are 600 dpi at least.

BIOGRAPHY

Max. 500 character size professional biography of the author(s).

CHECKING

The editing board checks the articles and informs the authors about suggested modifications. Since the author is responsible for the content of the article, the author is not liable to accept them.

CONTACT

Please send the manuscript in electronic format to the following e-mail address: femgomze@uni-miskolc.hu and epitoanyag@szte.org.hu or by post: Scientific Society of the Silicate Industry, Budapest, Bécsi út 122–124., H-1034, HUNGARY

We kindly ask the authors to give their e-mail address and phone number on behalf of the quick conciliation.

Építőanyag – *Journal of Silicate Based and Composite Materials*, Quarterly peer-reviewed periodical of the Hungarian Scientific Society of the Silicate Industry, SZTE.
http://epitoanyag.org.hu